CRANFIELD UNIVERSITY

SARAH YASIR

INNOVATION REPORT
DEVELOPMENT OF NI3AL CORROSION RESISTANT COATINGS FOR SS347 HEAT STORAGE COMPONENTS IN PRESENCE OF MOLTEN NITRATE SALT

SCHOOL OF AEROSPACE, TRANSPORT AND MANUFACTURING

Engineering Doctorate
Academic Year: 2015 - 2020

Supervisor: Dr Adrianus Indrat Aria, Prof Jose Luis Endrino
July 2020

CRANFIELD UNIVERSITY

SCHOOL OF AEROSPACE, TRANSPORT AND MANUFACTURING

Eng D Sustainable Materials and Manufacturing

Academic Year 2015 - 2020

SARAH YASIR

DEVELOPMENT OF NI3AL CORROSION RESISTANT COATINGS FOR SS347 HEAT STORAGE COMPONENTS IN PRESENCE OF MOLTEN NITRATE SALT

Supervisor: Dr Adrianus Indrat Aria, Prof Jose Luis Endrino

July 2020

This Innovation report is submitted in partial fulfilment of the requirements for the degree of Engineering Doctorate

ABSTRACT

Climate change is an inevitable global issue with long term consequences for the sustainable development. It is a crucial time to review this climate issue with ensured determination. There is a need and demand for alternative sources to generate power rather than the conventional burning of fuels due to impact on environment. Renewable energy sources are those natural reserves that are refilled continually, including wind, solar, biomass and geothermal. A number of technologies have been developed to use solar energy for power generation. Among them, an important feature of concentrated solar power plants is the potential to incorporate thermal storage. Thermal energy storage allows generation beyond sunset and in times of cloud cover. Several possibilities for heat transfer fluid and thermal energy storage have been identified. From a wide range of materials, molten nitrate salt is selected because of adequate heat storage and transfer capability. Different approaches to prolong life by suppressing corrosion have been suggested in the literature, coating is a promising option because coatings are believed to provide shield to suppress corrosion. Among different coatings, nickel aluminide has been claimed to possess high-temperature mechanical strength and it has a remarkable oxidation resistance performance as substrate component. Moreover, nickel aluminide has low solubility in the molten nitrate salt. Ni_3Al coatings are much preferred to be used as corrosion resistant coatings as they possess strength at high temperature, oxidation protection and creep properties. Among different deposition techniques, plasma spray has been identified as most applicable because it is versatile, adaptable, cost effective. It also has high deposition rate, deposition efficiency and less environmental impact, more importantly it is easy to scale up.

Corrosion behaviour of stainless steel 347 (SS347) and Ni_3Al coated SS347 was investigated in molten nitrate salt (60wt% $NaNO_3$ + 40wt% KNO_3) immersion at 565^oC for 500 hours intervals up to 3000 hours. A growth of stratified oxide layers was observed on SS347 sample surface comprising of $NaFeO_2$, Fe_2O_3 and Fe_3O_4. The Ni_3Al coated SS347 samples were observed to undergo rapid

oxidation within first 500 hours. Apparent Mass change for bare SS347 was 4 mg/cm^2/yr, equivalent to oxide growth rate of ~ 5 µm/yr. Mass change for Ni_3Al coated SS347 was 29.8 mg/cm^2/yr, equivalent to oxide growth rate of ~ 44.6 µm/yr for first 500 hours and 0.5 mg/cm^2/yr, equivalent to oxide growth rate of ~ 0.7 µm/yr for 500 to 3000 hours. The results presented in this study suggest that Ni_3Al coating supresses the formation of oxide layers on the surface of stainless-steel substrates and can be used to suppress corrosion in presence of molten nitrate salts. The fact, that Ni_3Al coated SS347 gives mass change of one order of magnitude lower than the bare SS347, it means that these coatings can be used to prolong the lifetime of bare SS347 in molten nitrate salt at 565^{o}C, which is of relevance to thermal energy storage applications.

The Engineering Doctorate portfolio is structured as an innovation report and five submissions. A personal profile and a report on international industrial placement are also included in the portfolio.

Keywords:

Concentrated solar power, Nickel aluminide, Thermal energy storage, Heat transfer fluid, Plasma spray.

ACKNOWLEDGEMENTS

It is my pleasure to acknowledge the part of many individuals who contributed for completion of this project.

First of all, I would like to thank my mentors, Dr Adrianus Indrat Aria and Prof. Jose Luis Endrino, and my industrial mentor, Dr Elena Guillen for important ideas, new approaches and academic support and being available when needed. Thank you all for your continuous support and invaluable guidance during the last four years.

This EngD was part of EPSRC centre for Doctoral training in Sustainable Materials and Manufacturing, in collaboration with Cranfield University, University of Warwick and University of Exeter. Research was conducted as part of FRIENDS^2 project with funding from the European Union's Horizon 2020 research and innovation programme under the Marie Skłodowska-Curie grant agreement No 645725. I would like to express my gratitude to FRIENDS^2 project team in particular Ramon Escobar Galindo for all his support and encouragement. Additionally, I am highly appreciative for the enthusiasm and passion they always treated me with. I am grateful to Ivan Fernandez Martinez and Ambiörn Wennberg for hosting my international placement.

A big thanks to Cranfield University for the facilities and equipment required for successful completing of this project. A special thanks to Prof. John Nicholls for his expert advice on many matters and for being an inspiring figure. The project would not have been accomplished without provision from Cranfield University technicians and administrative staff. Special thanks to Dr Simon Gray for taking time out of busy schedule and helping me with low vacuum plasma spray coating deposition. Dr Christine Chalk and Mr Timothy Pryor for supervising health and safety requirements and assisting me to use furnaces and many other pieces of equipment. Mr Steve Pope for help with metallography. Dr Tracey Roberts and Mrs Christine Kimpton for supporting in evaluating deposited coatings using XRD, SEM and EDX. Mrs Sharon McGuire for all administrative help and support.

I would like to acknowledge my fellow office friends, Dr Luis Isern, Mr Tomasz Brzezinka, Ms Victoria Minns, Mr Rizal Nofrizal, Ms Siti Mohamad Badari, Mr Yading Wang and Mr Mohammad Hakim Khalili, for pleasant office environment.

Last but not least, I would like to express my most cordial appreciation to my family. I thank my parents, for supporting me throughout my life. Thanks to my husband Mr Ali Raza for his love and support, it would not have been possible without his unconditional support. Thanks to my daughters Ayesha and Aleena for being my inspiration.

TABLE OF CONTENTS

LIST OF FIGURES

LIST OF TABLES

LIST OF EQUATIONS

LIST OF ABBREVIATIONS

EngD	Engineering Doctorate
FRIENDS^2	Framework of Innovation for Engineering of New Durable Solar Surfaces
EU	European Union
CSP	Concentrated solar power
TES	Thermal energy storage
APS	Air plasma spray
SOA	State of the Art
R & D	Research and development
FEM	Finite element analysis method
GHGs	Greenhouse gases
PV	Photovoltaic
DNI	Direct normal irradiation
HTF	Heat transfer fluid
MW	Megawatt
MNS	Molten nitrate salt
UMS	Unspecified molten salt
UD	Unavailable data
UC	Under construction
PTC	Parabolic trough collector
LFR	Linear fresnel reflectors
PDC	Parabolic dish collector
CRT	Central receiver tower
HVOF	High velocity oxyfuel
SS	Stainless steel
LVPS	Low vacuum plasma spray
PVD	Physical vapour deposition
CVD	Chemical vapour deposition
HIPIMS	High-power impulse magnetron sputtering
PREN	Pitting resistance equivalent number
IPA	Isopropyl alcohol
MPa	Megapascal

SEM	Scanning electron microscope
EDX	Energy dispersive x-ray spectroscopy
XRD	x-ray diffraction
LCOE	Levelised cost of electricity

1 INTRODUCTION

This document provides an executive summary of the studies conducted to establish this thesis. The project was divided into several sections. The thesis was largely advanced experimentally, with most of the work carried out at Cranfield University. The full process has been recorded and detailed, from design, experiments, postprocessing characterisation and scale up. The Engineering Doctorate (EngD) portfolio is structured as an innovation report, five submissions, international placement report and a personal profile (Figure 1). Each submission has been customised to explain the processes used and summarise the results and conclusions.

Introduction to EngD portfolio is presented in this chapter. It features the research focus and approach used, research aim and objectives and defines structure of the Engineering Doctorate portfolio. The innovation in the research undertaken is also illustrated.

1.1 Research Focus and Approach

This proposed research is dedicated to the design and development of coatings to mitigate one of the most severe problems facing the energy industry, that is the corrosion caused by molten salt at high temperatures.

The research focus of this engineering doctorate study was on the investigation and development of protective surface coatings to suppress corrosion, to be used specifically in a molten nitrate salt environment at high temperatures. A literature search was carried out on concentrated solar power plants, explicitly corrosion issues associated with thermal energy storage in concentrated solar power plants, and strategies for corrosion protection with emphasis on anticorrosion coatings. In the course of this study, suitable materials were selected, coatings were designed, deposited and tested in the real-life depicting environment. A comprehensive characterisation of the anticorrosive coatings was carried out in order to identify the chemical structure and physical properties.

This research was conducted as part of FRIENDS^2 project. The project entitled Framework of Innovation for Engineering of New Durable Solar Surfaces (FRIENDS^2) includes two academic partners Helmholtz-Zentrum Dresden – Rossendorf, a research institution from Germany, and Cranfield University from the United Kingdom. It also includes industrial partner, Profactor, an applied research company from Austria, and two Spanish SMEs, Metal Estalki and Nano4Energy. The FRIENDS^2 project works under new Marie Curie scheme within Horizon 2020, the European Union (EU) Framework Programme for Research and Innovation, encouraging international and inter-sectorial partnership using staff exchanges.

1.2 Research Aims and Objectives

Some of the challenges in concentrated solar power (CSP) plants currently include enormous water consumption, dust accumulation on mirrors and solar collectors, selection of compatible system components with increasing temperature to improve efficiency, initial installation cost and hot corrosion in thermal energy storage (TES) system.[1–7] The issue with hot corrosion in thermal energy storage system is the motivation of this study. It may not be the biggest challenge, but it is certainly important to be addressed because TES is a vital part of CSP. The research question for this study is “can specialised coatings be used to suppress corrosion in thermal energy storage system, on exposure to molten nitrate salts?” The overall aim of this study is to design, develop and assess a corrosion resistant coating for use in molten nitrate salts above 500^{o}C. Several specific objectives have been devised to attain this goal, described as following.

1. Establish appropriate coating material candidates with good corrosion resistance in molten nitrate salts at elevated temperatures based on state of the art.
2. Develop an empirical model to predict normalised mass change with time.
3. Selection of deposition technique and manufacture of selected coatings.
4. Produce a protocol to evaluate corrosion resistance of samples.
5. Evaluate and compare corrosion resistance of bare substrate material and coated substrate samples.

1.3 Structure of the EngD Portfolio

Along with the personal profile and the innovation report, five submissions and a report on international industrial placement are included in the EngD portfolio. As displayed in Figure 1, five submissions were produced during the progression of EngD.

1.3.1 Submission 1: Literature Review

During the first year of the project, an important part of the work was devoted to an extensive literature search. The main corrosion failure mechanisms associated with TES were identified. The search focused on anticorrosion coatings for high temperature applications, with special emphasis on those devoted to protection against molten salt corrosion. As a result of this search, a state-of-the-art on anticorrosion coatings for CSP was prepared (Submission 1 Literature Review). Submission 1 (Literature Review) facilitates the framework for performance criteria which is validated through experimental work in submission 4 (Protective Coatings Development) and submission 5 (Strategy for Scaling Up of Developed Coatings).

1.3.2 Submission 2: Database of Properties of High Temperature Corrosion Resistance Coatings

A database of corrosion behaviour information of various alloys and coatings was compiled based on the previous studies reported in literature. Corrosion data were based on the studies conducted in molten nitrate salt as well as several other molten salt. An empirical model to predict mass change of different alloys was proposed. The proposed empirical model provides a guideline to select suitable material for supressing corrosion. Ni_3Al was proposed as the suitable material for coating based on the studied literature, the compiled database and the empirical model.

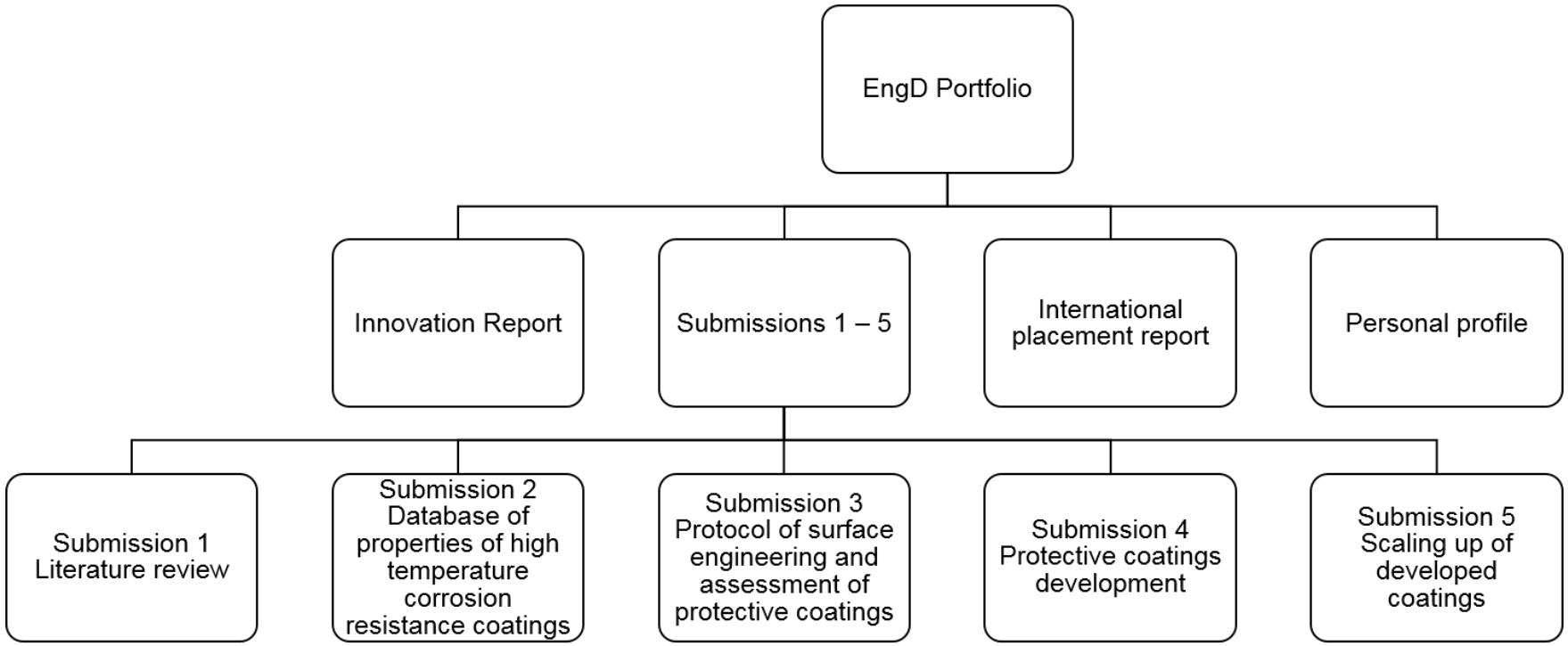

Figure 1: Engineering Doctorate portfolio consists of five submissions, international placement report, innovation report and a personal profile

1.3.3 Submission 3: Protocol for Surface Engineering and Assessment of Protective Coatings

The key purpose of this submission was to describe all the processes, experiments, analysis and characterisation methods used in this project. The first part of this submission establishes a methodology to deposit and characterise coatings and investigate them as candidates to be utilised as corrosion resistant coatings. The second part of this submission describes a methodology for corrosion tests. It helps to put into context the conditions used and the step by step process undertaken to assess the corrosion resistance of the samples. The characterisation techniques used are also described.

1.3.4 Submission 4: Protective Coatings Development

This document provides details of coating development, including selection of materials and deposition process. The deposited coatings were analysed using characterisation techniques provided in submission 3 (Protocol for surface engineering and assessment of protective coatings). The analysis of structure, morphology and composition of the developed coatings are included.

1.3.5 Submission 5: Scaling Up of Developed Coatings

This submission on scaling up of the coating deposition technique was put together to provide guidance on material and operational costs of the protective coating deposition processes used in this project. Atmospheric plasma spray (APS) deposition technique is capable of depositing Ni_3Al coatings with sub millimetres thickness on laboratory scale substrates. Air plasma spray (APS) has been used in a wide range of applications due to its versatility, flexibility, cost effectiveness, and high deposition efficiency (submission 1 Literature Review). Ni_3Al coatings were successfully deposited on 100x150 mm samples, for the first trial towards scalability.

1.3.6 International Industrial Placement Report

The international industrial placement provided a prospect to practice industrial work outside of the UK as part of EngD. Nano4Energy located in the Universidad

Politécnica de Madrid was selected with an intention to develop the coatings through a different deposition process. The details about the industrial placement are provided in this report.

1.3.7 Innovation Report

The innovation report summarises all submissions and provides the details of the evaluation of corrosion performance of developed coatings. The structure of the innovation report is presented in section 1.4.

1.3.8 Personal Profile

Personal profile of the author is also contained within the EngD portfolio. It summarises the development of key competencies for the EngD. Competencies were developed and advanced during the embedded MSc, international placement, conference presentations, FRIENDS^2 meetings, workshops and other activities carried out during the EngD program.

1.4 Structure of the Innovation Report

The purpose of this report is to demonstrate main findings of the research carried out as part of this Engineering Doctorate. This innovation report is structured as five chapters and one appendix. The first chapter includes the background of the study. The aims and objectives with the structure of engineering doctorate portfolio are also defined in chapter one. The second chapter provides a background on the concentrated solar power technology with focus on hot corrosion challenge associated with use of molten nitrate salt as thermal energy storage, and the use of coatings as the proposed solution. The third chapter comprises of all materials and experimental methods used in the study. Details about the coating deposition and characterisation of the corrosion resistance of coatings are presented in the fourth chapter along with the results. A discussion is included in chapter five, with conclusions and suggestions for future works are wrapped in chapter six. The appendix includes the safety information concerning the corrosion testing. The outline of each chapter is detailed in following section.

1.4.1 Chapter 1: Introduction

This chapter sketches the Engineering Doctorate programme and its constituents. It portrays fundamental focus of this study and research approach. The aim, objectives, and structure of portfolio are described in this chapter. It presents a summary of innovation and list of publications.

1.4.2 Chapter 2: Background of CSP Technology

This chapter presents the key areas of the research and offers the background information essential for the following chapters. It starts with introducing the relationship between wide concept of sustainability, the need for renewable energy and background of concentrated solar power technology. A description of thermal energy storage and direct storage is specified. The challenges of hot corrosion along with approaches to supress hot corrosion are provided. Current advances and limitations in the anticorrosion coatings are discussed and corrosion resistance coatings are proposed for use in direct thermal energy storage systems in CSP.

1.4.3 Chapter 3: Materials and Methodology

This chapter covers the material selection and experimental methodology for the development of coatings. The materials and methods used in this study are described in this chapter. The basic characterisation methods employed are also outlined.

1.4.4 Chapter 4: Results

The summary of corrosion test results obtained during the study are provided. The mass change, thickness, composition and morphology data of the samples exposed to molten nitrate salt at 565^{o}C are included.

1.4.5 Chapter 5: Discussion

A discussion on the gathered data is carried out and compared with previous studies in the literature.

1.4.6 Chapter 6: Conclusions

This chapter sketches the final conclusions including research limitations, reflections and recommendations for future work. Conclusions are depicted together with a viewpoint on the future research. It also presents a summary of innovation and findings, contributions and limitations.

1.5 Innovation

As stated, before the research was conducted as part of FRIENDS^2 project involving a number of academic and industrial partners. The intellectual contributions to knowledge and innovation specifically from my research carried out during the course of this engineering doctorate are listed below.

- Methods for materials selection have been provided. My contribution was down selection of the substrate and coating materials using literature review, database and regression fitting, and the selection of deposition technique using literature review. Selection, development and evaluation of Ni_3Al corrosion resistance coatings is provided for concentrated solar power plant with integrated thermal energy storage.
- Understanding of corrosion behaviour has been provided for bare SS347 and Ni_3Al coating. Experimental analysis demonstrating the growth of corrosion layers on stainless steel 347 has been provided. The corrosion layer growth is not seen in Ni_3Al coated SS347, instead a rapid oxidation within the coating has been observed within first 500 hours of solar salt immersion. The use of Ni_3Al coating to protect stainless steel in presence of molten nitrate salts is demonstrated with potential direct industrial impact. The mass change for Ni_3Al coated SS347 is an order of magnitude lower than bare SS347.

1.6 List of Publications

1.6.1 Internal Reports

Internal reports were submitted as part of FRIENDS^2 project (http://www.friends2project.eu/), to a European portal (https://cordis.europa.eu/project/rcn/194373/factsheet/en) Several deliverables

were accomplished as part of FRIENDS^2 project. This work was part of deliverables D2.1, D2.2, D2.3, D2.4, D4.1, D4.2, D4.3 and D4.4.

- D2.1 Improvement potential of state of the art (SOA) of protective coatings: determination of improvement potential for state-of-the-art protective surface coatings and definition of future research and development (R&D) directions
- D2.2 Simulation results with finite element analysis method (FEM) analysis: report on the simulated results obtained for protective coatings with FEM analysis including optimized parameters (composition, thickness, materials) determined.
- D2.3 Surface engineering of protective coatings: protocol on the preparation of anti-corrosion coatings
- D2.4 Scaling up of protective coatings: report of the scaling up results.
- D4.1 Durability tests: report on the evaluation of the corrosion and degradation processes occurring when the coatings are exposed to high temperatures or corrosive environments (surface protective coatings).
- D4.2 Database of properties of high temperature resistance coatings: database of composition, structure, and optical properties of high temperature resistance solar thermal coatings.
- D4.3 Field tests: report on field tests planned and practiced by staff
- D4.4 Selection of coatings for scaling-up: report about scale-up progress and candidates.

Part of this study was also included as contributions to the annual reports for the FRIENDS^2 project.

- D6.1 Kick off meeting report
- D6.2 Annual report 1st year
- D6.3 Mid-term report
- D6.4 Annual report 3rd year
- D6.5 Final meeting report

1.6.2 Conference Presentations

Conference presentations done during the course of EngD are listed below.

- “Nickel-Aluminide Based Anticorrosion Coatings Prepared by Plasma Spray for Concentrating Solar Power Applications” Materials Research Society Spring Meeting, Phoenix, USA, April 2019 (Oral presentation).
- Manufacturing Doctoral Community PhD Poster Presentation Day, Cranfield, UK, May 2019 (Poster presentation).
- “Nickel-aluminide based anticorrosion coatings prepared by plasma spray for concentrating solar power applications”, European Conference on Nanofilms, Cranfield, UK, March 2018 (Poster presentation).
- “Corrosion resistant coatings for concentrated solar power”, Conference and Student Presentations – Sustainable Materials and Manufacturing Centre for Doctoral Training, London, UK, March 2018 (Oral and Poster presentation).
- “Nickel-Aluminium Based Anticorrosion Coatings Prepared by Plasma Spray for CSP Applications”, Materials Research Society Spring Meeting, Phoenix, USA, April 2017 (Oral presentation).
- 5th Annual Conference of the Centre for Industrial Sustainability, Cambridge University, UK, 2016 (Poster presentation).
- Nickel-aluminium based anticorrosion coatings prepared by Plasma Spray for high temperature industrial applications”, 15th International Conference on Plasma Surface Engineering, Garmisch-Partenkirchen Germany, September 2016 (Poster presentation).

1.6.3 Journal Papers

The following paper has been prepared for publication in surface and coatings technology journal. This will be submitted on 15th July 2020 to the journal.

S. Yasir, J. L. Endrino, E. G. Rodriguez, A. I. Aria, “Suppression of stainless steel 347 corrosion in molten nitrate salts by plasma sprayed Ni_3Al coatings”.

2 BACKGROUND OF CSP TECHNOLOGY

Climate change is a global issue with long term consequences for sustainable development. It is a crucial time to review this climate issue with ensured determination. The world's energy expenditure has been gradually growing and is estimated to continue increasing.[8] Global temperature growth must be limited to 1.5 degrees to reach climate neutrality by 2050.[9] UK is set to decrease greenhouse gas emissions (GHGs) to 'net-zero' by 2050, stopping the UK's part to global warming within 30 years.[10] This could be achieved by attaining sustainable changes to energy, transport and food manufacture industries.[9] There is a need and demand for alternative sources to generate power rather than the conventional burning of fuels due to impact on environment. Development of new technologies enabling use of renewable energy sources has got special attention. Renewable energy sources are those natural reserves that are refilled continually. Sustainability advancements encourage the use of renewable energy that comes from natural resources that include wind, solar, biomass and geothermal.[11]

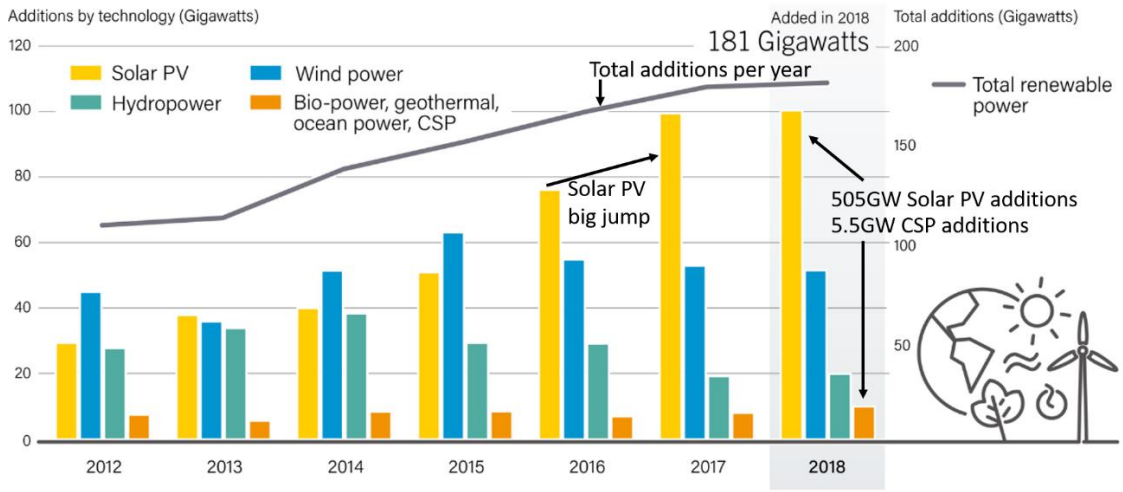

Figure 2: Total annual additions per year of renewable energy including Solar PV, wind power, hydropower, bio-power, geothermal, ocean power and CSP for years 2012-2018. Bar plots are additions by technology and the solid line is total additions of all technologies per year. An addition of 5.5 GW in CSP is observed by the end of 2018.[12]

2.1 Solar Energy for Power Generation

The use of renewable energy is increasing in many individual countries and areas; however, some challenges need to be addressed before further growth. One of the promising renewable energy source is the solar energy, primarily inspired by the enormous energy from the sun.[13] The energy consumption for the entire year on earth can be supplied by one hour of sunlight.[14] Solar energy can be used for power generation through two main technologies concentrated solar power (CSP) or photovoltaics (PV). The CSP technique uses mirrors or lenses to focus sunlight onto a receiver, a heat transfer fluid (HTF) is heated in the receiver. The HTF is used to generate steam to drive a turbine for electricity generation. PV utilises solar cells for direct conversion of solar energy to electricity. After years of stable progression a substantial increment of approximately 181 gigawatts in renewable power capacity has been observed during 2018 (Figure 2).[12] Solar PV increased to 505.5 GW while CSP increased to 5.5GW by end of year 2018 (Figure 2).[15] One of the reasons for this difference could be that direct normal solar irradiation (DNI) is required for efficient operation of CSP plants (Figure 3).[16] The solar energy is not evenly dispersed, DNI is area specific and for this reason CSP technology is used in limited number of countries including China, USA and Spain (Table 1). [11,13,17–21]

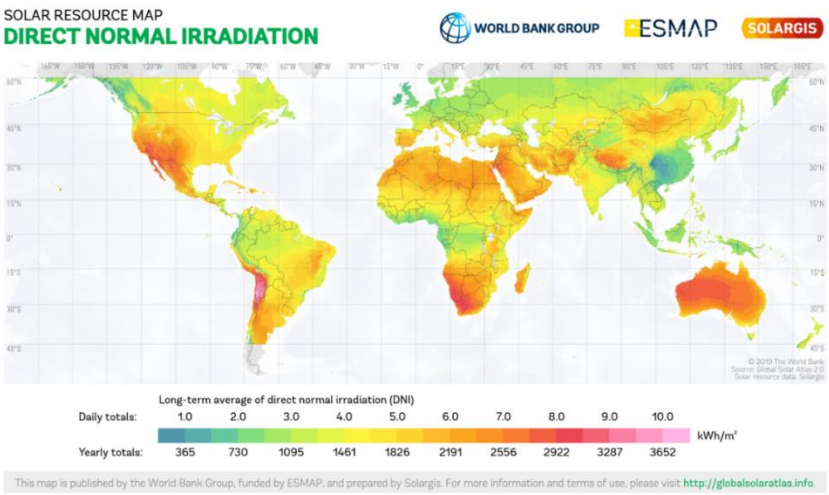

Figure 3: Global solar direct normal irradiation across the world kWh/m², displaying areas with direct normal irradiation in red colour. Direct normal irradiation is needed for efficient operation of concentrating solar power plants.[16]

Table 1: A list of concentrated solar power plants in different counties with thermal energy storage type, storage capacity, heat transfer fluid and expected electricity generation

CSP Plant	Country	Power (MW)	Thermal energy storage	Storage Capacity (hours)	Heat Transfer Fluid	Expected electricity generation (MWh/yr.)	Year	Ref
DEWA	UAE	100	Direct	15	MNS	UD	2021	[17]
Likana Solar	Chile	390	Direct	13	UMS	2800000	2021	[17]
Tamarugal	Chile	450	Direct	13	UMS	2600000	2021	[17]
Aurora Solar	Australia	150	Direct	8	MNS	1800000	2020	[17]
Minos	Greece	52	Indirect	2	MNS	UD	2020	[17]
Copiapó	Chile	260	Direct	14	MNS	500000	2019	[13]
Atacama-1	Chile	110	Direct	17.5	MNS	UD	2018	[13]
Goldmud	China	200	Direct	15	MNS	1120000	2018	[13]

Noor III	Morocco	134	Direct	7	UMS	UD	2018	[17]
Redstone	SA	100	Direct	12	UMS	480000	2018	[13]
Shouhang Dunhuang II	China	100	Direct	11	UMS	390000	2018	[17]
SUPCON	China	50	Direct	7	UMS	146000	2018	[17]
DSG	China	135	Direct	3.7	MNS	628448	2017	[17]
Shouhang Dunhuang I	China	10	Direct	15	UMS	UD	2016	[17]
Crescent Dunes	USA	110	Direct	10	MNS	500,000	2015	[13], [18]
Ivanpah	USA	392	None	UD	Water	UD	2014	[18]
SUPCON	China	10	Direct	2	UMS	UD	2013	[17]
Gemasolar	Spain	19.9	Direct	15	MNS	80000	2011	[13], [18]
PS 20	Spain	20	UD	1	UD	48000	2009	[18], [19]
PS 10	Spain	11	UD	1	UD	23400	2007	[18], [19]
Golden Tower	China	100	Direct	8	MNS	UD	UC	[17]
Hami	China	50	Direct	8	MNS	UD	UC	[17]

Luneng Haixi	China	50	Direct	12	UMS	160000	UC	[17]
Qinghai Gonghe	China	50	Direct	6	UMS	UD	UC	[17]
Shangyi	China	50	Indirect	4	UMS	UD	UD	[17]
Yumen	China	50	Direct	6	UMS	UD	UC	[17]

- MNS –Molten nitrate salt
- UMS – Unspecified molten salt
- UD – Unavailable data
- UC - Under construction

2.2 Environmental Impact of Power Generation Technologies

Solar PV operation is emissions free, however a huge amount of emission is indirectly released in the production process, as number of harmful materials are used for cleansing the semiconductor surface, including hydrochloric, sulfuric or nitric acid, that cause health and safety hazards.[22–30] Silicon-based PV cells involve a lot of energy input in their production, that usually comes from coal.[27] Wind energy is considered a clean, sustainable and emission free, however, it can contribute to noise pollution caused by airflow and movement of mechanical parts of turbine, which can affect the scenery and can cause damage to flying wildlife.[31–39] CSP has much lower environmental impact compared to other power generation plants as no fuel is used and there is no risk of oil or methane leakages.[40] CSP becomes dispatchable with integration of TES, making them of higher value than other power generation technologies.[40–46] The energy can be stored rather than distributing it and can be released on demand. Dispatchability is significant to supply power through the grid on demand.

Nevertheless, solar energy is intermittent.[11] The solar irradiation is available for a limited amount of time throughout the 24 hours. Also, the amount of solar energy that can be used for power generation depends on seasonal and weather changes significantly. There is a spread of normal irradiation, low solar radiations and cloud cover throughout 24 hours, resulting in discrepancy between demand and supply. The discrepancy between demand and supply of solar PV generation is demonstrated using duck chart representing twenty-four hours variable electricity demand in California, with no energy storage system (Figure 4).[47] A high demand and low power generation exists early morning, while during sunny afternoons demand is low and solar generation is high creating a potential over generation.[48] Energy storage is required to balance the differences in the demand and supply and to flatten the duck curve. The energy can be stored and distributed when demand is high, instead of distributing it all the time. For continuous power generation, a reasonably priced and consistent energy storage method is required.[14,49]

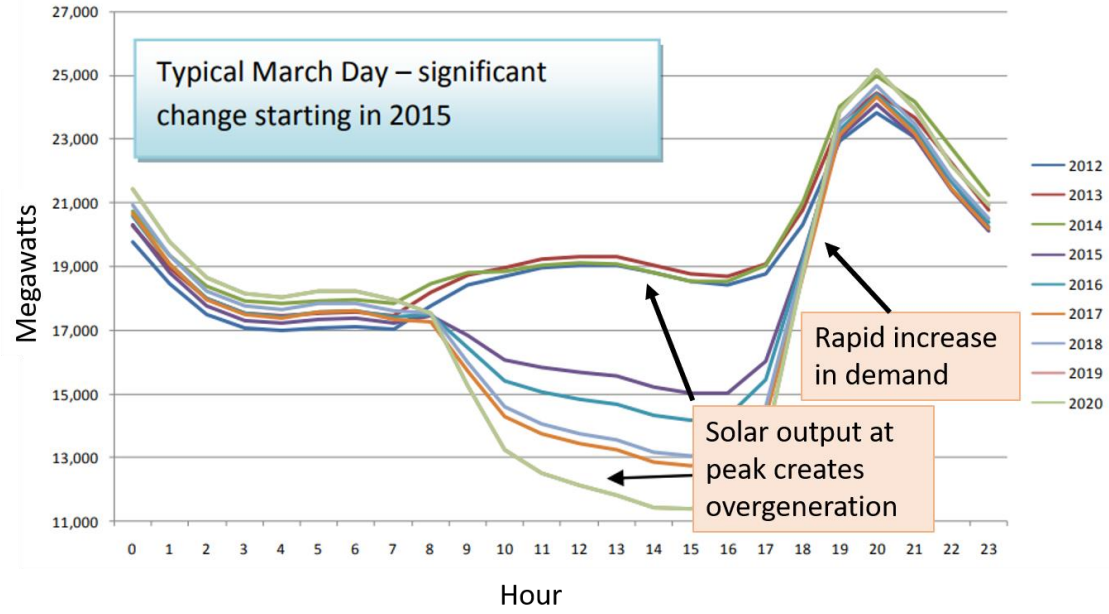

Figure 4: The duck curve presenting the mismatch of energy between demand and supply for a typical March day in California (without energy storage capacity). An average of about 20,000-megawatt power transported in the grid for 24 hours of a day. Overgeneration from solar PV during the middle of the day and rapid increase in demand during hours with no solar irradiation is revealed in the plot highlighting need for energy storage. The use of TES can remove the discrepancies in the curve.[47]

2.3 Energy Storage

One of the key features in CSP plants is the capacity for integrated thermal energy storage. There are four commonly used CSP technologies available at present including parabolic trough collector (PTC), linear fresnel reflectors (LFR), parabolic dish collector (PDC) and central receiver tower (CRT) (Figure 5).[4,50–54] Solar PV stores energy as electrochemical storage in batteries. Batteries have environmental effect during production, utilisation, storage, operation, removal and recycling.[55] Some metals and non-metals included in battery production can jeopardise human health by toxic exposure to Pb, Cd, Hg, As and Cr.[55–62] CSP systems are capable of storing energy as thermal storage. The thermal energy storage leads to overall efficiency, enhanced reliability, improved economics, operating costs, and reduced environmental pollution with less carbon dioxide

(CO_2) emissions.[63] The capability to store heat permits CSP plants to produce electricity during the periods of cloud cover and low solar radiations.[64] CSP plants with big storage capabilities could produce electricity throughout day and night. The capability of TES integration in the CSP plants makes it more appealing than other renewables technologies because of its high practicality and proficiency commercially.[65]

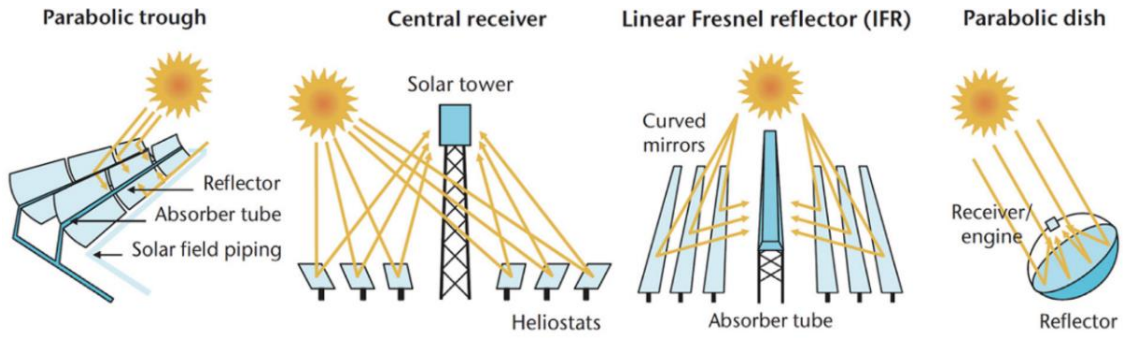

Figure 5: Schematic of four different available CSP technologies: Parabolic trough, central receiver, linear Fresnel reflector and parabolic dish.[50]

2.4 Thermal Energy Storage

Thermal energy could be stored in the form of chemical heat storage, latent heat storage or sensible heat storage.[66] Chemical heat storage has the highest storage capacity, but it is restricted by the need for complicated reactors to carry out specific chemical reactions.[67] Phase change materials used as latent heat storage have limitations because of material compatibility and high cost.[63] Sensible heat storage is industrialised and low cost technology. Sensible heat storage materials can be solid state or liquid state. Some of the frequently used solid state thermal storage materials include sand-rock minerals, concrete, ferroalloys and fire bricks. These materials have working temperatures ranging from 200^{o}C to 1200^{o}C, possess high thermal conductivities and are low-cost. Some of the frequently used liquid state thermal storage materials include oils, liquid metals and molten salt. The molten salt as one of the most suitable materials for use in solar power plants is selected because of excellent thermal stability at high temperatures and heat storage capacity.[15,55,63,68–82] Some of the main requirements for storage material are material compatibility, high thermal

storage capacity, high heat transfer capability, specific heat, latent heat, viscosity and cost.

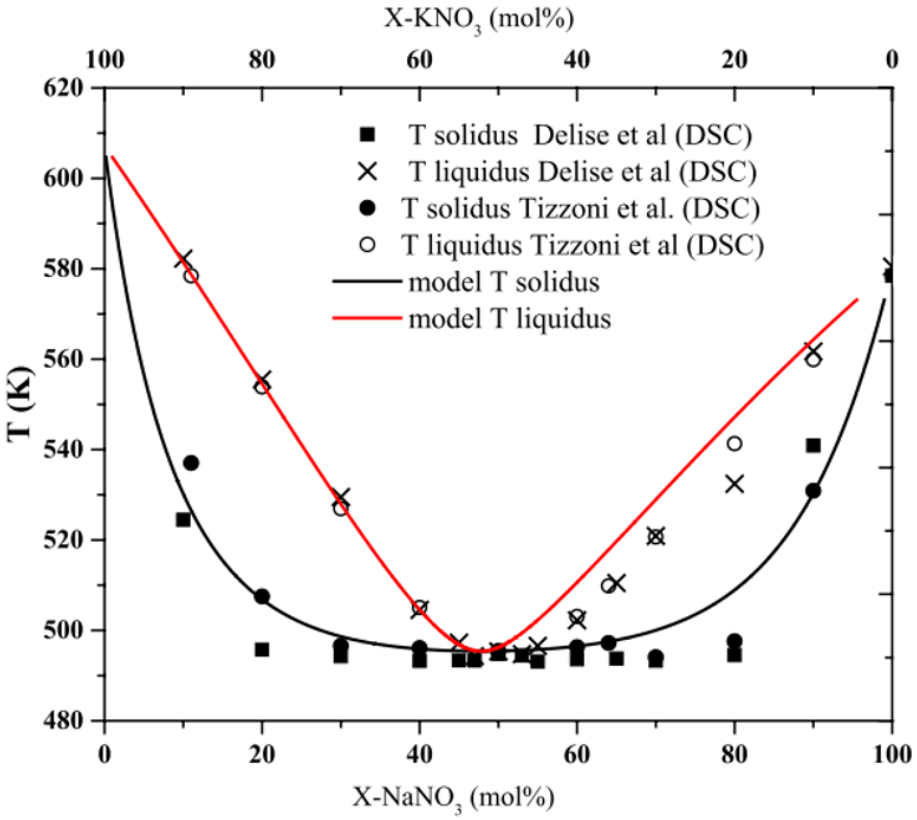

Figure 6: $NaNO_3$–KNO_3 phase diagram, comparison between the model (line) and experimental data (dots). The calculated equilibrium curves are plotted along with the experimental data. Very small deviations of about 4 K can be observed.[83]

Heat transfer fluid could also be used as thermal energy storage medium for carefully chosen material (Table 2). In direct storage systems, same material is used for thermal energy storage and heat transfer fluid, thus avoiding heat transfer loses and boosting efficiency. While in Indirect storage systems, different materials are used for thermal energy storage and heat transfer fluid.[84] In direct storage system, same material is not essential to be used as HTF and TES. But in this study, the scope is limited to one material being used as both TES and HTF. Direct storage avoids heat transfer losses and boosts efficiency. The most commonly used material for energy storage is molten salt.[66] A feasible medium for TES and HTF in concentrating solar power towers, is a molten salt with low melting point, high temperature stability low vapour pressure, low viscosity and

high thermal conductivities.[17,86] One of the mostly used salt is molten nitrate salt. Molten nitrate salt are non-flammable with high thermal stability and high density,[71] low vapor pressure,[87] lower melting temperature and low cost as compared to chlorides and carbonates. The molten nitrate salt mix, 60wt% $NaNO_3$ + 40wt% KNO_3 known as solar salt is stable, with sufficient heat storage and transfer capability and low melting point.[88–90] A sum-up of a few phase diagrams for binary solar salt mix is presented in Figure 6.[83,91–99] The minimum melting point has been measured to be close to 220°C for a mixture of 50mol% $NaNO_3$ + 50mol% KNO_3,[91,96,97] which is to 46wt% $NaNO_3$ + 54wt% KNO_3 based on literature. The melting point for (64mol% $NaNO_3$ + 36mol% KNO_3) or (60wt% $NaNO_3$ + 40wt% KNO_3) salt mix is 221ºC. The melting point for solar salt used in this study is not eutectic, its melting point is slightly higher than the minimum melting point. This salt was chosen because it is much more economical than the eutectic mix.[97,100] Solar Salt (60wt% $NaNO_3$ + 40wt% KNO_3) is used as HTF and TES in this study.

2.5 Molten Salt Corrosion in CSP Plants

Regardless of the clear advantages of using molten salt as HTF in CSP plants, one of the challenges associated with molten salts is corrosion at elevated temperatures.[100–106] The term hot corrosion is usually employed to describe the accelerated degradation of materials induced by molten salt at an elevated temperature.[107] Corrosion occurs naturally as the decay of a material or its properties due to reaction with surroundings. Corrosion in molten salt can result both from oxidation of the base metal and solubility-driven dissolution reactions.[108] The compatibility of piping and container in contact with molten salt is a big issue. The selection of material for different components depends on working temperature. Figure 7 illustrates a typical central tower plant with TES using a two-tank molten salt configuration. From the cold-salt tank (290ºC), the salt is pumped to the tower receiver and heated up to 565ºC, to be stored in one hot-salt tank (565ºC). There are several examples of plants using this technology as for example Atacama (Abengoa)[109] and Torresol (Sener).[17]

Table 2: Advantages and limitations of different HTFs.[110]

HTF	Advantages	Limitations	Ref
Molten salts Solar salt	Solar salt has high heat capacity and low cost allow for direct thermal storage, non-toxic, non-flammable.	Solar salt has upper temperature limit is roughly 600^{o}C, high melting point, around 220^{o}C for solar salt.	88
Air	Well-known, non-expensive, extensive temperature range, direct cycle is possible.	Limited heat transfer, large pumping power, indirect storage needed.	111
Water / steam	Well- known, non-expensive, direct cycle is possible.	Limited temperature range, high pressure required for direct cycle, direct storage only in small scale, indirect solution is required for larger systems.	14
Liquid metals Na, PbBi	Na is stable up to 833^{o}C, low reactivity and cost. PbBi is stable up to 1670^{o}C, low melting point 125^{o}C, inert in air and water.	Na is highly combustive in water. Lead is toxic.	112–115

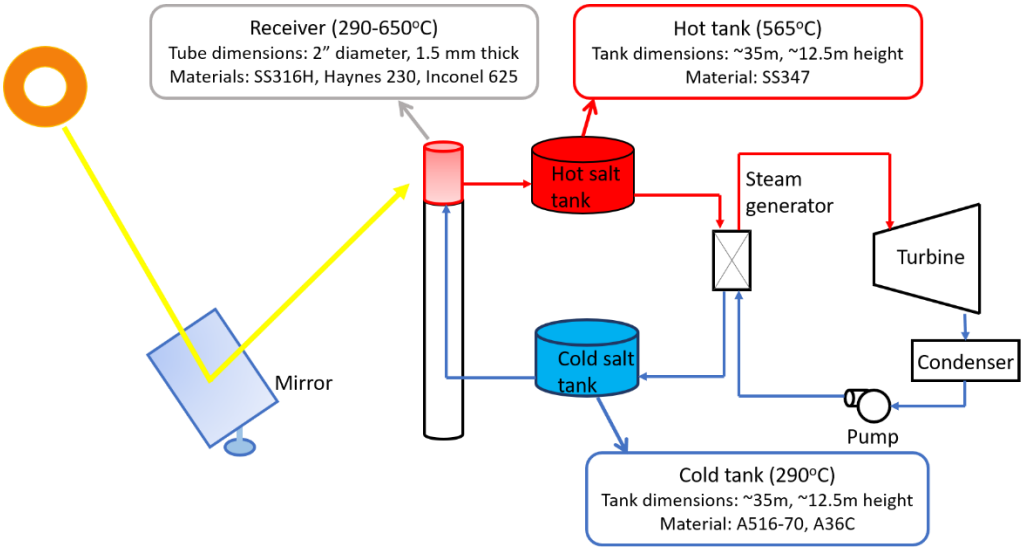

Figure 7: Central tower CSP plant with two tank direct molten salt storage, steam generator, turbine, condenser and a pump. The solar radiation is concentrated on the receiver at top of central tower by programmed mirrors. Heat transfer fluid is heated, stored in hot salt tank, and is used to generate steam when required. The hot salt tank and connected components are hotspots for corrosion due to molten salt.

2.6 Current Corrosion Suppression Strategies

In order to suppress corrosion, several strategies have been explored (Figure 8). The commonly used solution is to use thicker walls as it would extend the lifetime operation of the material. However, it does not solve the corrosion issue and may not be applicable for components with fixed dimensions or tight tolerance.[116] The use of high purity salt to avoid corrosion aggravation from impurities like chloride and water has been proposed but not widely implemented due to higher costs.[116–118] Nickel-based superalloys have also been recommended, as they provide high temperature stability and resistance for molten salt corrosion compared to iron-based alloys.[116,119,120] However, they are significantly more expensive as compared to structural stainless steel.[119,120]

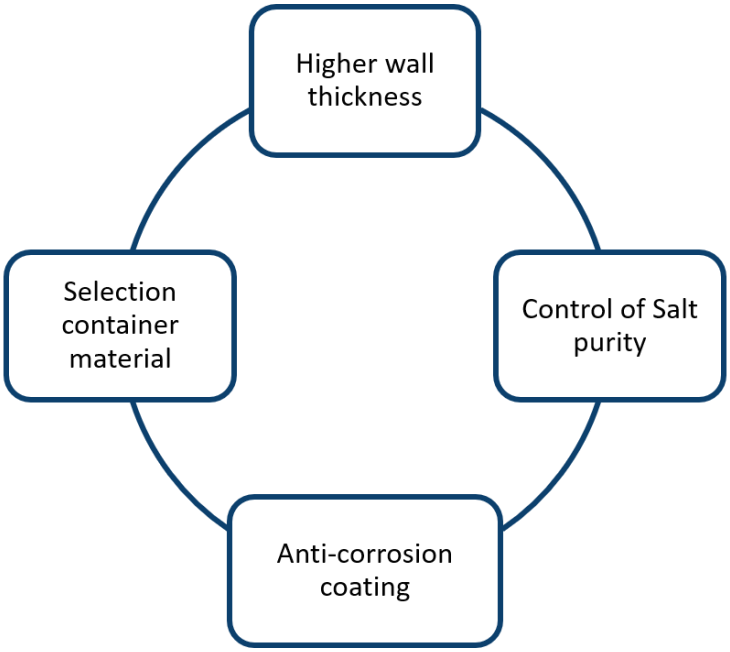

Figure 8: Current corrosion protection strategies used for molten salt TES in CSP. Higher wall thickness, use of high purity salt, selection of specialised alloys is among the different strategies currently employed for corrosion suppression. Anti-corrosion coating is attractive because corrosion protection of coating can be used with structural properties of substrate material.

2.7 Proposed Corrosion Resistant Coatings for TES

Among various strategies employed to supress corrosion in CSP plants, one of the solutions is to apply protective coating layer to the substrate (Figure 8, Table 3).[121] The use of corrosion resistant coatings has been considered as the most viable solution.[120,122–124] Coating techniques such as physical vapour deposition and plasma spraying provide barrier to suppress corrosion while maintaining the structural stability of substrate material.[125] Corrosion resistant coatings for thermal energy storage components, in presence of molten nitrate salt, should be able to achieve degradation rates lower than 30 µm/year as the normal lifespan of CSP plants is 30 years.[126,127] Although corrosion rate for SS347 has been measured to be 4-13 µm/yr, it is one of the high cost specialised alloy. The aim of corrosion resistance coatings is to provide protection to all substrates so that a low-cost stainless-steel substrate can be used with the coatings for thermal energy storage container. The hot tank wall with stainless steel can offer

degradation rates lower than 30 µm/year, depending on the wall thickness. Usually a 3mm corrosion allowance is added to the tank walls,[128] with a minimum wall thickness of 6mm.[129] The suppression of corrosion is more difficult in tubing, pipes, pumps and heat exchanger due to dimensions. The need for excessive use of material could be avoided by using corrosion resistant coating. The following factors need to be taken into account while choosing coating material suitable for use in molten nitrate salt environment:

- The coatings to be used should necessarily own a capacity to form a steady, slow-growing, passivating surface oxide.
- The coatings should have good adhesion and metallurgical stability in contact with the substrate. The chemical potential of elements in the coating and substrate should differ to only a slight extent; otherwise, excess phases, often with unfavourable morphologies, form under the coating and act as stress concentrators and crack initiators.[130]
- They should have microstructural strength to keep their protective properties for prolonged service life, at high temperatures. They should also have resistance to developing cracks or fractures to preserve coating strength when under the influence of thermal and mechanical stresses.

Table 3: Selection of nickel aluminide coatings prepared by plasma spray deposition

Material	Substrate	Technique	Test	Ref
Ni_3Al	Steel	Plasma spray	___	[131]
Ni_3Al	Boiler steels	Plasma spray	Tested for corrosion in industrial thermal plant boiler	[132]
Ni_3Al	Boiler steels	Plasma spray	Molten salt (Na_2SO_4-60%V_2O_5) at 900°C for 50 cycles.	[133]
Ni_3Al	Fe superalloy	Shrouded plasma spray	___	[134]
Ni_3Al	Steel	Shrouded plasma spray	Oxidation test at 900°C for 50 cycles	[135]
Ni_3Al	Mild steel	APS	___	[136]
Ni-5wt% Al	Steel	APS, HVOF	Microstructure and residual stress	[137]
Ni-5wt% Al	___	APS, HVOF	Oxidation and microstructure evolution during deposition	[138]
Ni85% Al15%	Stainless steel	Plasma spray	Micro hardness, adhesion strength and porosity of the coatings were measured and compared	[139]

3 MATERIALS AND METHODOLOGY

The experimental work for this study was conducted to evaluate the corrosion behaviour of Ni_3Al coated SS347 samples on exposure to molten nitrate salt at 565°C. The methodology used for selection of substrates, coating materials and coating deposition along with coating characterisation in this study are described in detail in submission 3 (Protocol of surface engineering and assessment of protective coatings).

3.1 Material Selection

To select a suitable candidate for corrosion resistant coating, a database of high temperature resistant coatings, and corrosion resistance of alloys was compiled. That was followed by linear regression fitting, corrosion rate prediction and literature review conducted to identify the - state - of - art for corrosion resistance coatings in molten nitrate salt (Figure 9). Details on these can be found in submission 1 (Literature Review) and submission 2 (Database of Properties of High Temperature Corrosion Resistance Coatings). A summary of coating material selection is provided here.

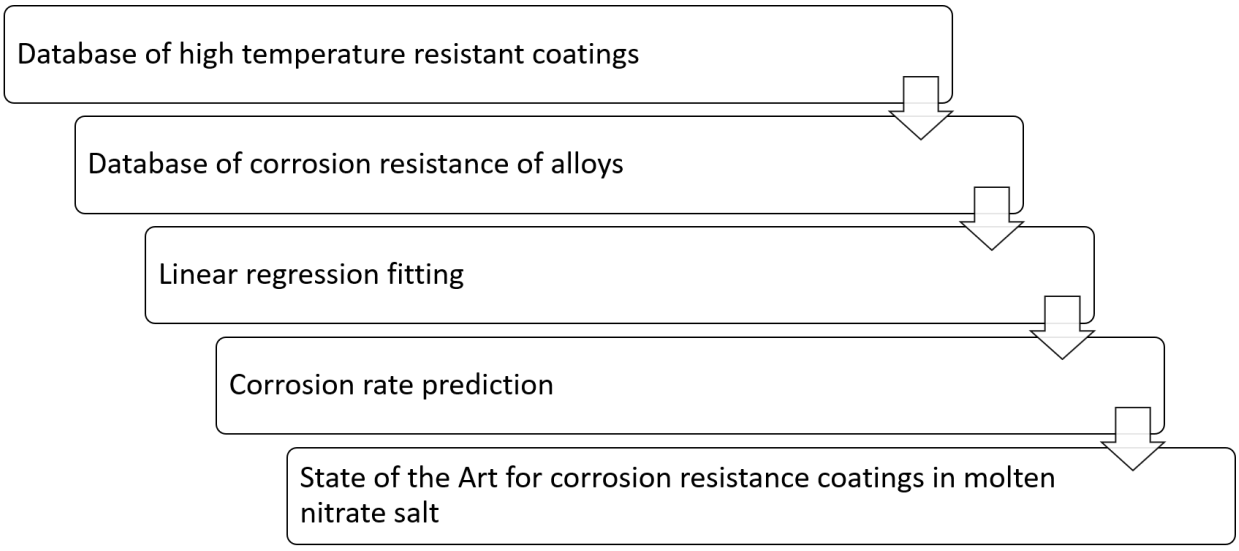

Figure 9: Flow chart of material selection process including database of high temperature resistant coatings and alloys, linear regression fitting, prediction of corrosion rate and state of art for corrosion resistance coatings in molten nitrate salt

3.1.1 Constraints for Material Selection

This research was conducted as part of FRIENDS[2] project in collaboration with academic and industrial partners, some constraints were setup according to current standards used by industrial partners, as listed below.

- Solar salt is the TES medium for this study. It is commonly used as thermal energy storage in CSP plants due to its properties mentioned in section 2.1 as well as low cost and availability.[100,105,140] This salt is being used in Andasol – Spain, Atacama – Chile, Aurora solar – Austrailia, Casablanca – Spain, Crescent Dunes - USA, Copiapo – Chile, Delingha – China, Gemasolar – Spain, Golmud – China, Noor III – Morocco, Solana - Arizona.[13,17,18,141,142] This specific salt is used to ensure that the test condition is the actual condition of TES in order to understand the behaviour of materials in real life situation. Hence the selected material for the container should be compatible with molten nitrate salt, to minimize the corrosion progression. Standard 98% purity solar salt will be used.
- The typical working temperature of hot salt storage tank in CSP central tower plant is 565^{o}C (Figure 7).[140] An accelerated test can be conducted at higher temperature however, the solar salt will not be suitable because of decomposition temperature of 565^{o}C. The corrosion tests will be conducted at 565^{o}C for this study. The selected material should be stable at 565^{o}C.
- The proposed solution has to be scalable. A 300 MW plant with 8 hours storage requires ~ 22,500 metric tons of molten salts and salt container of size ~ 35 m diameter, ~ 12.5 m height. The selected materials and the coating deposition technique should have the capability to be scaled up to this size.
- Container material cost for the above-mentioned dimensions is ~ £ 1.7 M with 15 mm thick SS347 wall. If, however the wall thickness is doubled to provide corrosion allowance as mentioned as one of the strategies for corrosion suppression the material cost will also be doubled to ~ £ 3.4 M. The container material cost with the use of selected coatings, should not exceed the cost of double wall thickness with SS347.

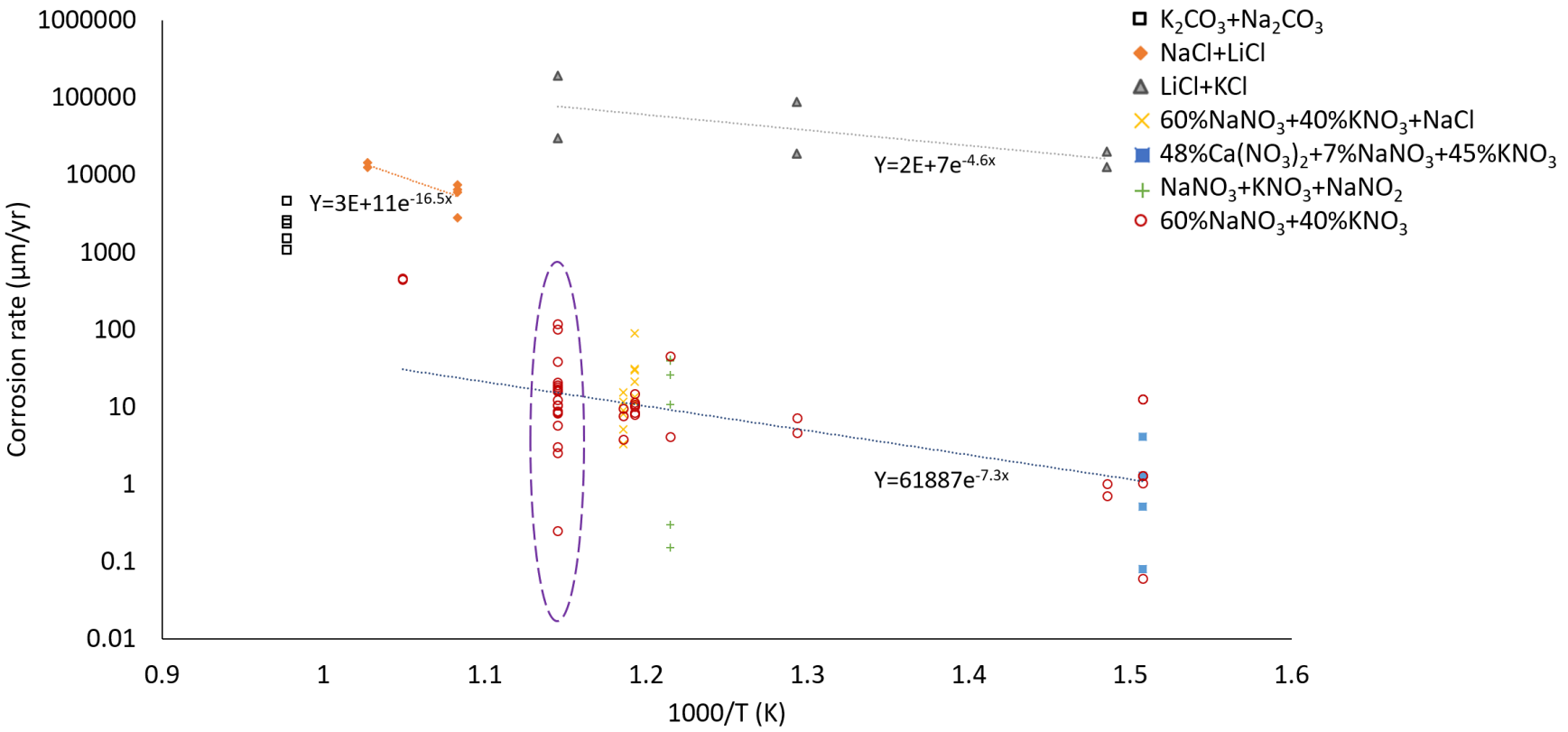

Figure 10: Corrosion rate of stainless steels, iron and nickel alloys in presence of various molten salt at 390°C to 680°C. Corrosion rate varies significantly at any single temperature. There is a three orders of magnitude variation in corrosion rate for molten nitrate salt (60wt% $NaNO_3$ + 40wt% KNO_3) at 600°C (dotted outlined).

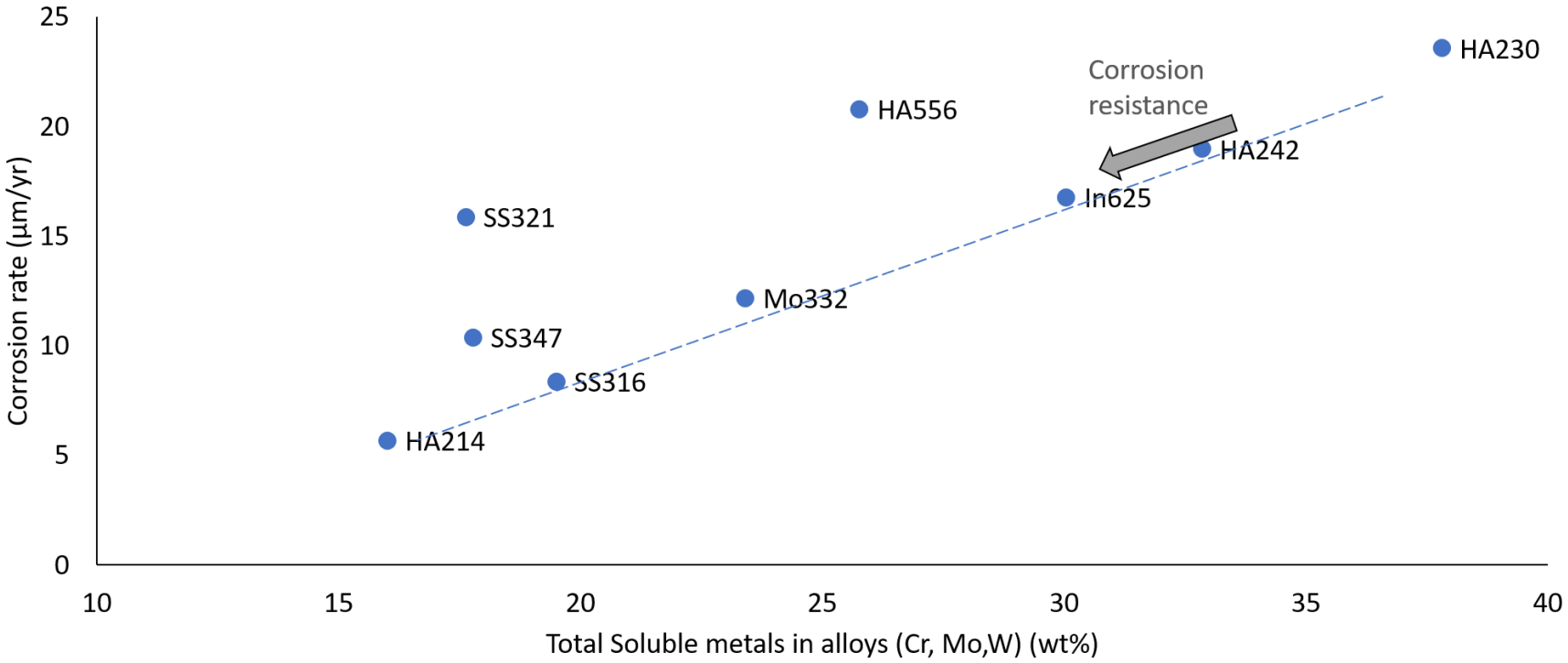

Figure 11: Corrosion rate of various alloys plotted as a function of total soluble metals in molten nitrate salt environment at 600°C. There is dependency between corrosion rate and elemental composition of alloy.

3.1.2 Substrate Material

It is worth mentioning that CSP components are mostly made of high temperature iron-based alloys such as stainless steel.[143] These alloys are typically used for heat exchange components and thermal energy storage systems. These are preferred because of exceptional strength, creep resistance at high temperature, low corrosion rates in molten salt and lower cost compared to Ni based alloys. SS347 contains niobium, which overcomes the problem of carbide formation during weldability due to presence of carbon in some stainless steel.[144] Stainless steel (SS), precisely SS347 is selected as based on the literature review in submission 1 (Literature Review) and the linear regression presented in submission 2 (Database of properties of high temperature corrosion resistance coatings).

3.1.3 Database of High Temperature Resistant Coatings

A database for high temperature resistant coatings used in various molten salt environments at high temperature was compiled. In a number of cases, MCrAlY as bond coat has been used with some topcoat for protection in molten salt at high temperature.[121,124,145–154] MCrAlY provides oxidation and corrosion resistance owing to formation of Al_2O_3 and Cr_2O_3. MCrAlY bond coat avoids thermal mismatch at high temperature between the topcoat and substrate.[121,145,147,148,150,155–157] Ni-Cr coatings have been found to provide protection in sulphate vanadate salt environment at 900^{o}C. The oxidation and corrosion resistance was attributed to formation of $NiCrO_2$.[124,158,159] Ni-Al has been found to provide oxidation resistance due to formation of continuous, compact and fully adherent Al_2O_3.[131,160–163] However, Cr gets dissolved in nitrate salts making MCrAlY or Ni-Cr incompatible solution.[101,103,105,120,164–167]

3.1.4 Database of Corrosion Resistance of Alloys

Corrosion resistance of various alloys was plotted as a function of temperature to understand the behaviour for different molten salt environments (Figure 10). A big variation in corrosion rate is observed at any single temperature. In case of molten nitrate salt at 600^{o}C, three orders of magnitude variation in corrosion rate

was noticed. To further grasp this variation corrosion rate was plotted for various alloys in molten nitrate salt at 600°C, as a function of total soluble metal in alloys (Figure 11). A dependency between corrosion rate and elemental composition of alloy was revealed in the plot (Figure 11).

3.1.5 Poisson Regression Fitting

The dependency between corrosion rate and elemental composition was used for linear regression fitting. A regression analysis was used for prediction of corrosion performance of alloys in corrosive molten nitrate salt environment at elevated temperature. The starting point of the regression model is measured corrosion rate values based on previous corrosion behaviour in literature.[143] Poisson regression can be applied in case of count data of independent events, corrosion rate can be interpreted as a count, from zero to infinity, of corrosion events per unit time with each event independent to each other. An offset, denoted herein as Log CR_0, is required to allow Poisson regression of rate data instead of the count data itself (Equation (3-1)). The Poisson regression fitting provides a relationship between the calculated corrosion rate and the relative amount of elemental metal alloy as follows:

$$Log\ CR = \sum_{\alpha=1}^{n} C_\alpha A_\alpha + Log\ CR_o \qquad \textbf{(3-1) Regression fitting}$$

where

C_α = The regression coefficient for each element in alloy

A_α = The percentage amount of each element in alloy

n = Number of elements to be considered

CR = Corrosion rate per unit alloy

CR_o = A constant with value corresponding to the Percentage composition of all considered elements per unit alloy

In this study, the number of elements considered (n) is 12, which includes Fe, Ni, Co, Mn, Cr, Mo, W, Al, Si, Ti, Nb and others, as these are the elements known to be constituent of Fe-based alloys and Ni-based alloys. Any additional elements, other than Fe, Ni, Co, Mn, Cr, Mo, W, Al, Si, Ti and Nb, in alloy are included in others elements category. The regression fitting (equation (3-1)) is able to replicate the experimental measured values from literature (Figure 12).

A dimensionless coefficient is assigned to each elemental constituent of alloy, as a solution of regression fitting model (Table 4). Elements with positive fitting coefficients corelate positively to corrosion while negative fitting coefficients corelate negatively to corrosion. This suggests that the elements with positive fitting coefficients contribute physically to the corrosion while elements with negative fitting coefficients contribute in supressing the corrosion. The larger values have stronger effect on corrosion compared to smaller values. A best alloy composition to minimize corrosion can be achieved, by using elements that corelate negative and avoiding elements that corelate positive to corrosion. The corrosion can be minimized by using an alloy comprising of large percentage of elements with negative fitting coefficient and small percentage of elements with positive fitting coefficients.

Ni with a positive fitting coefficient contributes towards corrosion in pure solar salt, however in presence of chloride or nitrite impurities it behaves differently with negative coefficient. Fe contributes towards corrosion in pure salt as well as salt with chloride impurities. Cr does not promote corrosion for pure salt but with impurities it contributes towards corrosion, same is the case with Mn. Mo seems good with impurities but not good with pure salt, while Al suppresses corrosion for pure salt and with chlorides but behaves neutral in salt with impurities. A combination of Ni and Al seems best as Ni suppresses corrosion in presence of chloride or nitrite impurities and Al supresses corrosion in case of pure salt (Table 4). The linear regression fitting makes it possible to predict corrosion behaviour of various alloy compositions with help of corrosion rate values (Table 5). This linear regression fitting is able to replicate the experimental test results found in literature (Figure 12). The predicted corrosion rate values are in agreement with

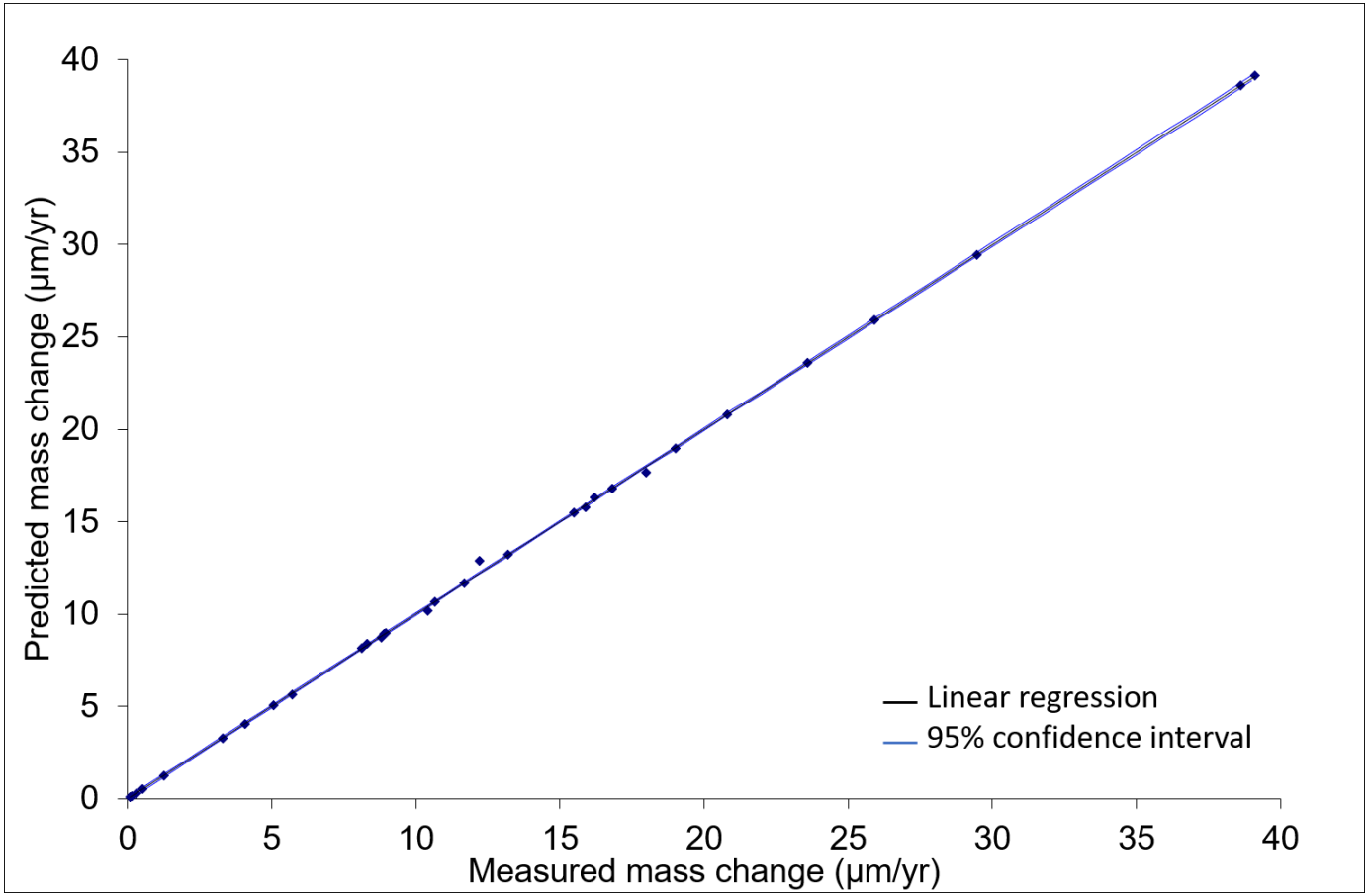

Figure 12: Measured corrosion rate from literature plotted versus predicted corrosion rate calculated using the regression fitting for molten nitrate salt (ref. [100,105,143,164,168–172]). The solid line is linear regression, dotted line is 95% confidence interval. The predicted values are in good agreement with the measured values.

Table 4: Table of coefficients assigned to different elements, the elements with positive fitting coefficients corelate positively to corrosion while negative fitting coefficients corelate negatively to corrosion. The larger values have stronger effect on corrosion as compared to smaller values

Test Conditions		Fitting coefficients for different elements											
Molten Salt	Temp (^oC)	Co	Ni	Fe	Mn	Cr	Mo	W	Al	Si	Ti	Nb	Other
60%$NaNO_3$+40%KNO_3	600	0.02	0.03	0.03	-0.65	0.03	0.03	0.04	-0.41	0.69	2.09	-0.23	0.87
60%$NaNO_3$+40%KNO_3+ 1%NaCl	570	0	-0.12	0.02	0.01	0.12	0.04	0	-0.03	0	0	0	0
$NaNO_3$-KNO_3-$NaNO_2$	550	0	-0.92	-0.01	3.15	0.39	-1.38	0	0	0.63	0	0	7.76

Table 5: Corrosion rate for various possible combinations of Ni and Al, using the linear regression fitting for solar salt at 600ºC

Alloy	Corrosion rate (μm/yr)
SS 347	10.7
Ni	27.6
Al	0
NiAl	0
$NiAl_3$	0
Ni_2Al_3	0
Ni_3Al	0

the measured values from literature with a few outliers.[100,105,143,164,168–172] The reason for outliers could be discrepancy in composition or change in structural properties of alloy as the regression fitting is based on elemental composition and does not take into account any changes in the structural properties of the alloy.

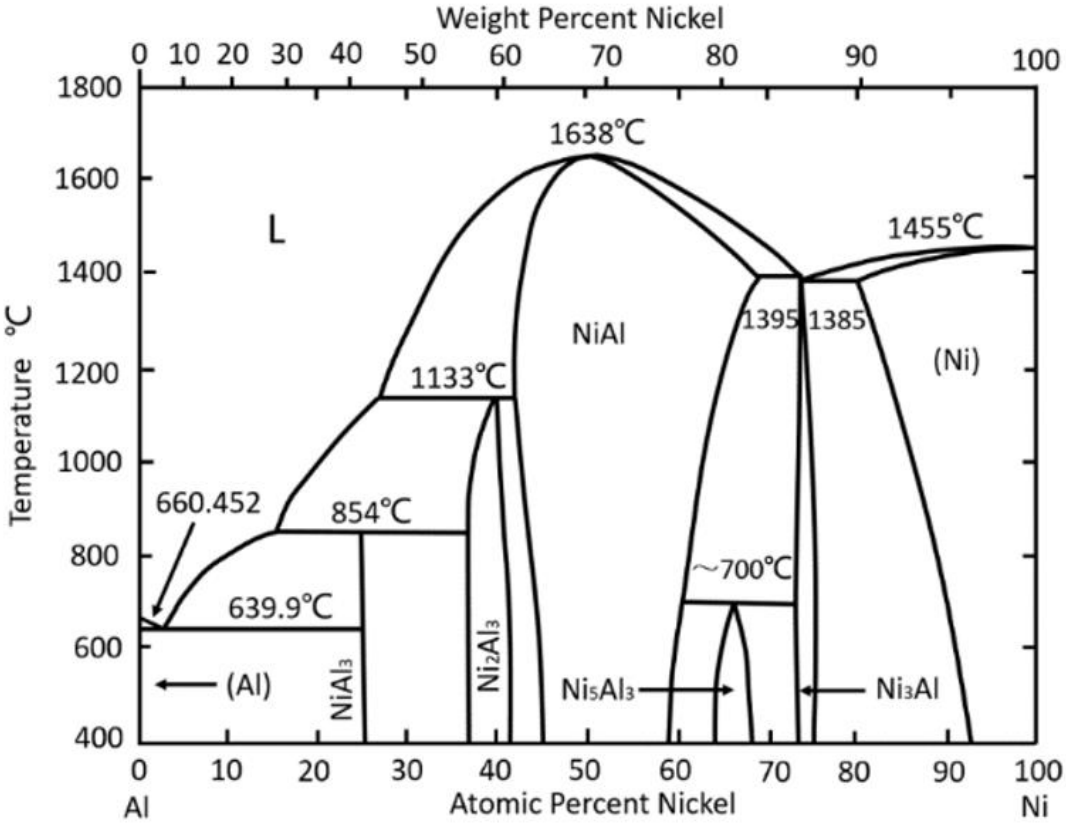

Figure 13: Binary phase diagram of Nickel Aluminium system.[173]

3.1.6 Selected Corrosion Resistant Coating for Molten Nitrate Salt

Due to large variation in operational temperature, it is best practice to match the thermal properties of the coating with substrate material, to minimize cracking or spallation with temperature change.[167] For stainless steel substrate, commonly used in TES, the most suitable coating material would ideally be Fe-based, Cr-based or Ni-based. Cr-based material forms a slow growing chromium oxide under oxidising environment. However, it has a high solubility in solar salt.[101,103,105,120,164–167] Ni-based coating is preferred over Fe- based because of

its ability to form protective oxide layer whilst Fe oxide is non-passivating.[106] Ni-base alloys are much more resistant to molten nitrate corrosion than iron-base alloys. It has been reported that increasing Ni concentration improves resistance to molten nitrate corrosion in Ni- base alloys. Ni-based coatings have been reportedly used to provide wear, oxidation and hot corrosion resistance in ash and flue gases inside coal-fire boiler.[134,174] Aluminide coatings provide corrosion resistance to molten nitrates and carbonates salts. Among many potential different combinations of Ni-based coatings, $NiAl_x$ are favoured because of their strong adhesion, high thermal conductivity, attractive stiffness, good oxidation resistance and metal-like electric conductivity.[136,175] Nickel Aluminides perform well by combining high temperature strength with oxidation resistance. Nickel aluminide in the form of Ni_2Al_3 coatings showed very low mass changes after 1000 hours immersion in solar salt at 580ºC.[120] Nickel aluminide in the form of NiVAl has been used, reporting a mass change of 0.11 nm/h after 2000 hrs immersion in solar salt at 500ºC, reducing the mass change by more than two orders of magnitude as compared to uncoated high temperature $9Cr^{-1}Mo$ (Grade P91) steel.[116] The Al_3Ni, Al_3Ni_5 and Al_3Ni_2 have lower melting points of ~640°C, ~700°C and ~1133°C respectively, and therefore not suitable in high temperature environment (Figure 13).[176] The possible high temperature candidates are NiAl, and Ni_3Al with melting points of ~ 1638°C and ~ 1385°C respectively (Figure 13). A minimum amount of aluminium is required to form continuous oxide on oxidation, minimum amounts of 25%, 30%, and 35% aluminium have been suggested in literature to form a continuous oxide.[108,177–179] For this study the amount of aluminium is proposed to be such as to avoid brittleness upon oxidation and to be able to form a continuous oxide. Using large concentrations of Al reduce the melting point, and compromises creep strength hence its percentage needs to be limited. Aluminium content has been suggested to be kept below 6% to avoid brittleness after oxidation.[101,123] Among NiAl, and Ni_3Al phases of nickel aluminide, Ni_3Al appears be a good candidate because amount of Al is low enough to prevent brittleness after oxidation.[101] Ni_3Al coating was effective in decreasing the mass gain to about one-third as compared to uncoated Fe-based superalloy in molten salt (Na_2SO_4 – 60%V_2O_5) at 900ºC.[124] The Ni_3Al

coating have been effectively used in coal-fired boiler at 450^{o}C, 900^{o}C and $NaNO_3$-(KNO_3)-Na_2O_2 molten salt at 650^{o}C.[101,180,181] Numerous studies on Ni_3Al coatings and their corrosion resistance in different high-temperature atmospheres have been reported in the literature. However, long term corrosion behaviour of Ni_3Al coatings has not been investigated in realistic solar salt TES environment.

3.2 Methodology for Deposition

The methodology used for coating deposition method along with coating characterisation used in this study are described in detail in submission 3 (Protocol for Surface Engineering and Assessment of Protective Coatings), a brief description is provided as follows.

3.2.1 Deposition Technique Selection

Coatings can be tailored for a specific application by controlling their elemental composition, their microstructure, and by selection of deposition process. The deposition technique for coatings need to fulfil the following criteria.

- Deliver high density coatings (porosity < 10 %) to act as a barrier for inward or outward diffusion of elements.
- Provide thickness control to deposit thick enough coating (> 100 µm) to shield the inward or outward diffusion of elements.
- Deposit coating with good bond (adhesion strength > 20 MPa) with the substrate to avoid spallation with changing temperature.
- The coating deposition technique should have the capacity for scale up
- The deposition rate should be high enough (> 2 kg/hr) to enable lower labour cost.
- The deposition efficiency should be high (> 60 %) to minimize waste material.
- The deposition technique should not have bad impact on environment in form of CO_2 or harsh by-products.

3.2.2 Review of Deposition Techniques

A number of coating technologies were considered in comparison to the criteria mentioned above. The sol gel and electrodeposition do not provide good adhesion between coating and substrate because they are both low energy processes.[182,183] Thick coatings can be achieved using these methods. Dense coatings can be achieved by post heat treatment however it imposes size limitation by oven size or vacuum chamber requirement, hence making it difficult to scale up. The popular physical vapour deposition (PVD) methods are sputtering and evaporation. The PVD sputtering is line of sight process, keeping material cost low. However, material consumption is high because the target cannot be deposited after certain usages.[182,184,185] This method is not readily scalable due to size limitation by chamber capacity. PVD evaporation process requires high vacuum, making it high cost method.[184,185] Tabular coating structure is deposited using this process, tabular structure does not provide corrosion protection. This process is not easily scalable due to size limitation by chamber capacity. Chemical vapour deposition (CVD) method has high vacuum requirement which also makes it high cost method.[182–187] The coatings deposited using plasma spray are not dense enough as deposited by PVD or CVD processes but are of acceptable density. Plasma spraying is versatile (can be used with a variety of substrate and coating material), adaptable (can be used in low vacuum mode or in atmospheric pressure) cost effective (does not require high vacuum system or clean system), has high deposition rate and deposition efficiency (distance between spray gun and substrate is comparatively low), less environmental impact and more importantly it is easy to scale up.[121,182,188–190] This method has capacity for scaling up effortlessly as it does not require an enclosed chamber. The plasma spray method satisfies all the required criteria for coating deposition (Section 3.2.1 Deposition technique selection) hence plasma spray being cost effective and readily scalable has been selected as the process for deposition of corrosion resistant coatings in this study.[191]

3.2.3 Plasma Spray Deposition

The plasma sprayed coatings are deposited from propelling molten particles hitting the substrate (Figure 15, Figure 14). The details of plasma spray deposition process are provided in Submission 3 (Protocol for Surface Engineering of Protective Coatings). The plasma spraying process is affected by a large number of parameters (Submission 3 Protocol for Surface Engineering of Protective Coatings). Coating characteristics can be controlled by a huge and relatively complex parameter space, including particle size, particle velocities, temperature, powder feed rate, spraying distance, design of spray gun, gas environment, and plasma input power.[134,152] Some parameters, such as gas flow rate and powder feed rate, are determined by equipment capacity, shape of nozzle gun, compressor pressure, geometry and power of gun. While other parameters, like input power and spray distance can be varied depending on the powder and substrate. Hence the input power and spray distance were varied to optimize the deposited coatings.

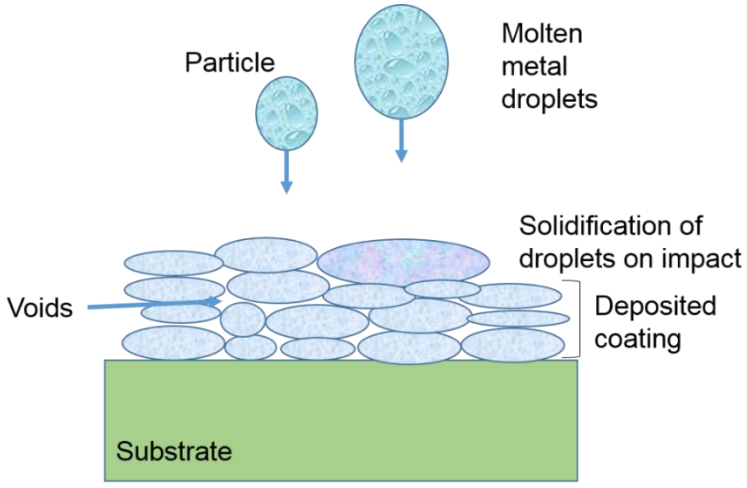

Figure 14: Schematic of plasma spray coating deposition showing the structure of coating. Coating becomes lamellar because of solidification of particles upon impact on the substrate

Table 6: Summary of substrate materials and dimensions

	LVPS	APS	APS	High-power impulse magnetron sputtering
Substrate material	SS 347	SS 347	SS 304	SS 347
Dimensions	75 × 30 × 1 mm	20 mm diameter, 2 mm thick discs 10 mm diameter, 2 mm thick discs	10 mm diameter, 2 mm thick discs	10 mm diameter 2 mm thick discs, 150 × 70 × 1 mm
Powder material	$NiAl_3$, Ni-18 (Trial run)	Ni_3Al Al_2O_3	Ni_3Al Al_2O_3	Ni_3Al

Table 7: Deposition parameters used for air plasma spray deposition

Parameters	Values
Ni_3Al particles size	20 – 45 µm
Argon flow rate	36700 ± 10 sccm
Hydrogen flow rate	7000 ± 10 sccm
Powder feed rate	67 ± 5 g/min
Input power	29KW, 31KW, 34KW
Spray distance	100mm, 150mm

3.3 Deposition of coatings

The deposition of coating is explained in detail in submission 3 (Protocol for Surface Engineering and Assessment of Protective Coatings) and submission 4 (Protective Coatings Development). A brief description is provided as follows.

3.3.1 Powder Description

Three different powders were used for this study for comparison purposes (Table 6).

- Nickel-18 powder (MCrAlY Tecphy, 10 – 35 µm spheroid particles) (Trial run)
- $NiAl_3$ powder (480NS Sulzer Metco, 20 – 45 µm spheroid particles) (Trial run)
- Ni_3Al powder (Sandvik osprey, 20 – 45 µm spheroid particles)

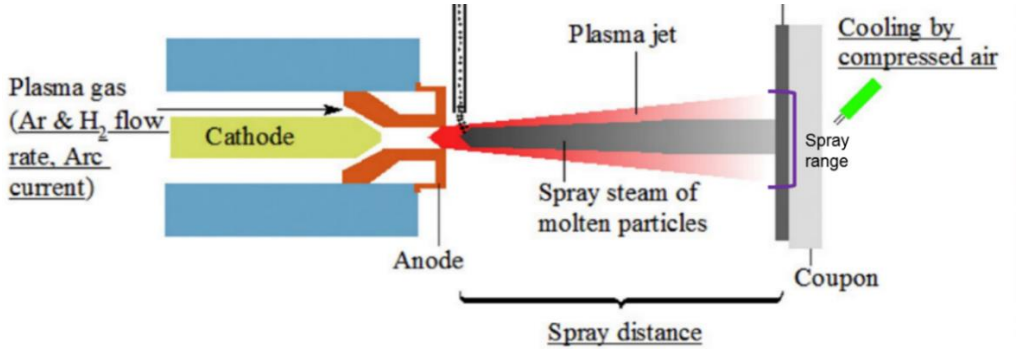

Figure 15: Schematic of plasma spray process displaying cathode and anode in the plasma spray gun with plasma jet and the range of spray jet reaching the substrate and the plasma gun to substrate distance.[2]

3.3.2 Substrate Description

Three different dimensions of SS347 substrate samples were utilised. Rectangular samples approximately 75 × 30 × 1 mm and discs samples with two different diameters of approximately 20 mm, 10 mm and 2 mm thickness were used in the study (Table 6). SS304 with dimensions approximately 10 mm in diameter and 2 mm in thickness, was also used for comparison purposes.

3.3.3 Coating Deposition

Nickel-18 and $NiAl_3$ powder were used to prepare coatings on SS347, with dimensions approximately 75 × 30 × 1 mm, using low vacuum plasma spray (LVPS) coating system for trail run. After literature review Ni_3Al was selected as the best candidate for the coatings and hence the study was focused on the corrosion behaviour of Ni_3Al coating in comparison with the substrate. Ni_3Al powder was used to prepare coatings on circular coupons of SS347, with dimensions approximately 20 mm in diameter and 2 mm in thickness and 10 mm in diameter and 2 mm in thickness, using air plasma spray (APS) deposition (Table 6, Figure 16, Figure 17). Ni_3Al powder was used to prepare coatings on circular coupons of SS304, with dimensions approximately 10 mm in diameter and 2 mm in thickness, using air plasma spray (APS) deposition (Table 6). Ni_3Al target was used to prepare coatings on circular coupons of SS347 and SS304, with dimensions approximately 10 mm in diameter and 2 mm in thickness, using high-power impulse magnetron sputtering (HIPMIS) (Table 6). The details of deposition set up and spray parameters used for depositing the coatings can be found in submission 3 (Protocol for surface engineering of protective coatings).

3.4 Characterisation of Coated Samples

The coatings were characterised using scanning electron microscope (SEM), energy dispersive x-ray spectroscopy (EDX) and x-ray diffraction (XRD) analysis. The APS deposited Ni_3Al coated SS347, with 34000 KW input power and 100 mm gun to substrate distance, meet all the requisite coating requirements and hence are discussed further in this innovation report (Table 8). The detailed coating characterisation of all coatings is provided in detail in submission 4 (Protective coatings development).

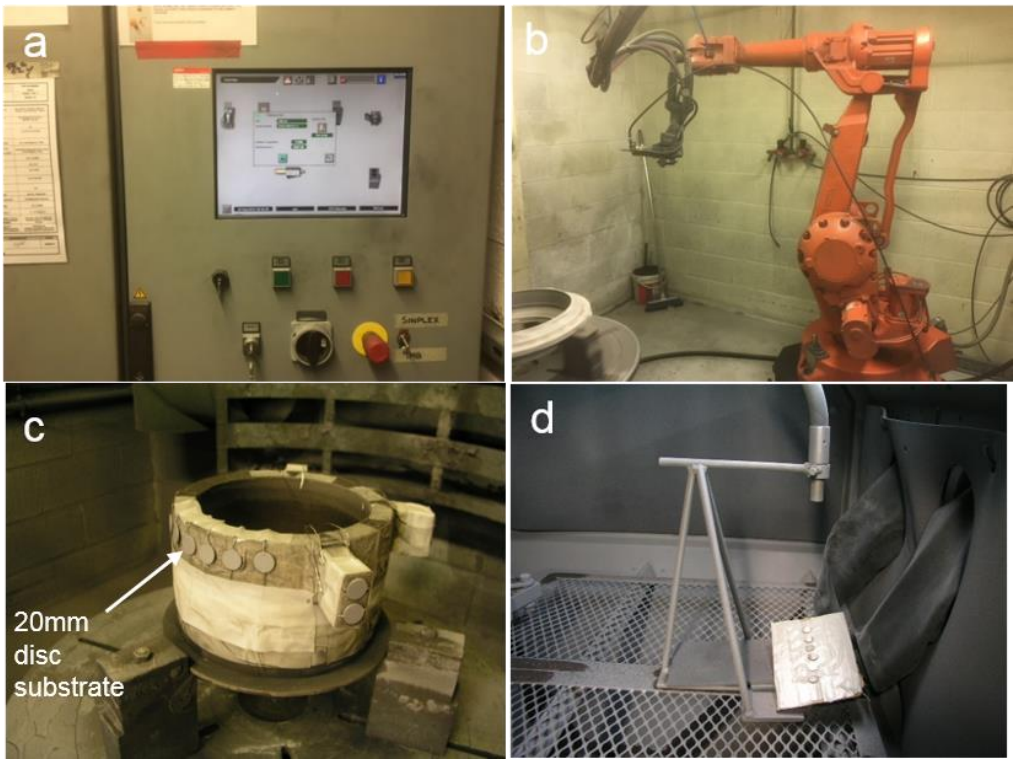

Figure 16: The Air Plasma Spray (APS; Multicoat system, 9MPE-CL feeder and 9M spray gun) (a) Control panel used for operating the plasma spray system (b) Plasma spray gun attached to robotic arm, the movement of plasma spray gun is controlled using the robotic arm (c) 20 mm samples attached on the specimen holder

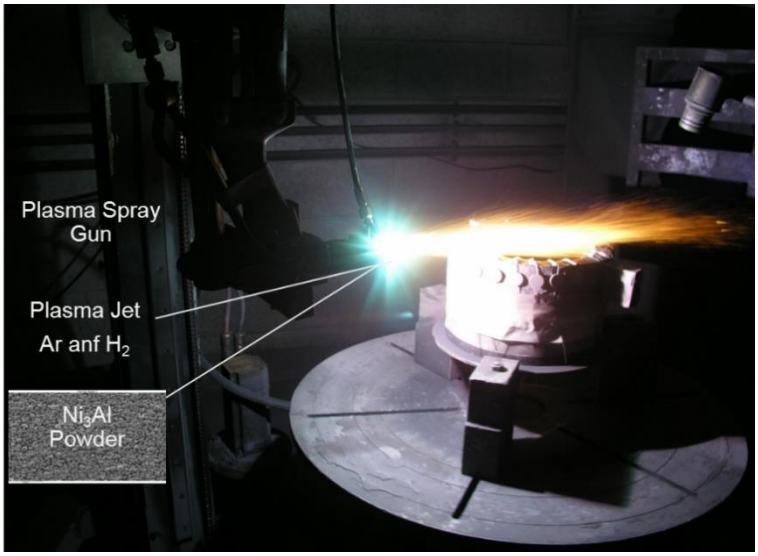

Figure 17: Deposition of coating with Ni_3Al powder using air plasma spray gun in presence of argon and hydrogen during process using the air plasma spray system shown in Figure 16.

3.5 Corrosion Test

The corrosion performance of bare and coated SS347 was investigated by immersion in solar salt at 565^{o}C up to 3000 hours (Figure 18). The methodology used for corrosion performance test is provided in detail in Submission 3 (Protocol for Surface Engineering of Protective Coatings). Only corrosion assessment for bare SS347 and APS deposited Ni_3Al coated SS347 samples is presented and discussed in this innovation report. Although other samples were also tested, however the results are not presented in the portfolio. A brief description of corrosion test procedure (Figure 18) is as follows:

- The molten nitrate (60%$NaNO_3$ - 40%KNO_3) salt mixture was introduced into ~ 10 ml alumina crucibles.
- Crucibles were introduced to furnace at 400^{o}C for 24 hours to ensure a homogeneous molten state.
- Samples were individually immersed in the crucibles and placed in the furnace at 565^{o}C.

- The samples were removed after every 500 hours interval, to be weighed and characterised.
- The test was carried out at 565°C for up to 3000 hours.

Table 8: The samples tested for corrosion resistance on molten nitrate salt immersion at 565ºC, presented in this innovation report.

Sample	Test duration	Temperature
Bare SS347	3000	565°C
APS Ni_3Al Coated SS347	3000	565°C

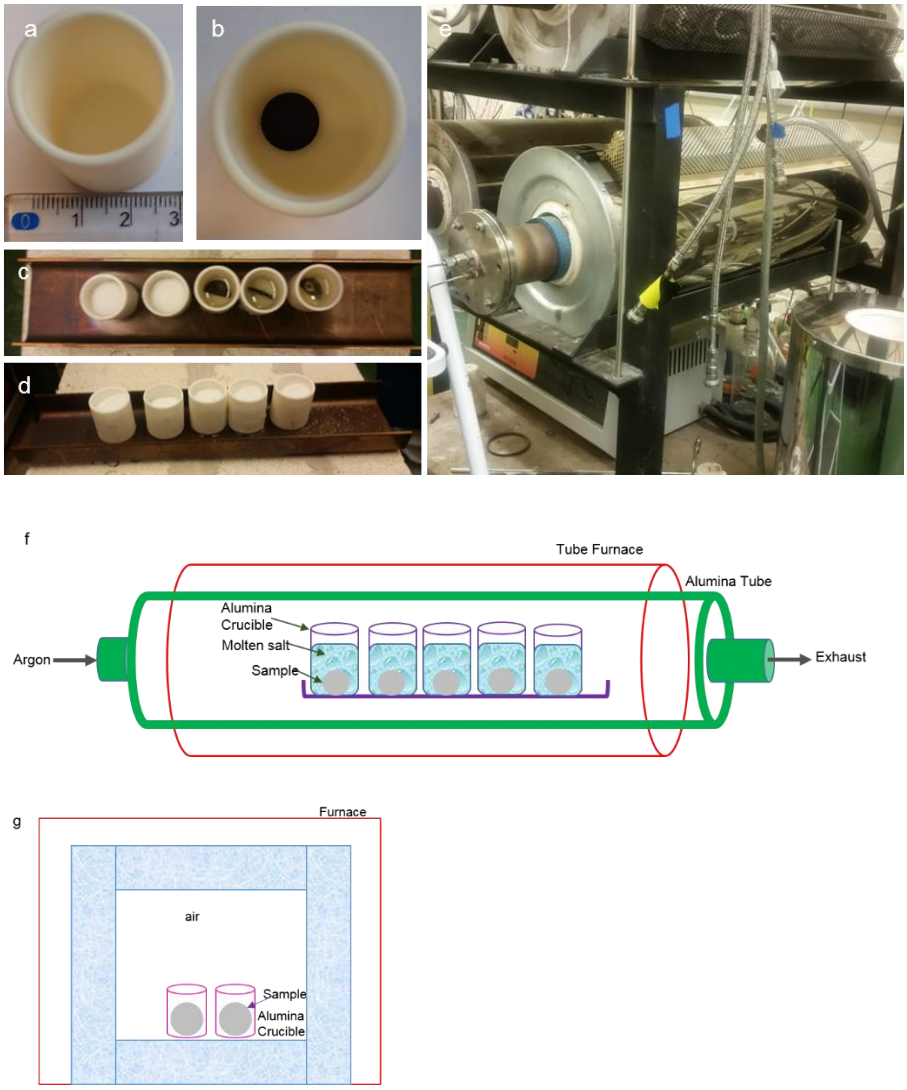

Figure 18: (a) Crucible made of alumina with 23.5 mm top diameter (b) 10 mm sample placed in the crucible (c) samples placed in the crucibles filled with solar salt heated to 400ºC (d) crucibles topped up with more salt ready for test at 565ºC (e) The furnace used for corrosion test with argon used as purge gas (f) Schematic of the corrosion test displaying crucibles filled with molten nitrate salt and samples placed inside a tube furnace (g) The furnace used for oxidation test in air

4 RESULTS

The Ni_3Al coated SS347 and bare SS347 stainless steel samples were immersed in solar salt at 565^oC for up to 3000 hours, to investigate their corrosion mechanism and calculate mass changes. Only corrosion assessment for bare SS347 and APS Ni_3Al coated SS347 samples are discussed and presented in this innovation report. Although other samples were also tested, the results are not presented in this innovation report. The characterisation of other samples is provided in submission 4 (Protective coatings development).

4.1 The Microstructure and Morphology of Bare SS347 in Solar Salt

4.1.1 Visual Inspection

The bare SS347 sample before exposure to solar salt shows a silver coloured smooth surface finish (Figure 19a, Figure 20a), that is a typical characteristic of commercially available stainless steel. After solar salt immersion, white coloured salt deposits were observed on the sample surface when removed from the furnace. These salt particles were removed during the cleaning process (Submission 3 Protocol for Surface Engineering and Assessment of Protective Coatings).

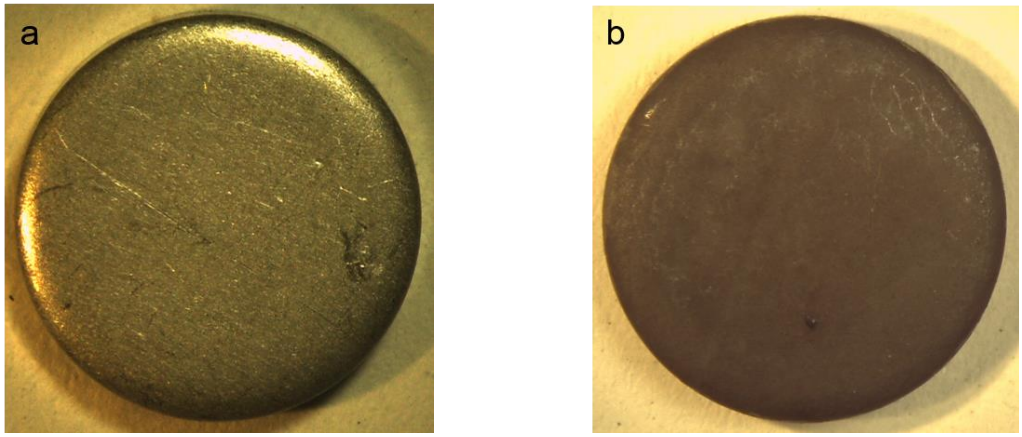

Figure 19: Pictures of the bare SS347 sample (a) at 0 hour, (b) after 3000 hours exposure to solar salt at 565^oC

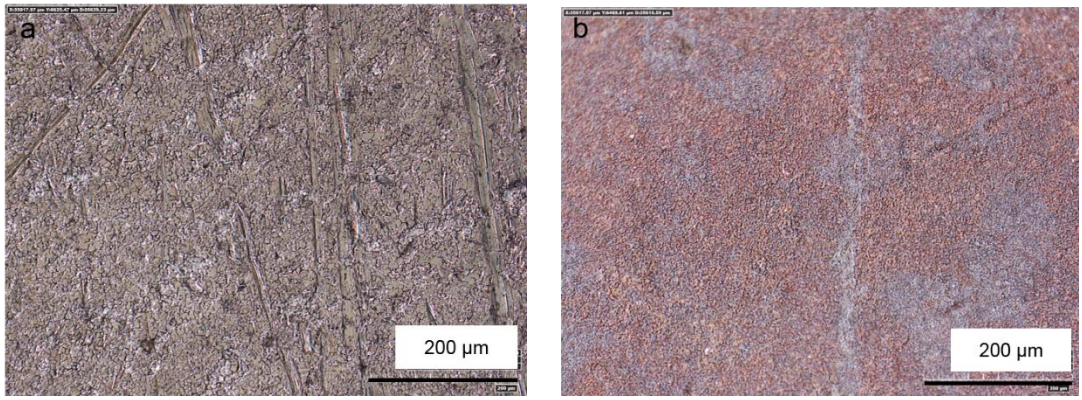

Figure 20: Optical microscope pictures of the bare SS347 sample (a) at 0 hour, (b) after 3000 hours exposure to solar salt at 565ºC

The shiny bright silver like appearance of stainless steel was replaced by a dark brown layer that covered the entire surface of each sample after 500 hours nitrate salt immersion at 565ºC. This dark colour and richer texture were also detected at 3000 hours (Figure 19b, Figure 20b). This suggests that the surface morphology of substrate changes within the first 500 hours and further changes are insignificant at least visually after longer immersion. No holes, cavities, pitting, intergranular attack or other localized attacks were observed in the bare SS347 after 3000 hours molten salt immersion at 100X magnification (Figure 19b, Figure 20b). Smaller holes or cavities in submicron sizes might be present, although could not be observed at this magnification. Higher resolution images are needed to establish the presence of smaller holes or cavities.

4.1.2 Surface Microstructure and Morphology

The morphology of corrosion products on the sample surface was analysed using SEM secondary electrons images. The SEM analysis of bare SS347 at 0 hour shows a typical smooth stainless steel surface with average grain size of ~ 4 µm and surface roughness of ~ 500 nm (Figure 21a, Figure 21b). Some dark regions are observed in the cross-section image, which could be due to difference in morphology, porosity, structure or phase (Figure 21b). The surface morphology looks different after 3000 hours solar salt immersion. SEM image of bare SS347 reveals a surface with average surface roughness of ~ 580 nm and surface features of average size ~ 1 µm (Figure 21c). There was no micro size pitting

observed on SEM surface images of samples after exposure to nitrate salt at 565^{o}C at 750X magnification. In order to validate that no pitting took place, sample needs to be characterised at higher resolution using SEM images or some different techniques. No distortion through the grain boundaries is observed, eliminating the likelihood of intergranular corrosion. It is suggested the only form of corrosion taken place is the general corrosion. The SEM cross-section after 3000 hours immersion exhibits distinguishable ad-layers which were not seen before at 0 hour (Figure 21d). The stratification in the oxide layers could be due to different elemental composition, crystalline structure, or phase. The darker topmost layer implies incorporation of light elements on the surface. There are some microcavities observed in the layer below, but no micro-size pitting is detected (Figure 21d).

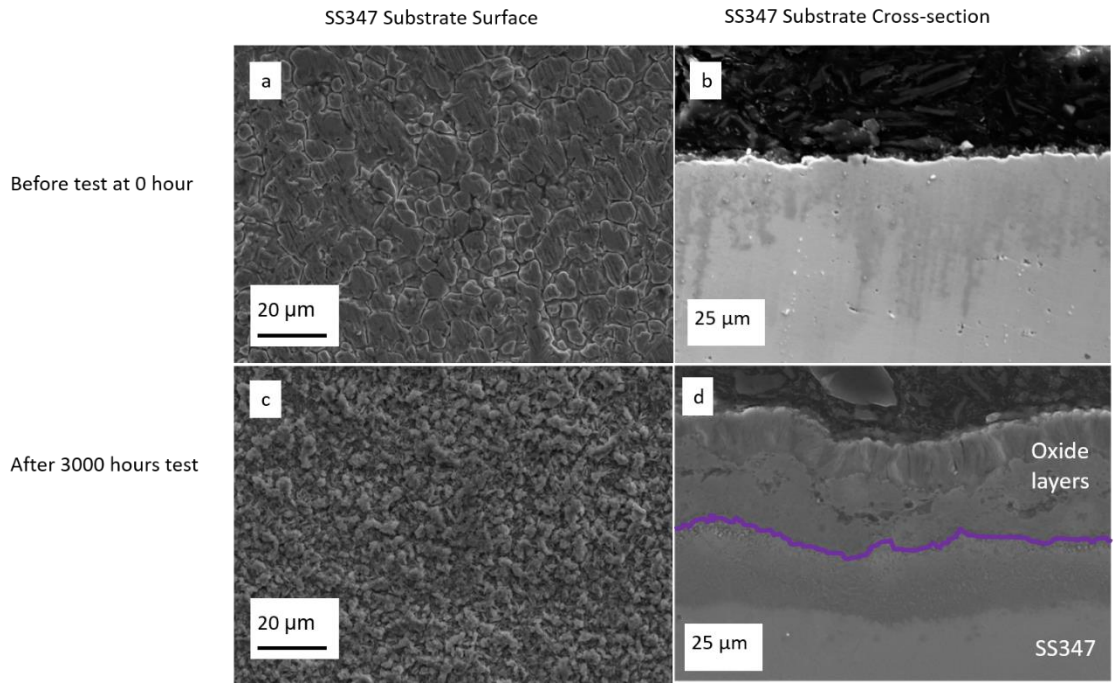

Figure 21: SEM images of surface and cross-section of bare SS347 taken at 0 hr (a, b) and 3000 hrs (c, d) of immersion in solar salt. All tests were done using solar salts at 565^{o}C and images were taken using secondary electron detector.

4.1.3 Structural Phase

X-ray diffraction spectra were collected every 500 hours, to further understand the evolution of grown layer observed in the SEM analysis, (Figure 22). The XRD spectrum

of the bare SS347 before test (at 0 hours) exhibits the peaks that can be attributed to CrFeNi (peak 1, Figure 22), which is typical for stainless steel. There is a change in the composition within first 500 hours of molten nitrate salt immersion. After 500 hours, the diffraction peaks attributed to $NaFeO_2$ (peak 2, Figure 22) and Fe_3O_4 (peak 3, Figure 22) phases can be observed in XRD spectrum.[192] Diffused peak could suggest inhomogeneous configuration in a solid solution.[193] The spectra remains unchanged from 1000 to 2500 hours, with all obvious peaks associated with $NaFeO_2$ and Fe_3O_4. The XRD spectrum displays peaks, corresponding to $NaFeO_2$ (peak 2, Figure 22), Fe_3O_4 (peak 3, Figure 22), Fe_2O_3 (peak 4, Figure 22).and $(Cr, Fe)_2O_3$ (peak 5, Figure 22) after 3000 hours immersion in molten salt.

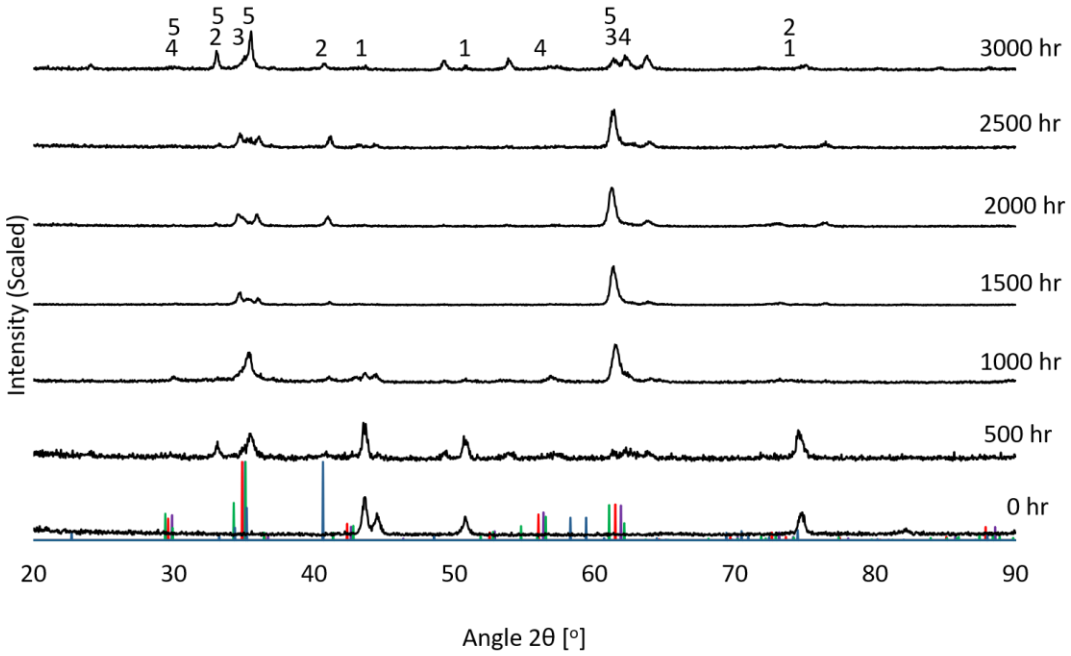

Figure 22: XRD patterns of bare SS347 sample before test at 0 hour and after 500, 1000, 1500, 2000, 2500, 3000 hours interval solar salt immersion at 565°C. Main peaks are highlighted, peak 1 corresponds to cubic CrFeNi, peak 2 corresponds to trigonal $NaFe_2O_3$ [1,0,-1,1] at 2θ peak of 35.2 and [1,0,-1,2] at 40.6, peak 3 corresponds to cubic Fe_3O_4 [2,2,0] at 2θ peak of 29.6, [3,1,1] at 34.8, [4,0,0] at 42.4 and [5,1,1] at 61.5, peak 4 corresponds to cubic Fe_2NiO_4 [2,2,0] at 2θ peak of 29.8, [3,1,1] at 35.1 and [4,4,0] at 61.9 and peak 5 corresponds to tetragonal Cr_2FeO_4 [1,0,3] at 2θ peak of 34.3, [2,1,1] at 35.1, [3,2,1] at 56.5, [2,2,4] at 61 and [4,0,0] at 62.1 according to the PDF-2 International Centre for Diffraction Data (ICDD) database[194] and Materials project.[192]

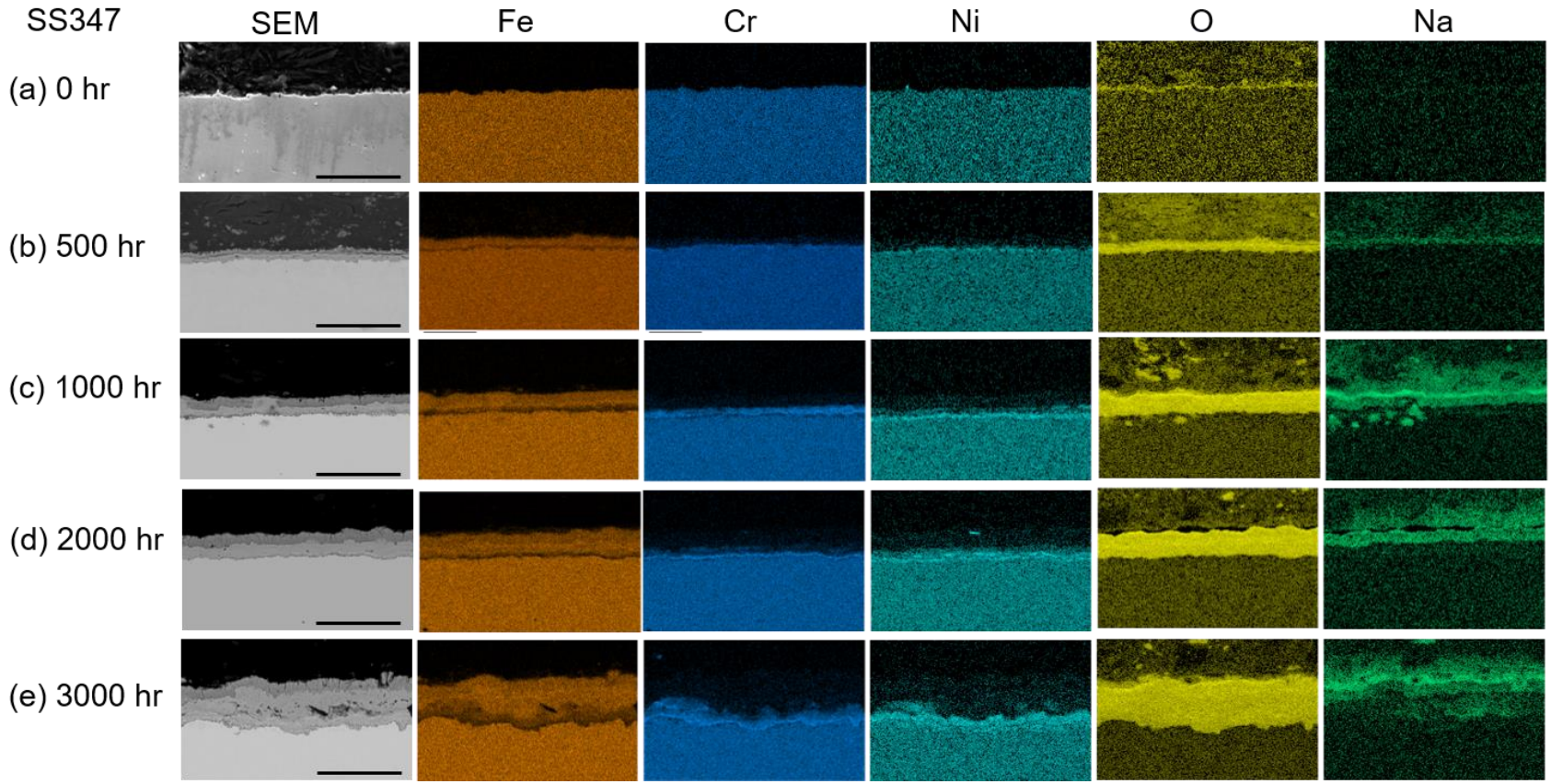

Figure 23: Elemental analysis by EDX elemental analysis of bare SS347 sample cross-section at (a) 0 hr, (b) 500 hrs, (c) 1000 hrs, (d) 2000 hrs, (e) 3000 hrs, of immersion in molten salt at 565°C. Inward diffusion of O and Na and outward diffusion of Fe could be clearly observed on SS347 (a–e). All scale bars represent 50 µm.

4.1.4 Elemental Composition

EDX map for bare SS347 at 0 hours reveals homogeneous existence of Fe, Cr and Ni typical for stainless steel (Figure 23a). Difference in topography with some dark regions are observed, which could be due to difference in morphology, porosity, height, structure or phase. After 500 hours, oxide layers are observed on SS347 surface (Figure 23b). The outermost layer is observed to be comprising of Na, O and Fe layer. The layer underneath contains Fe and O but no Na. After 1000 and 2000 hours, the oxide layers grow in thickness (Figure 23c, Figure 23d). Bare SS347 after 3000 hours molten salt immersion, shows the grown oxide layers with increased thickness (Figure 23e). The outermost layer, (layer I) ~10 µm thick is observed to be Na, O and Fe rich, whereas the rest of layers contain Fe and O. The layer II underneath is ~ 19 µm thick contains Fe and O but no Na.

4.1.5 The Oxide Layers Composition

Elemental composition of different elements in the grown oxide layers is plotted as a function of the distance from substrate surface after 3000 hours solar salt immersion (Figure 24). The zero level is set at the interface between substrate and the grown layers, with positive distance towards grown oxide layers and negative distance within the substrate. There is variation of elemental distribution in the grown oxide layers with Fe and O presence in all oxide layers. Comparing the elemental atomic percentage at different distances from SS347 surface after 3000 hours molten salt immersion, established the oxide in outermost layer (layer I) as $NaFeO_2$, validating XRD analysis (Figure 24). Layer II is identified as Fe_2O_3. Some discrepancy is observed between EDX map and the elemental composition plot. A depletion layer can be observed in EDX map (Figure 23b, c, d and e), however it is not quantified in the plots of elemental composition of constituent elements with time (Figure 24). It might be a part of layer II or a contrast effect or it could be due to precipitation of Ni, because of more signal from Ni it overshadows Fe. The thickness of individual grown stratified layers (I, II and III) increases at different rates with immersion time (Figure 25, Figure 26). The oxide thickness growth rate is 0.03 µm/hr, equivalent to 262.8 µm/yr for first 500 hours and 0.01 µm/hr, equivalent to 87.6 µm/yr for first 500 – 3000 hours (Figure 25).

This implies that the oxides grow in thickness with a higher rate for first 500 hour and the rate is lower after 500 hours up to 3000 hours. The thickness of all of oxide layers formed on the substrate surface was measured, after every 500 hours interval up to 3000 hours solar salt immersion at 565^{o}C, using SEM images and image analysis software.

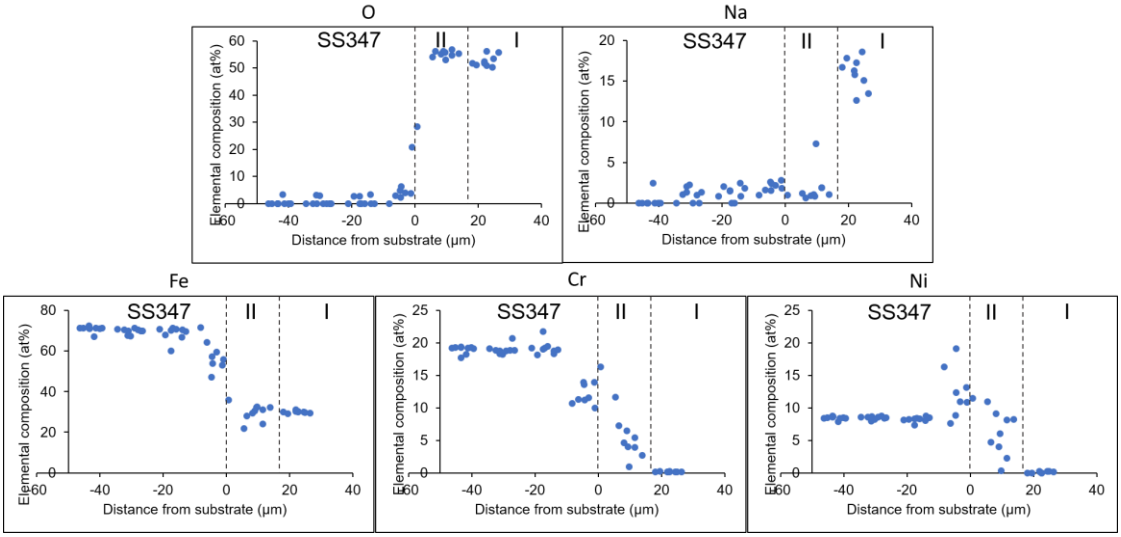

Figure 24: Elemental composition percentage of O, Na, Fe and Ni obtained using EDX, plotted as a function of distance from the bare SS347 sample surface after 3000 hrs immersion in solar salts at 565^{o}C. There is difference in elemental percentage in layer I, layer II and substrate.

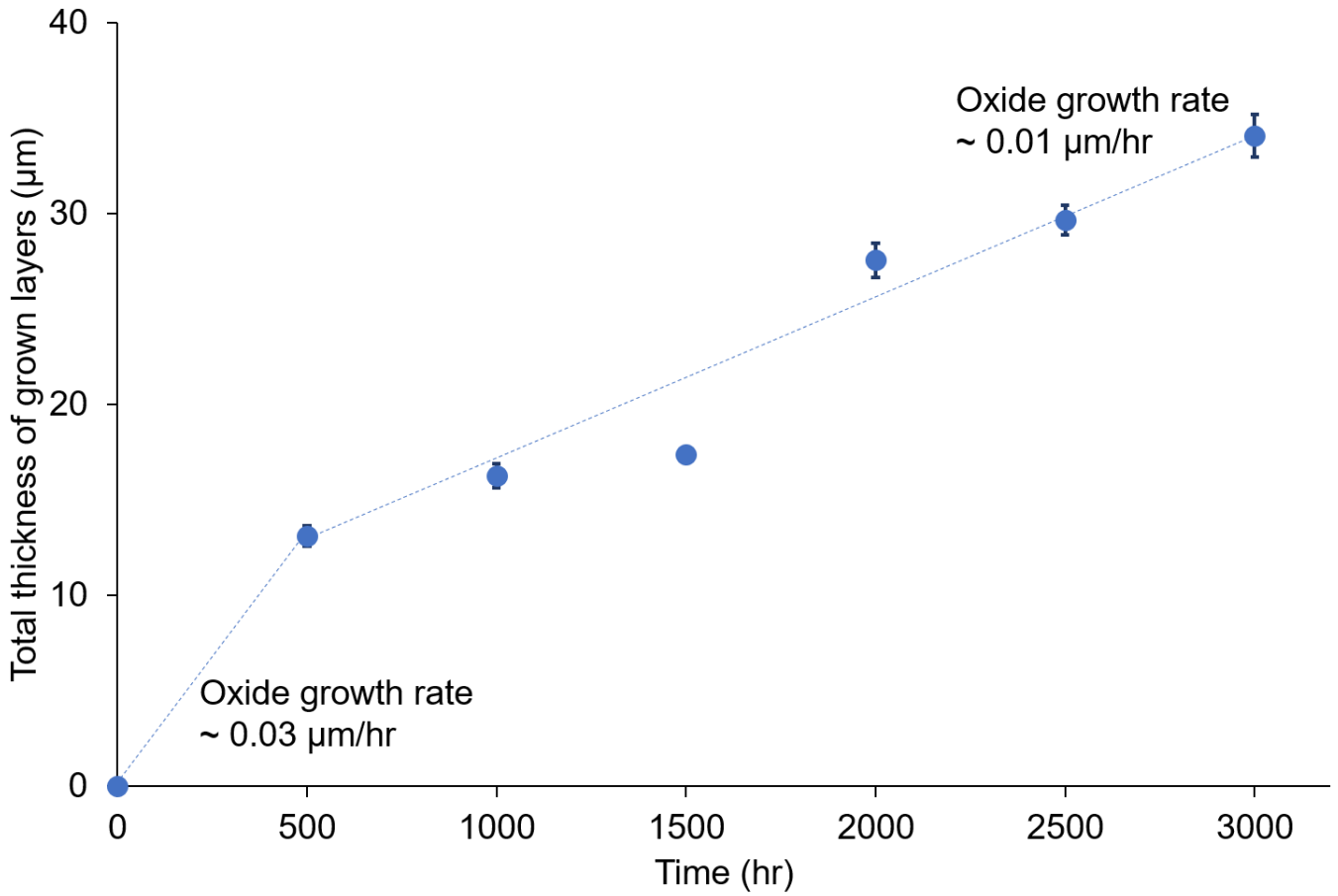

Figure 25: Total thickness of all grown oxide layer (μm) is plotted as a function of solar salt immersion time (hour) for bare SS347. The thickness grows with immersion time. The oxide growth rate is 0.03 μm/hr for 0 – 500 hrs and 0.01 μm/hr for 500-3000 hrs.

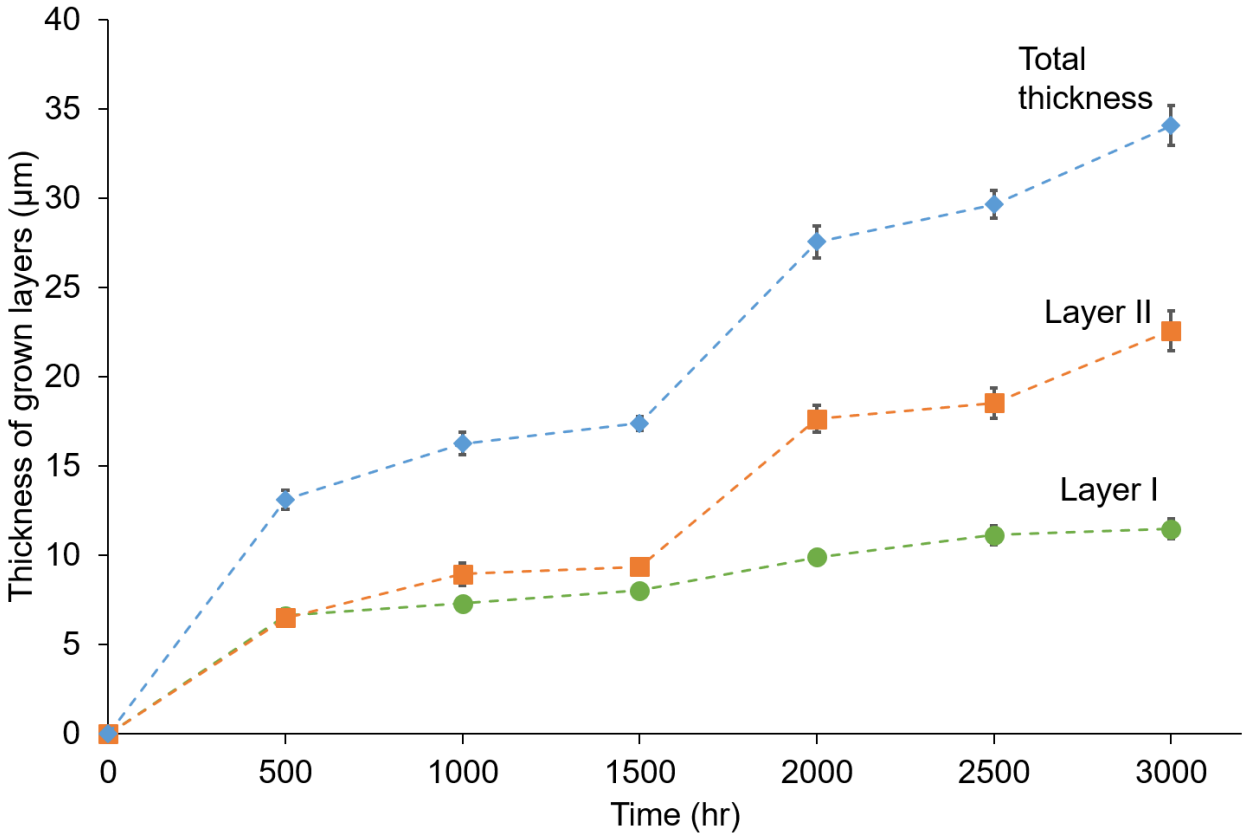

Figure 26: The thickness of individual grown layers is plotted as a function of time for bare SS347 sample to understand the increase in thickness with time. The oxides layers extended with increasing thickness over time. The oxide growth rate is 0.003 µm/hr for layer I and 0.007 µm/hr for layer II. The thickness of all oxide layers formed above the substrate was measured, after every 500 hours up to 3000 hours of corrosion test in solar salt at 565°C, using SEM images and image analysis software.

4.2 The Microstructure and Morphology of Ni3Al Coated SS347 in Solar Salt

4.2.1 Visual Inspection

Visual inspection of the Ni_3Al coated SS347 sample before exposure to solar salt shows a grey coloured surface finish (Figure 27a, Figure 28a). Surface colour remains the same after 500 hours exposure to nitrate salt. After 3000 hours, no difference is observed visually in the appearance of the Ni_3Al coated SS347 surface. This suggests no change in sample surface took place even after 3000 hours exposure to molten nitrate salt. No holes, cavities, pitting, intergranular attack or other localized attacks on macroscale were observed in the Ni_3Al coated SS347 samples after 3000 hours exposure to molten salt at 100X magnification (Figure 27b, Figure 28b).

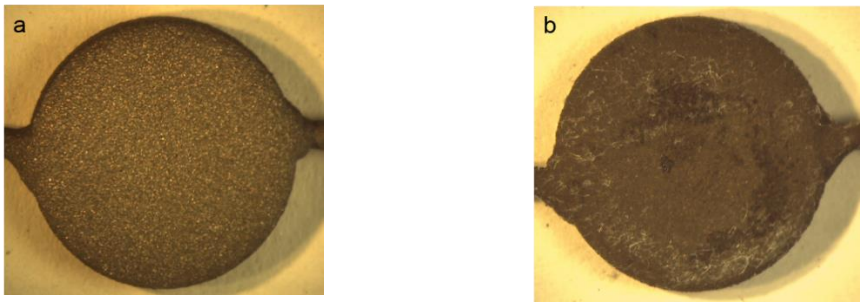

Figure 27: Pictures of the Ni_3Al coated SS347 sample (a) at 0 hour, (b) after 3000 hours solar salt immersion

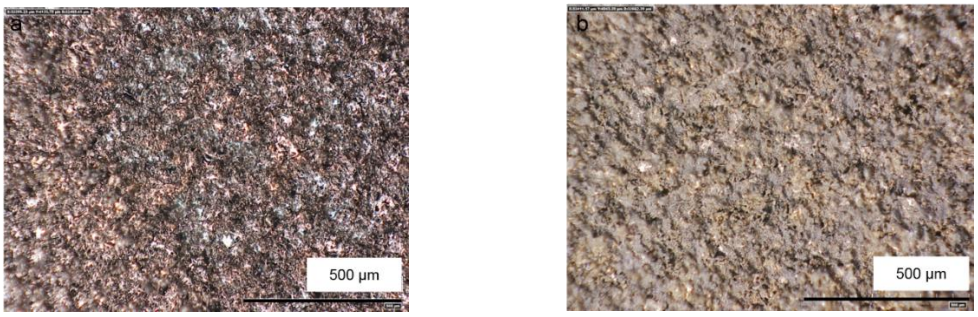

Figure 28: Optical microscope pictures of Ni_3Al coated SS347 sample (a) at 0 hour, (b) after 3000 hours solar salt immersion

4.2.2 Surface Microstructure and Morphology

The SEM image of the Ni_3Al coated SS347 sample surface, at time 0 hours, shows a typical plasma sprayed coating morphology, observed as splats of coating material on the surface with average lateral size of 5 μm and an average surface roughness of 6 μm (Figure 29a). The SEM image of the Ni_3Al coated SS347 sample cross-section at time 0 hours, exhibits a lamellar structure with few un-melted particles, which is typical for plasma sprayed coatings (Figure 29b). After 3000 hours immersion, the SEM image of the Ni_3Al coated SS347 sample surface shows additional surface features in addition to original morphology with surface features of average size of 1 μm and an average surface roughness of 5 μm (Figure 29c). The Ni_3Al coated SS347 sample cross-section looks similar to 0 hour but with less cavities within lamellar structure. Some of the lamellar structure have amalgamated into a more continuous structure. No visible degradation or oxide growth on the surface is apparent which suggests the corrosion resistance by the coating (Figure 29).[177]

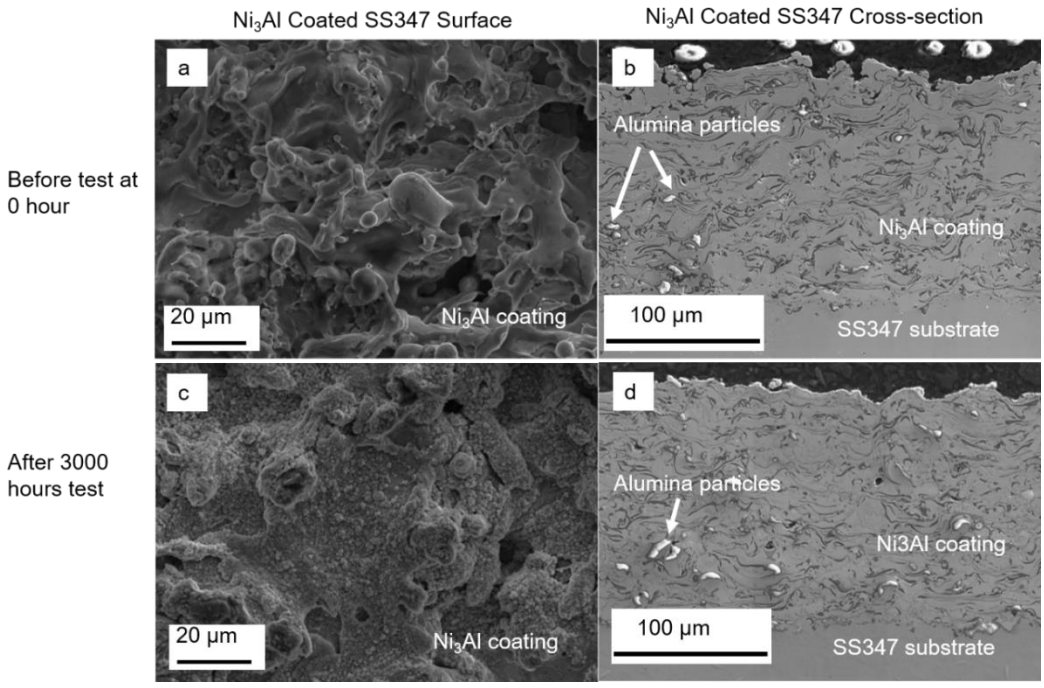

Figure 29: SEM images of surface and cross-section of Ni_3Al coated SS347 taken at 0 hr (a, b) and 3000 hrs (c, d) of solar salt immersion. All tests were done using 60 wt. % NaNO3 + 40 wt. % KNO3 salts at 565°C and images were taken using secondary electron detector.

4.2.3 Structural Phase

The XRD analysis was performed to analyse any changes in the Ni_3Al coated SS347 sample surfaces after exposure to solar salt for different time intervals (Figure 30). The XRD pattern of the Ni_3Al coated SS347 sample before test at 0 hours displays peaks corresponding to Ni_3Al.[192] There is a change in the composition within first 500 hours of solar salt immersion. After 500 hours, diffraction peaks corresponding to NiO in addition to Ni_3Al are observed. The peak around 76° seems to be shifted due to compressive stress in the coating.[195–200] The spectra remains same up to 3000 hours (Figure 30).[134,201–203]

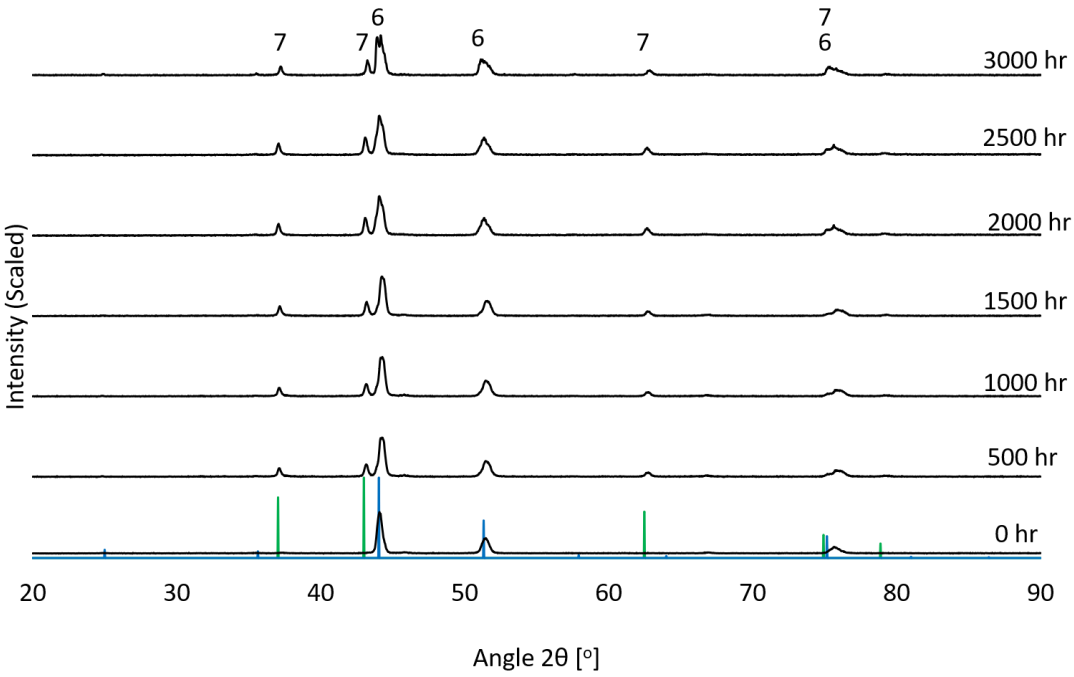

Figure 30: XRD spectrum of Ni_3Al coated SS347 sample before test at 0 hour, after 500, 1000, 1500, 2000, 2500, and 3000 hours solar salt immersion at 565°C. Main peaks are highlighted, peak 6 corresponds to Ni_3Al [1,1,0] at 2θ peak of 44, [2,0,0] at 51.3 and [2,2,0] at 75.2 and peak 7 corresponds to NiO [1,1,1] at 2θ peak of 37, [2,0,0] at 43, [2,2,0] at 62.5, [3,1,1] at 74.9 and [2,2,2] at 78.8 according to the PDF-2 International Centre for Diffraction Data (ICDD) database[194] and materials project.[192]

4.2.4 Elemental Composition

The EDX map of the Ni_3Al coated SS347 sample cross-section at 0 hour confirms the presence of Al and Ni in the coating (Figure 31a). The EDX map of the Ni_3Al coated SS347 sample cross-section after 3000 hours solar salt immersion displays Ni, Al and O (Figure 31b). The only difference in the elemental map after 3000 hours is the additional presence of O, no Na is observed in the coating or substrate (Figure 31b). Al is more susceptible to O compared to Ni at room temperature. There is some discrepancy between the XRD and EDX analysis. No AlO_x has been observed in the XRD spectrum however the EDX maps suggest the presence of AlO_x. It could be due to the reason that AlO_x is not in crystalline form and hence not detected in the XRD analysis. Elemental composition of different elements in the grown oxide layers is plotted as a function of the distance from substrate surface after 3000 hours molten salt immersion (Figure 32). The zero level is set at the interface between substrate and the coating, with positive distance towards the coating and negative distance within the substrate. There is no noticeable difference in the elemental composition of Ni_3Al coated SS347 before and after 3000 hours immersion. The lamellar structure of the plasma sprayed coatings might be the reason for fluctuation in elemental composition of Ni and Al within the coating. Elemental concentration of the coated sample plotted as a function of immersion time is plotted for further understanding of the process (Figure 32).

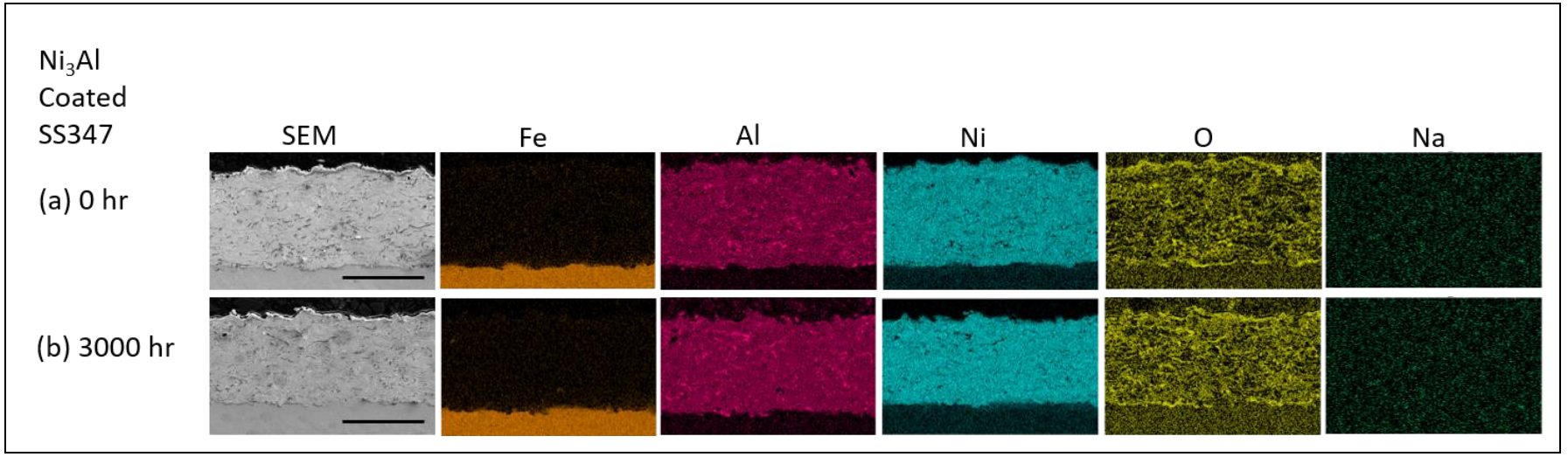

Figure 31:. Elemental analysis by EDX elemental analysis of Ni_3Al coated SS347 at (a) 0 hr and (b) 3000 hrs of immersion in molten salt at 565°C. There is no visible change in Ni_3Al coated SS347 for 3000 hrs. All scale bars represent 50 µm.

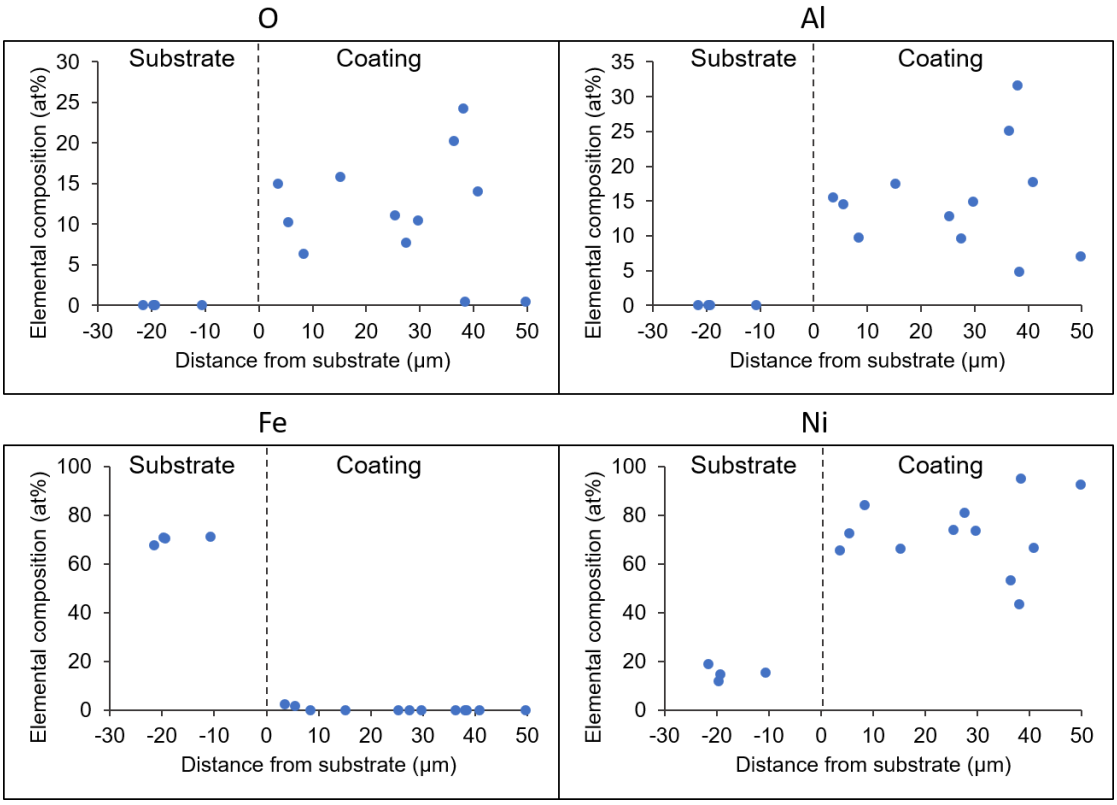

Figure 32: Elemental composition percentage of O, Al, Fe and Ni obtained using EDX, plotted as a function of distance from the Ni_3Al coated SS347 sample surface after 3000 hrs immersion in solar salts at 565ºC.

4.3 Oxidation Test in Air

The bare SS347 and Ni_3Al coated samples were subjected to oxidation test in air for up to 500 hours with 100 hours intervals. The XRD patterns of the coated samples before and after the corrosion test for 500 hours are presented (Figure 33 and Figure 34). The peaks in the XRD spectrum of bare SS347 after 500 hours oxidation are same as the bare SS347 sample before test (Figure 33). The peaks in the XRD spectrum of Ni_3Al coated samples after 500 hours oxidation are similar to the sample without test, but have some emerging peaks similar to the peaks for sample after 500 hour exposure to solar salt (Figure 34).

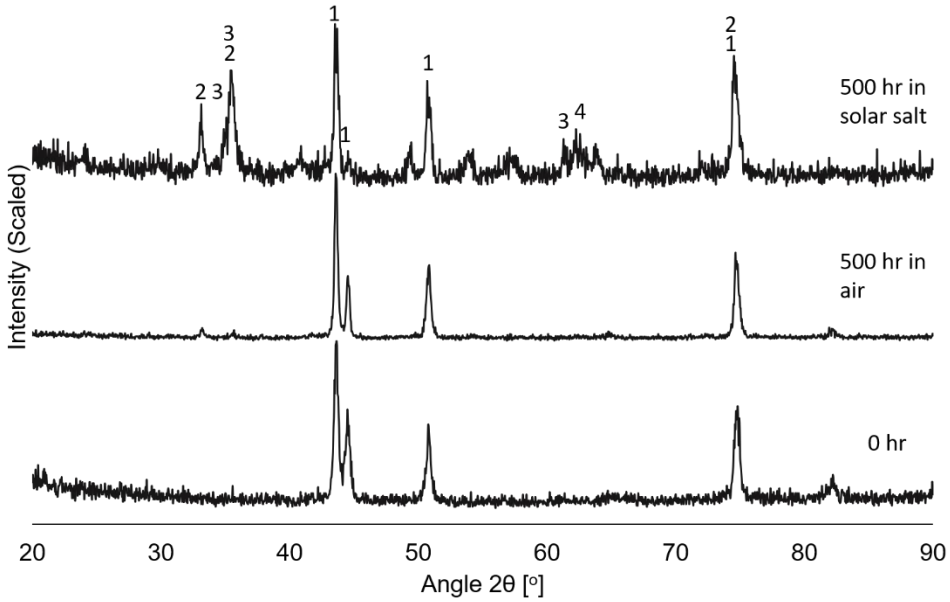

Figure 33: XRD spectrum of the bare SS347 before and after 500 hours oxidation test at 565°C. Main peaks are highlighted, peak 1 corresponds to cubic CrFeNi, peak 2 corresponds to trigonal $NaFe_2O_3$ [1,0,-1,1] at 2θ peak of 35, peak 3 corresponds to cubic Fe_3O_4 [2,2,0] at 2θ peak of 34.8 and [5,1,1] at 61.5 and peak 4 corresponds to cubic Fe_2NiO_4 [4,4,0] at 61.9, according to the PDF-2 International Centre for Diffraction Data (ICDD) database[194] and Materials project.[192]

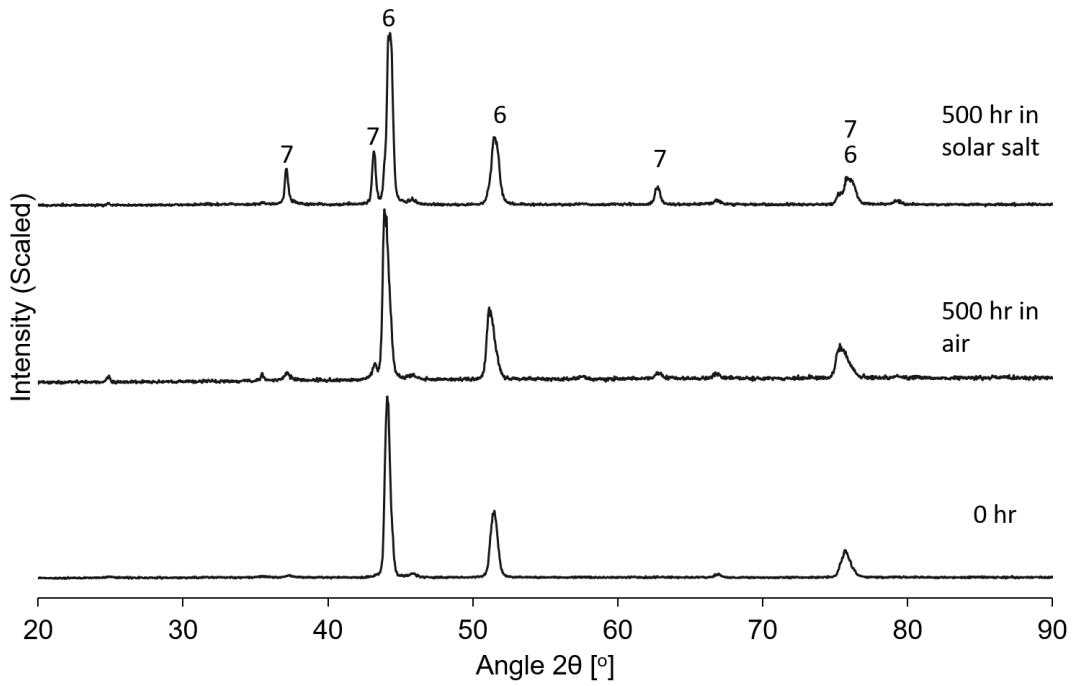

Figure 34: XRD spectrum of coated SS347 before and after 500 hours oxidation test at 565°C. Main peaks are highlighted, peak 6 corresponds to Ni_3Al [1,1,0] at 2θ peak of 44, [2,0,0] at 51.3 and [2,2,0] at 75.2 and peak 7 corresponds to NiO [1,1,1] at 2θ peak of 37, [2,0,0] at 43, [2,2,0] at 62.5 and [2,2,2] at 78.8 according to the PDF-2 International Centre for Diffraction Data (ICDD) database[194] and materials project.[192]

4.4 Corrosion kinetics

Different methods have been used to calculate mass change in literature. Standard practice for evaluating corrosion test samples is provided in ASTM G1-90.[204] ASTM G1-90 is relevant in the case of spallation of some or all grown oxides. Here it is not followed as the focus was on exploration of composition and thickness of the grown oxide layers. Therefore, corrosion rate, which requires removal of oxide product from sample, is not calculated here, instead normalised mass change per time is provided as an indication of corrosion behaviour. Mass of samples after every 500 hours immersion interval was measured up to 3000 hours of corrosion test in molten nitrate salt at 565°C. Mass of samples after every 100 hours was measured up to 500 hours of oxidation test in air at 565°C. Mass change (mg) was calculated by accumulated difference in mass from previous

time interval, not from initial mass. Calculated mass change (mg) was normalised per unit area (cm^2). Mass change per unit area (mg/cm^2) is plotted as a function of immersion time (hours) (Figure 35). The mass change in bare SS347 increases monotonically with increase in solar salt immersion time, that is in agreement with previous studies. From mass change viewpoint, the performance of bare SS347 is good enough, however the change in thickness and composition should also be considered. The mass change in Ni_3Al coated SS347 is quite noteworthy. It is observed to increase considerably fast within the first 500 hours and subsequently stabilise at a negligible increase rate. By looking at the plot it seems like the mass change in bare SS347 and Ni_3Al coated SS347 is similar, however the mass change in Ni_3Al coated SS347 reaches a plateau, stabilising with minimal increase after fast increase within first 500 hours. The Ni_3Al coated SS347 could be pre-treated by annealing in air to reach the plateau prior to introduction in molten salt. The thickness of all grown layers is plotted as a function of mass change of bare SS347 sample to understand the correlation between thickness and mass change (Figure 36).

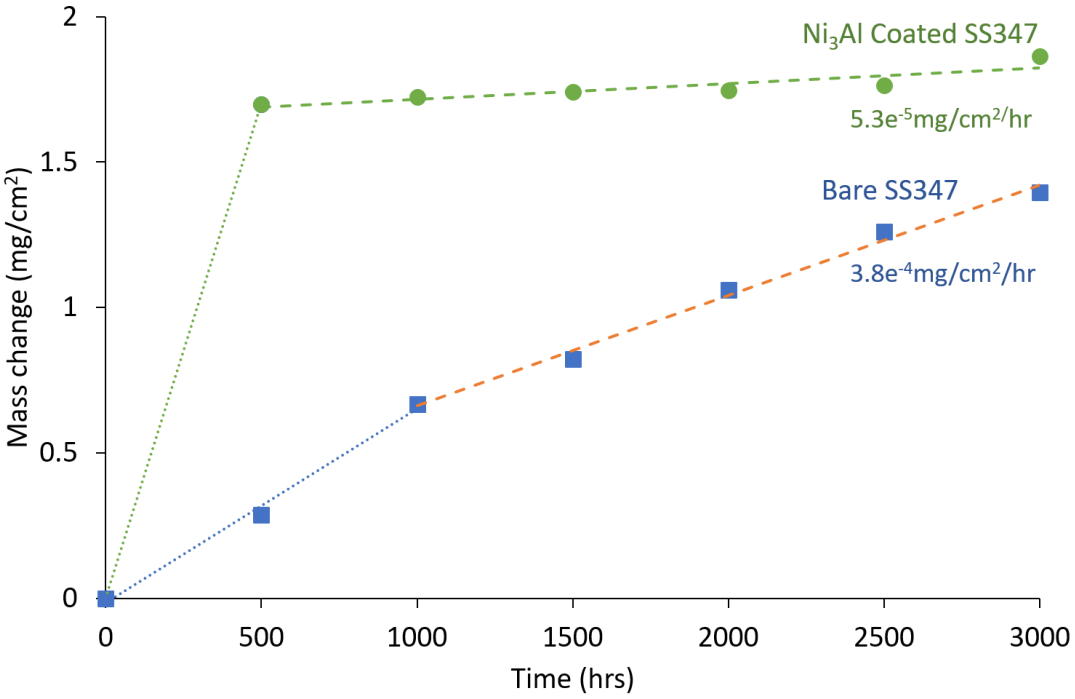

Figure 35: Time dependent mass change (mg/cm^2) of bare SS347 and Ni_3Al coated SS347 in solar salt at 565^{o}C. The behaviour in molten salt was observed for 3000 hrs based on measurements every 500 hrs. Here, the mass change is presented as an absolute accumulative value. Dotted lines are regression analysis. The rate of mass change is 5.3e^{-5} mg/cm^2/hr for Ni_3Al coated SS347 after first 500 hours, whereas 3.8e^{-4} mg/cm^2/hr for bare SS347.

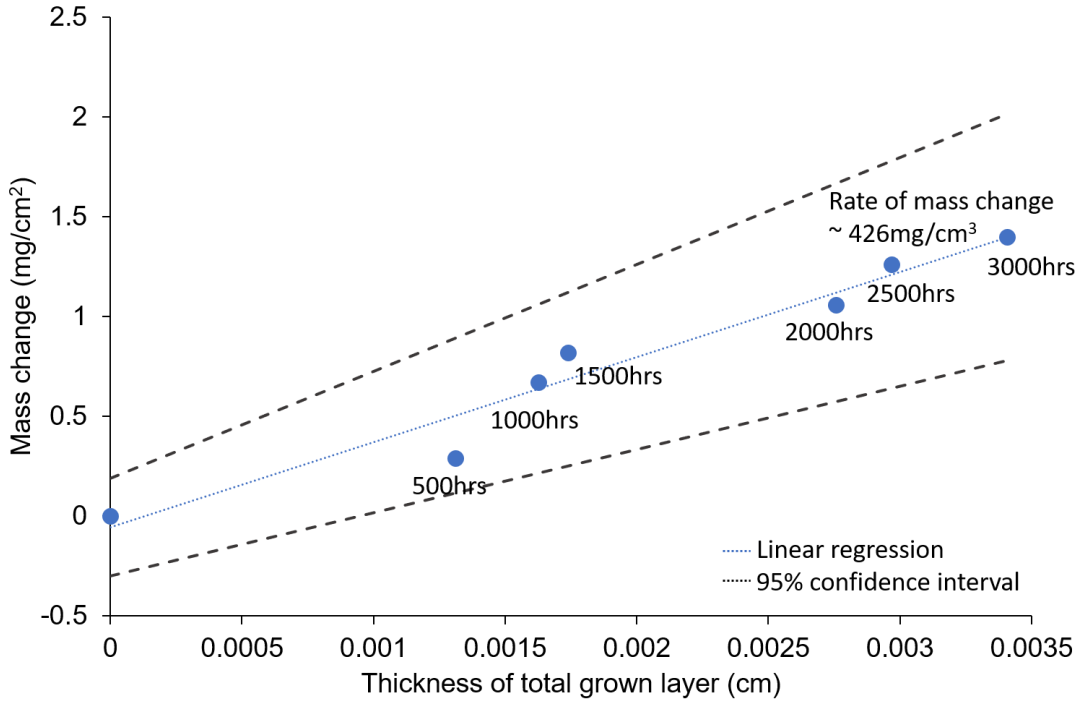

Figure 36: The mass change is plotted as a function of thickness of total grown layers for bare SS347 sample to understand the correlation between thickness and mass change. The oxides layer extended with increasing thickness over time. The slope of plot is 426 mg/cm^3. The thickness of all of oxide layers formed above the substrate was measured, after every 500 hours up to 3000 hours of corrosion test in solar salt at 565^{o}C, using SEM images and image analysis software.

5 DISCUSSION

Corrosion occurs naturally as the decay of a material or its properties due to reaction with surroundings. Hot corrosion does more damage to the components of systems than oxidation. Corrosion in molten salt can result both from oxidation of the base metal and from solubility-driven dissolution reactions.[108] If the solubility of the alloy in the molten salt is significant, excessive corrosion can be expected. Also, corrosion can be complicated by diffusion effects. If the alloy has different affinities for the environment, selective removal of some components can take place. As these components diffuse outwards, vacancies move inwards and segregate to form visible voids.[205]

The corrosion mechanism in nitrate salt are associated with nitrate reduction reactions.[206] Oxidation of metal and chromium dissolution are proposed to be the main reason for the metal loss in nitrate salt.[103] Chromium can be easily removed from the grown surface oxide on alloys because of its solubility, whereas nickel and iron do not form soluble species on exposure to molten nitrate salt.[207] Molten nitrates are moderately weak bases below 600°C.[207] The basicity of the salt mixture is stated to rise with rising temperature, facilitating integration of sodium in the grown oxides.[105] The stability of KNO_3 is typically better than $NaNO_3$.[208] Nitrates and alkali oxides are formed when nitrate salt breakdown above 540^{o}C. These oxide ions impact the corrosiveness of salt. The nitrate melts can be categorised as conventional Lux-Flood bases.[209] Molten salt behaves as bases in the Lux-Flood acid-base concept i.e., oxide ion givers, eliminating oxide layers from the material exposed to them.[207] Initially oxidation occurs resulting in formation of oxides which are subsequently dissolved in the molten salt. Corrosion is also enhanced by the presence of oxygen and water vapor in the molten salt.[210]

5.1 SS347

The surface of bare SS347 samples was analysed after molten nitrate salt immersion at 565°C. Corrosion observed is believed to be general surface corrosion, as no presence of pitting or intergranular corrosion was observed

visually, or in the SEM analysis of the surface and cross-section for the bare SS347 after molten nitrate salt immersion up to 3000 hours (Figure 19, Figure 21). Based on visual inspection of the surface of bare SS347, the surface colour has changed from shiny grey to dull dark colour after molten nitrate salt immersion (Figure 19, Figure 20). The dark colour is homogeneous all over, it could be due to physical changes e.g. surface roughness or chemical change in composition or both. The change in colour after molten nitrate salt immersion is obvious and signifies the formation of oxide layers.

The XRD spectrum disclosed the growth of four distinct oxides, including sodium iron oxide ($NaFeO_2$) and iron oxide (Fe_2O_3 and Fe_3O_4) after molten salt immersion (Figure 22). The EDX map results are in conformity of findings from previous studies.[211] Oxide layer formation was observed with an increasing thickness and separation of layers with increasing duration of exposure to nitrate salt.[212] A multilayer oxide growth is noticeable in the EDX elemental map (Figure 23). Iron is generally present in the entire grown oxide layers; iron is present in iron oxide and sodium iron oxide. However, iron distribution does not seem to be continuous over the thickness of the entire oxide layers. At the lower regions, iron is depleted while chromium and nickel are enriched. As the Fe and Cr diffuse outward to form oxides a layer rich in Ni is observed in the substrate below the interface. A nickel enriched region is displayed adjacent to the grown oxides inside the substrate, indicating that iron and chromium concentration is reduced due to outward diffusion to form oxides on the surface of substrate.[164] The inner layer is an iron oxide that contains a significant amount of chromium, as well as some nickel.[100] EDX and XRD analysis, strongly suggests there is sodium observed on the substrate surface, in the form of $NaFeO_x$. There was formation of three corrosion phases, sodium iron oxide ($NaFeO_2$), iron oxide and hematite (Fe_2O_3).

The outermost layer is concentrated with Na, believed to come from the nitrate salt mixture. It is determined to be $NaFeO_2$, which is usual corrosion outcome of Fe base alloys in molten salt.[100,213–215] Presence of sodium in oxidation layers is normal for high temperature iron alloys, beyond 600°C.[105] The sodium iron oxide is not present in the sample before corrosion test, it is present in the sample after

500 hour of corrosion test and getting higher in intensity in the sample after 1500 hour of corrosion test (Figure 22). That indicates reaction with molten salt leads to formation of sodium iron oxide. Sodium iron oxide outer layer with an iron oxide layer beneath it has been observed for molten nitrate exposure at 600^{o}C.[172] The sodium iron oxide has also been observed during past studies.[216] This outermost layer is followed by an iron oxide, probably Fe_3O_4 or Fe_2O_3 layer beneath which is a layer consisting of chromium oxide. Two types of iron oxide formation have been observed Fe_2O_3 and Fe_3O_4. The corrosion products comprising of $FeCrO_4$, Fe_2O_3 and $NaFeO_2$ outer layer have been reported after 2000 hour exposure to ternary nitrate salt.[169] Chromium forms an oxide layer on the surface of bare SS347 sample as a chromium deficient region is observed below this chromium oxide layer. This could be because chromium migrates and diffuses outwards, leaving a chromium deficient layer below.[105,170,211] The absence of chromium in outer layers confirms the fact that chromium is soluble in molten nitrate salt.[108,164,172,207,217,218]

5.2 Ni_3Al coated SS347

Based on visual inspection, no difference is observed on the surface of Ni_3Al coated SS347 after nitrate salt immersion. This suggests no change to sample surface takes place after 3000 hours molten nitrate salt immersion. XRD spectrum exhibited formation of NiO in the coating after nitrate salt immersion. EDX map revealed presence of Ni, Al and O in the coating, implying formation of Ni and Al oxide within the coating. No Na was observed in the coating or substrate in EDX or XRD analysis.

5.3 Corrosion Kinetics

The formation kinetics of the oxide layers is explained using schematic diagram (Figure 37). Bare SS347 and Coated SS347 samples were immersed in solar salt at 565^{o}C (Figure 37a, Figure 37e). Immersion in molten nitrate salts introduces oxide layers on surface of bare SS347 that grow in thickness with increasing immersion time. Within first 500 hours two layers were observed on the bare SS347 sample surface. Layer I is the outermost layer with higher Na

concentration compared to layer II (Figure 37b). Suggesting Fe out diffusion from the bare SS347 sample, Fe reacts with O and Na from the molten salt to form $NaFeO_x$ and FeO_x, detected in the XRD spectrum. EDX mapping displays two layered oxide formation corresponding to $NaFeO_x$ and FeO_x.[177] The $NaFeO_x$ has been identified as $NaFeO_2$, and the FeO_x as Fe_2O_3. The diffusion kinetics are similar from 500 to 3000 hours with outward diffusion of Fe. The two grown oxide layers grow in thickness as observed using EDX map (Figure 37b - d), showing further Fe diffusion outwards from the substrate and mixing with O and Na inwards from the salt (Figure 37b - d). The amount of Na is higher in the top layer and O is higher in the top two layers. Absence of Cr in outer layers I and II confirms the solubility of Cr in molten salts.

In contrast to the bare SS347, the Ni_3Al coated SS347 sample behaves differently. After 500 hours in the solar salt, O is observed to have diffused into the coatings to form NiO and Al_2O_3(Figure 37e). This was confirmed with XRD and EDX maps as well as mass gain (Figure 22, Figure 23 and Figure 34). After 500 hours the O continue to diffuse into the coatings (Figure 37). After 1500 hours O still diffuses in but in lower amounts (Figure 37). The kinetics for the Ni_3Al coated sample remain the same and crystalline structure of coating does not change after 3000 hours of molten nitrate salt immersion (Figure 30, Figure 31 and Figure 37). No out diffusion of Fe, Ni or Cr has been observed from the substrate towards the interface or coatings, O continue to diffuse in the coatings. No Na has been observed in the coatings or the substrate. In comparison to CrO_x which is soluble in nitrate salt, AlO_x and NiO_x are stable and dense enough to create a diffusion behaviour. The fact that no Na has been observed in coating or substrate implies that, AlO_x and NiO_x act as a barrier for outward diffusion of Fe, Cr and Ni from substrate and inward diffusion of Na into coating or substrate. Hence showing the protective nature of the coatings, as it prevents any diffusion of Na or O from the solar salt into the substrate and also prevents any outwards diffusion of substrate elements.

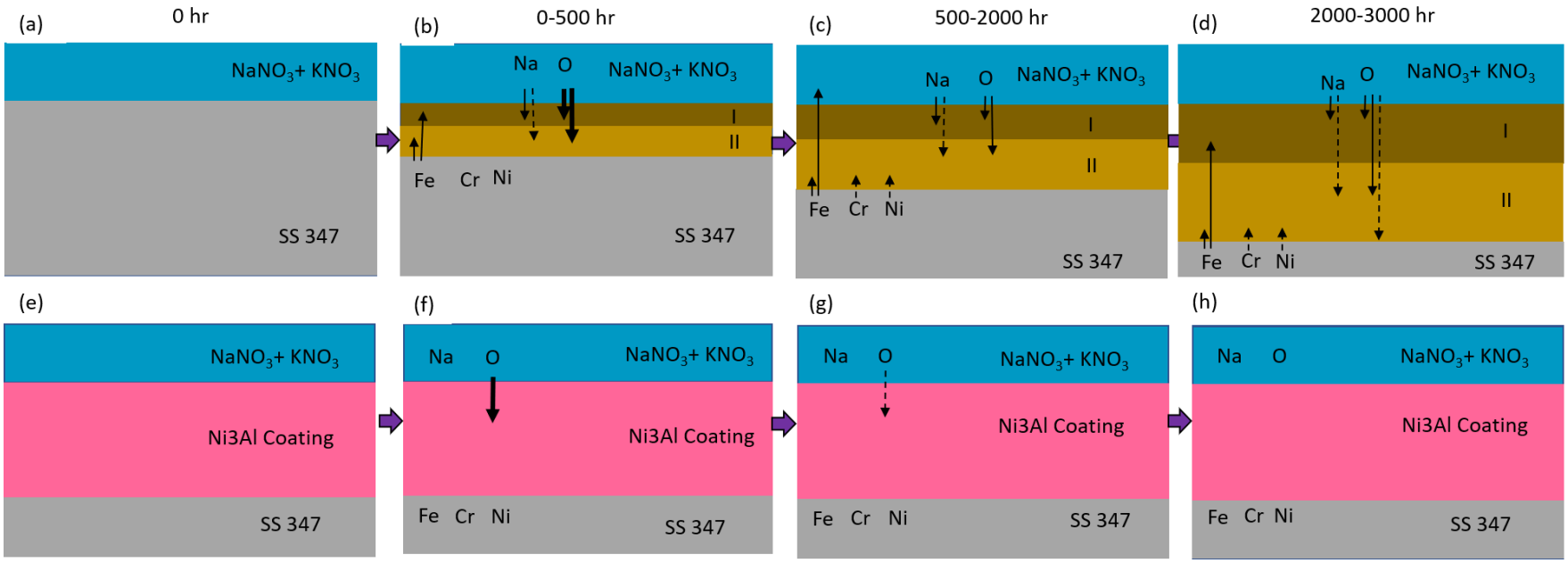

Figure 37: Schematic of time dependent corrosion mechanism of (a–d) bare SS347 and (e–h) Ni_3Al coated SS347 with immersion in molten nitrate salts at 565°C. On bare SS347, (b) the uptake of O is strong, and the diffusion of Na is slow within first 500 hrs, (c, d) which then slows down when the test reaches 3000 hrs and beyond. For Ni_3Al coated SS347, (f) the uptake of O is very strong within first 500 hrs. (g, h) Beyond 500 hrs, the O diffusion slows down significantly. The solid thick line is used to show a high rate of diffusion, solid thin line for intermediate rate of diffusion, and dotted line the lower rate of diffusion.

5.4 Mass change

The mass change in bare SS347 sample increases almost linearly up to 3000 hours solar salt immersion. The mass change appears to be due to the formation and growth of oxides on the surface of sample. The mass change, for oxidation in air and for solar salt immersion, is very similar for up to 500 hours. The thickness of all grown oxide layers is plotted as a function of mass change of bare SS347 sample to understand the correlation between thickness and mass change (Figure 36). The density can be estimated from the slope of the plot between the mass change and the change in thickness of all grown oxide layers. Small disc samples were used during this study, the samples thickness increases slightly with solar salt immersion because of grown oxide layers. For a sample with density ρ and volume V', the mass m is given by;

$$m = \rho V' \quad \textbf{(5-1)}$$

Mass

Where V' is the sum of volume of sample and grown oxide layers, V is the volume of SS347 sample with thickness H and ΔV is the volume of grown oxide layers with thickness h.

$$V' = V + \Delta V \quad \textbf{(5-2)}$$

Volume

The volume V of the sample with radius r and thickness H can be given by

$$V \propto r^2 H \quad \textbf{(5-3)}$$

Therefore

$$V' \propto r^2 H + r^2 h \quad \textbf{(5-4)}$$

The thickness h of the grown oxide layers is very small compared to the constant thickness H and radius r of the SS347 sample. Taking derivative of volume with respect to h,

$$\frac{dV'}{dh} \propto r^2 \quad \textbf{(5-5)}$$

Taking derivative of equation (5-1) with respect to h,

$$\frac{dm}{dh} = \frac{d\rho}{dh}V' + \rho\frac{\mathrm{d}V'}{\mathrm{dh}} \quad \textbf{(5-6)}$$

It can be assumed that the sample has homogeneous porosity and composition, and thus density remains constant.

$$\frac{d\rho}{dh} = 0 \quad \textbf{(5-7)}$$

Density

Implying,

$$\frac{dm}{dh} = \rho\frac{\mathrm{d}V'}{\mathrm{dh}} \quad \textbf{(5-8)}$$

Hence,

$$\frac{dm}{dh} \propto \rho\, r^2 \quad \textbf{(5-9)}$$

The slope of the plot in Figure 36, gives value of mass change per unit area per thickness, as shown below in equation (5-10).

$$\frac{dm/_A}{dh} = 426\ \mathrm{mg/cm3} \approx 0.5\ \mathrm{g/\ cm3} \quad \textbf{(5-10)}$$

The density of grown oxide in outer layer (layer I, $NaFe_2O_3$ (bulk)) is ~ 4.6 g/cm^3 and density of grown oxide in inner layer (layer II, Fe_3O_4 (bulk)) is ~ 4 g/cm^3 (Figure 23). This suggests that the actual density of the grown oxide layer is 4.6/0.5 = 9.2% of the density of bulk. Suggesting that the substrate and the grown oxide layers are very porous, ~ 90% porosity, or may be some of the mass changes are unaccounted. These unaccounted mass changes could be

independent from the formation of oxide layers, e.g., dissolution to the salt. Some changes in volume could occur because of phase change or precipitation. The oxide layers grow in thickness with increasing immersion time (Figure 25).

The mass change in Ni_3Al coated sample is quite noteworthy (Figure 38). It is observed to increase considerably fast within first 500 hours, and subsequently stabilise at a negligible increase rate. Looking at the varying trend in mass change, it is important to note that the mass change with immersion time needs to be approximated in a piecewise manner (Figure 39). It is reasonable to have average mass change as there is no steady state for bare SS347. It is particularly important for Ni_3Al coated samples as the mass change follows a specific trend for 0 to 500 hours and a completely different trend for 500 to 3000 hours. Important information regarding time dependant mass change could be lost if both distinctive trends are considered for coated sample. If mass change was calculated based on longest immerse time, the mass change with immersion time would be 5.4 $mg/cm^2/yr$, equivalent to oxide growth rate of ~8.1 µm/yr, which is incorrect for both regimes and does not capture change in mechanism. Whereas if mass change is calculated piecewise, the mass change with immersion time would be 29.8 $mg/cm^2/yr$ for 0 to 500 hours and 0.5 $mg/cm^2/yr$ for 500 to 3000 hours for Ni_3Al coated SS347. Hence the oxide growth rate would be ~44.6 µm/yr for 0 to 500 hours and ~0.7 µm/yr for 500 to 3000 hours for Ni_3Al coated SS347. The rapid increase could be partially due to intake of oxygen by the coating with subsequent aluminium and nickel oxide formation. Oxidation test at atmospheric pressure was conducted without the nitrate salt to establish the cause for this initial rapid mass gain, whether it is due to intake of oxygen or due to interaction with solar salt. It was seen that Ni_3Al coated SS347 behaved similar in air. Air was enough for oxidation of Ni and Al in the coating. The fastest change in mass takes place in the first 100 hours of oxidation in air. The Ni_3Al coated sample gained substantial mass for 500 hours oxidation in air. It is speculated that the increase in mass change for coated samples initially is because of oxidation, due to intake of oxygen by the coating with subsequent aluminium and nickel oxide formation. Oxide development at the splat boundaries in the coating could be the reason for early high mass gain.[169] Fast uptake of O within first 500 hour is

because the coating is O_2 vacant. It acts as a sink and stabilises after filling up with O_2. It is suggested that after initial oxidation, the coating reach a saturation point with oxygen, hence stabilizing the mass. The actual mass change to be considered in case of coated sample would be the $OR_{steadystate}$ as the coatings could be pre-conditioned to reach the time t-1 before solar salt immersion (Figure 39).

It can be stated that the coating supresses, either delays or stops the formation of the oxides on the surface of the sample, however, fundamental mechanism is still unknown, and the exact nature of the process cannot be ensured within the scope of this study. The coating grows dense after the oxide development resulting in initial mass gain, preventing any further diffusion.[169] This implies the coatings are protective, inhibiting any oxide formation on the substrate surface.

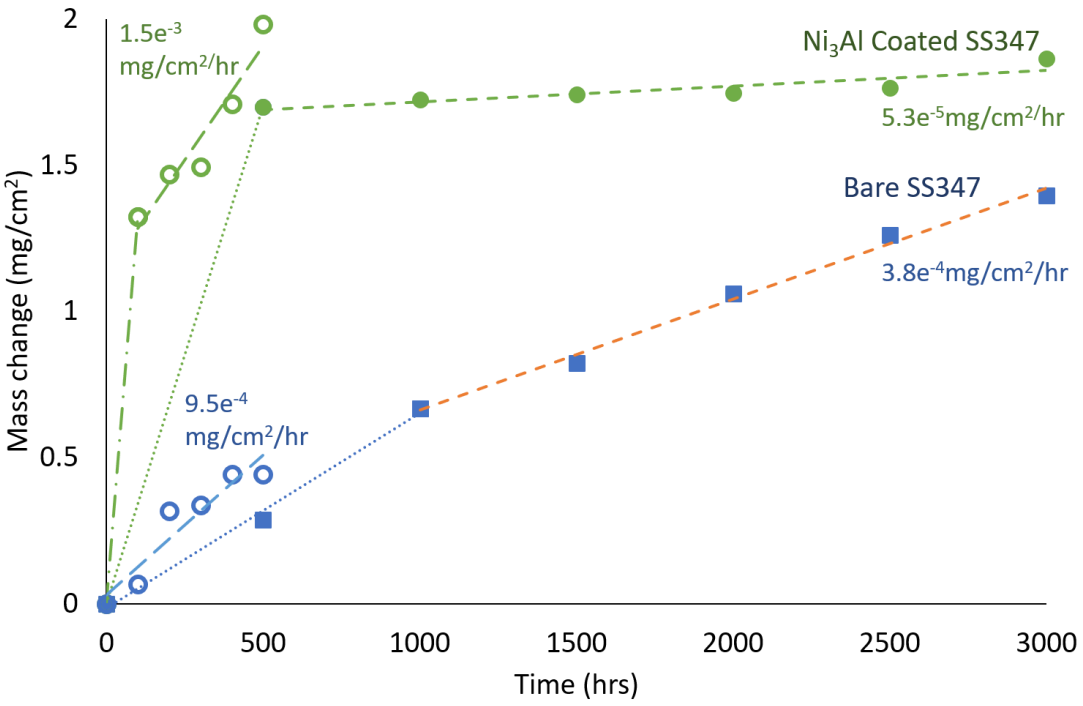

Figure 38: Time dependent mass change (mg/cm^2) of SS347 and Ni_3Al coated SS347 in air (un-filled markers) and solar salt (solid fill markers) at 565^{o}C. The behaviour in molten salt was observed for 3000 hrs based on measurements every 500 hrs, while that in air was observed for 500 hrs based on measurement every 100 hrs. Here, the mass change is presented as an absolute accumulative value.

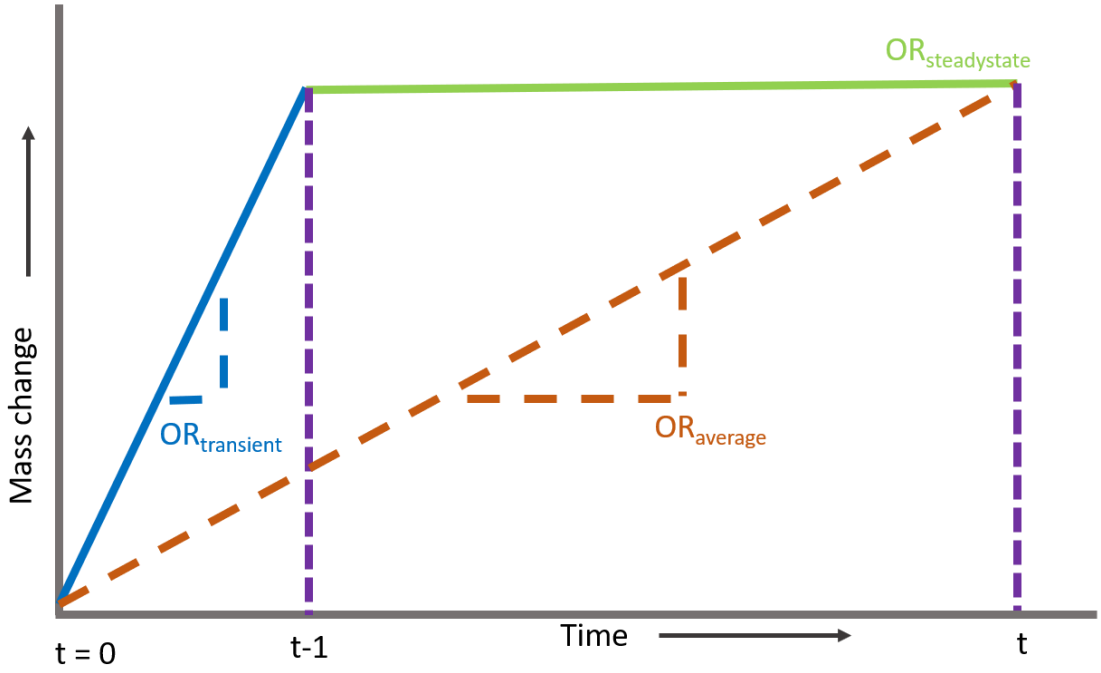

Figure 39: Mass change is the slope of the curve, plotted for mass change against time. $OR_{transient}$ is the oxide growth rate in the transient behaviour and $OR_{steady\ state}$ apparent oxide growth rate for a steady state behaviour is not equal to zero.

6 CONCLUSIONS

The main goal of the project was to test the hypothesis that "Ni_3Al coatings will provide corrosion resistance in solar salt at 565^oC". Several precise objectives were devised to attain this goal. In conclusion, the project has successfully met the objectives. The details of how the research met objectives is described as follows.

1. Critical literature review of state - of - the - art alloys in presence of molten salt is provided. A number of technologies have been developed to use solar energy for power generation. Among them, an important feature of concentrating solar power (CSP) plants is the potential incorporated thermal storage. The capability to store heat permits plants to produce electricity during the periods of cloud cover and low solar radiations. Several possibilities for HTF and TES have been identified. From wide range of materials, solar salt was selected as appropriate because of high thermal stability and low cost as compared to chlorides and carbonates. Different approaches to prolong life by suppressing corrosion have been suggested in literature, coating is best because coatings are believed as a way to provide shield against corrosion while holding the mechanical properties of substrate. Among different coatings, Nickel aluminide has been claimed to possess high-temperature mechanical strength and has a remarkable oxidation resistance performance as substrate component and it has low solubility in the molten nitrate salt. Ni_3Al coatings are much preferred to be used as corrosion resistant coatings as they possess strength at raised temperature, oxidation protection and creep properties. Among different deposition techniques, plasma spray has been identified as most applicable because it is versatile, adaptable cost effective, has high deposition rate and deposition efficiency and less environmental impact, more importantly it is easy to scale up. A regression fitting has been used to predict corrosion rate in molten salt.
2. Ni_3Al coatings were developed by plasma spray technique on stainless steel 347 along with long term corrosion tests and corresponding materials characterisation.

3. Plasma spray is selected as the deposition process as it was identified based on literature. A protocol was produced to deposit nickel aluminide coatings using LVPS and APS has been established. Corrosion behaviour has been developed in molten nitrate (60 wt %$NaNO_3$ + 40 wt % KNO_3) salt at 565^oC for 3000 hours. Assessment was done using mass change measurement, SEM, EDX and XRD. A few trials were done with Ni-18 and $NiAl_3$ coatings deposited using LVPS technique. The Ni_3Al coated SS347 samples using APS deposition were produces and seen to be uniform, adherent, homogenous with very low porosity. The developed coatings were characterised using mass change measurement, SEM, EDX and XRD, according to protocol established in above point. The Ni_3Al coated SS347 samples using APS deposition were used for corrosion tests in molten nitrate $NaNO_3$:KNO_3 (60:40) salt at 565^oC for 500 hours intervals up to 3000 hours.
4. Evaluated and compared corrosion resistance of bare substrate material and coated substrate samples Underlying corrosion mechanisms in Ni_3Al coated SS347 have been identified. The corrosion tests were carried out to evaluate the performance of developed coatings in the solar salt at 565^oC for 500 hours intervals up to 3000 hours. Corrosion takes place on the bare SS347 sample after exposure to molten nitrate salt. Fe and Cr diffuse outwards from the bare SS347 sample. There is formation of $NaFeO_x$, FeO and $(Cr,Fe)O_x$ on the bare SS347 sample surface. The apparent mass change for bare SS347 is 4 mg/cm^2/yr, equivalent to oxide growth rate of ~ 5 µm/yr. For Ni_3Al coated SS347 samples, in the first few hundred hours coating gets oxidised quick, shown by densification and mass gain and presence of oxygen. However, there is no diffusion of Fe, Cr or Ni outwards from the substrate, and no Na inwards from molten salt, at least not observed during the 3000 hours exposure. The fact, that Ni_3Al coated SS347 gives mass change of one order of magnitude lower than the bare SS347, means it can be used to prolong the lifetime of bare SS347 in solar salt at 565^oC. Hence the hypothesis that "Ni_3Al coatings will provide corrosion resistance in solar salt at 565^oC" is verified. Apparent mass change with immersion time is measured ~ 29.8 mg/cm^2/yr for 0 to 500 hours and 0.5 mg/cm^2/yr for 500 to 3000 hours for Ni_3Al coated

SS347. The corresponding oxide growth rates are ~44.6 µm/yr for 0 to 500 hours and ~0.7 µm/yr for 500 to 3000 hours for Ni_3Al coated SS347.

6.1 Estimated Material Cost

A 300 MW CSP plant with 8 hours storage requires salt container of size ~ 35 m diameter, ~ 12.5 m height. The molten salt container made with 15 mm thick wall of SS347 costs ~ £ 1.7 M while the container made with 30 mm thick wall of SS347 would cost ~ £ 3.4 M. The material cost of raw slabs of Ni_3Al is ~ £ 10,000/metric tons. The total Ni_3Al needed for 100 µm thick coating is ~ 9.8 metric tons. Total material cost of Ni_3Al coatings with 25% coating efficiency is ~ £ 0.1 M and the total deposition cost is ~ £ 0.7 M. The molten salt container cost with Ni_3Al coated SS347 is ~ £ 2.4 M, including cost for 15 mm SS347, 100 µm thick coating material and deposition cost. Hence the material cost with coatings does not exceed cost of double wall thickness. Implying the use of proposed Ni_3Al coatings enable low manufacturing cost

6.2 Impact and Innovation

Primary impact of this study is the contribution to knowledge and capacity for developing corrosion resistance coating for use in TES integrated CSP plants. Among the existing CSP plants few have integrated TES while the others do not have TES. The capability to store heat permits plants to produce electricity during the periods of cloud cover and low solar radiations.[64] The use of TES could allow production of electricity throughout day and night.

CSP could flourish in the areas with abundance of direct normal sunlight, which is mostly near equator, where most underdeveloped countries are located. These countries could benefit from the greener electricity from CSP plants, however CSP without TES does not solve the purpose, TES is an integral part of CSP. The use of TES reduces the operating cost, yet the containment material of the TES system encounters corrosion problems, limiting the lifetime of the material. The use of proposed coatings enables longer lifespan of the TES containment system. This is one of innovation of this study because it enables large scale use

of the TES integrated CSP technology. To make CSP available to wider range of countries and population is by use of these coatings.

An innovative concept of using corrosion resistant coatings presented here has not been explored in the past for this particular application. The use of proposed coatings may allow ten times longer lifespan if the behaviour remains same when extrapolated. Protective coatings have been used in gas turbines and other applications in the past but not CSP-TES.[145,219,220] A comprehensive database of corrosion resistance information of several alloys and coatings in molten salt environments at different temperatures is compiled. A novel empirical model has been developed for predicting mass change of alloys and coatings for specific molten salt environments at certain temperatures based on previous studies reported in literature. The development of new protective coatings will affect the economy of CSP industry by preventing the need of expensive alloys for the use in thermal energy storage containers. The use of CSP technology is preferred over other power generation such as nuclear power plants because it helps environment by providing clean energy. In this work corrosion resistance of Ni_3Al protective coatings was evaluated for up to 3000 hours in solar salt environment at 565^{o}C. There has been a number of studies regarding corrosion tests of various alloys on exposure to molten nitrate salt however no work has been found to have explored the use of protective coatings to be used with molten nitrate salt at 565^{o}C.

One of the innovations of this study is that the use of proposed coatings the use of proposed coatings makes it economically viable to increase thermal storage capacity by enabling the use of material cost. The proposed coating enables low operating cost, by allowing the use of integrated TES in the CSP plants. As the use of TES system decreases the annual operation and maintenance costs.[221] A decrease in levelised electricity cost (LCOE) of about 10 % has been stated for integrating a 12 hour storage capacity TES system.[222] Any damage or destruction to storage system in a CSP could cause a substantial effect economically. As a precaution any such destruction due to corrosion should be to be addressed to avoid any possible risks of breakdown. The cost of breakdown would differ

dependent on the suffered damage, cost of amendments, cost of shut - down time and fines by local regulations.[13] The storage system consists of the storage medium, one or multiple storage tanks, piping, instruments and controls. The cost of the tank is only a fraction, about 15 to 30 % of the total cost of storage system.[11] A detailed design analysis for costs, economies and performance needs to be done for best possible TES composition and CSP plant setup.[129] One approach to keep the cost minimum is to use containment material that is compatible with the storage and heat transfer fluid. Assuming material for the container, the wall thickness of the container needs to be at least 30 mm thick to achieve 30 years lifespan.[21] The cost of commercial mixtures of molten nitrate (60wt% $NaNO_3$+ 40wt% KNO_3) salt is £ 0.30 / kg for Solar Salt, £ 0.72 for Hitec and £ 1.11 / kg for Hitec XL.[223] A typical two-tank TES system of molten salt in a CSP plant costs in the range of 30 to 40 GBP/kWhth, with 49% corresponding to molten salt, 16% for storage tanks, 10% for heat exchangers, 7% for construction's foundation, 4% for insulation, and 14% for other miscellaneous costs.[84] The TES system cost is about 15 to 25% of the total initial cost of the CSP plant.[13]

It is suggested that coating cost, time and coating quality are the factors influencing the total coating cost.[126] The proposed coatings for the thermal energy storage systems are technologically feasible and economically viable. The proposed coatings for the thermal energy storage systems are economically viable. APS technique is cost effective for use in large scale deposition of coatings. APS system can be placed inside the salt container for onsite deposition of anticorrosion coatings on the inner surface of the container. For a salt container with a diameter of 35 m and a height of 12.5 m, the total material cost for Ni_3Al coated SS 347 is calculated to be about £ 4.03 Million, which is less than half of that if it is to be made of HA214 (£ 8.59) and one fourth of the estimated cost if the container is to be made of In625 (£ 15.85). (submission 5 Scaling up of developed coatings). It will be cheaper than using specialised alloys such as HA217 or Inconel 625.[126] In comparison to stainless steel, it will be only fractionally expensive but will prolong the lifetime. The thickness of base material could be reduced to accommodate coating to moderate this fractional cost difference. Thus, Ni_3Al anticorrosion coating developed provides a viable solution

to allow the use of cheaper and machinable alloys in large scale CSP applications. Concentrated solar power can be used more widely with a lower levelized cost of electricity hence more clean energy and less carbon emissions from burning fossil fuels

6.3 Contribution to knowledge

This study has contributed to knowledge as following.

- A method to estimate corrosion rate from the slope of weight change versus time plot is specified, corrosion rate has to be measured from the overall trend in weight change rather than one value at maximum immersion time. Typically, corrosion rate is measured using the weight change at the maximum immersion time, however, the trend in weight change is not same during the entire molten salt immersion, hence does not provide the correct measurement of overall weight change trend.
- The weight change in relation to thickness has been studied for bare SS347.
- Ni_3Al coated SS347 undergoes rapid oxidation within first 500 hours of solar salt immersion at 565^{o}C.
- The use of Ni_3Al coating to protect stainless steel in presence of molten nitrate salts is demonstrated with potential direct industrial impact. The use of proposed coatings may allow ten times longer lifespan if the behaviour remains same when extrapolated and make it economically viable to increase thermal storage capacity.

6.4 Research Limitations & Suggested Future Work

In order to achieve a thorough understanding of the corrosion performance of the thermal energy storage system components in contact with molten nitrate salt, other alloys and coating systems should also be investigated for corrosion resistance. It was supposed during this study that the capacity to develop an adhesive and consistent oxide layer without cracks or pores, suggests the alloy and coating system possess good corrosion protection properties.

The above-mentioned corrosion evaluation of Ni_3Al coated SS347 stainless steel samples on exposure to molten nitrate salt at 565°C has established promising

corrosion resistance characteristics exhibited by the test samples. There is a huge parameter space, but it is not possible to test all within given timescale. Nevertheless, additional corrosion tests should be performed at different temperatures other than 565°C, test for 100 hours intervals for at least first 500 hours to gain understanding of corrosion initiation process and also cyclic corrosion tests should be performed. Different coating techniques should be tested. This will expand the grasp and knowledge of the corrosion behaviour of Ni_3Al coated SS347 stainless steel samples on exposure to molten nitrate salt at 565°C. Pure alumina coatings should be tested as well to check if they offer similar corrosion protection in presence of molten nitrate salt at 565°C. Another interesting study could be to examine and evaluate the molten nitrate salt during and after the corrosion tests.

It can be stated that the coating supresses, either delays or stops the formation of the oxides on the surface of the sample, but basic mechanisms are still unknown within the scope of this study. Because thickness of coating is ~ 100 µm which is much thicker than oxide layers formed on the bare SS347 samples at 3000 hours. It cannot be determined whether it is delaying or stopping the oxide formation on the surface. It is inconclusive at the moment for 3000 hours. Further tests with longer time or thinner coatings to understand mechanism if coating will delay or stop the oxidation, should be carried out.

There was limitation on the number of samples because of the size of the furnace. Hence only a number of selected samples were tested for corrosion for each 500 hours interval. It is suggested to test a larger number of samples to assess the corrosion performance, get better understanding and statistically significant results.

The above suggestions are to refine the investigations, however it would be interesting to see if future work focuses on different coating deposition techniques, for example HIPIMS produces thinner and higher-density coatings. The test with longer duration would allow to observe failure of bare substrate and coating. Further test with smaller time intervals during transient stage to understand the phenomena can be carried out, too. Accelerated test can reduce

the test time by increase in the test temperature. Oxidation test with longer duration to separate the effect of oxygen and molten salt. Corrosion test in molten salt and oxidation tests in air should be carried out in parallel for 100 hours intervals up to at least 1000 hours, to understand underlying mechanisms and differentiate between oxidation and corrosion result. Field test should be done to observe the coatings in actual environment with fluctuating solar flux, wind and dust as compared to steady temperatures in laboratory tests. It would be fascinating to precondition the coated samples by annealing them in air before introduction to molten nitrate salts at 565^{o}C.

REFERENCES

[1] Pennetta, S., Yu, S., Borghesani, P., Cholette, M., Barry, J. and Guan, Z., “An investigation on factors influencing dust accumulation on CSP mirrors,” AIP Conf. Proc. **1734** (2016).

[2] Rohani, S., Abdelnabi, N., Fluri, T., Heimsath, A., Wittwer, C. and Ainsua, J. G. P., “Optimized mirror cleaning strategies in PTC plants reducing the water consumption and the levelized cost of cleaning,” AIP Conf. Proc. **2126**(July) (2019).

[3] Sayyah, A., Horenstein, M. N. and Mazumder, M. K., “Mitigation of soiling losses in concentrating solar collectors,” Conf. Rec. IEEE Photovolt. Spec. Conf.(September 2015), 480–485 (2013).

[4] Xu, X., Vignarooban, K., Xu, B., Hsu, K. and Kannan, A. M., “Prospects and problems of concentrating solar power technologies for power generation in the desert regions,” Renew. Sustain. Energy Rev. **53**, 1106–1131 (2016).

[5] Fares, M. S. Ben and Abderafi, S., “Water consumption analysis of Moroccan concentrating solar power station,” Sol. Energy **172**(June), 146–151 (2018).

[6] Santos, J. J. C. S., Palacio, J. C. E., Reyes, A. M. M., Carvalho, M., Freire, A. J. R. and Barone, M. A., “Concentrating Solar Power,” Adv. Renew. Energies Power Technol. **1**(2), 373–402 (2018).

[7] Mazumder, M., Horenstein, M., Stark, J., Hudelson, J. N., Sayyah, A., Heiling, C. and Yellowhair, J., “Electrodynamic removal of dust from solar mirrors and its applications in concentrated solar power (CSP) plants,” 2014 IEEE Ind. Appl. Soc. Annu. Meet. IAS 2014(December) (2014).

[8] BRITISH PETROLEUM COMPANY. (1981). BP statistical review of world energy. London, B. P. C., “67 th edition Contents is one of the most widely respected,” Stat. Rev. World Energy, 1–56 (2018).

[9] UNCCS., “Climate action and support trends,” United Nations Clim. Chang.

Secr. (2019).

[10] Stark, C., Thompson, M., Andrew, T., Beasley, G., Bellamy, O., Budden, P., Cole, C., Darke, J., Davies, E., Feliciano, D. and Gault, A., “Net Zero The UK’s contribution to stopping global warming,” 277 (2019).

[11] Liu, M., Steven Tay, N. H., Bell, S., Belusko, M., Jacob, R., Will, G., Saman, W. and Bruno, F., “Review on concentrating solar power plants and new developments in high temperature thermal energy storage technologies,” Renew. Sustain. Energy Rev. **53**, 1411–1432 (2016).

[12] Members, R. E. N., [Renewables 2019 Global Status Report] (2019).

[13] Walczak, M., Pineda, F., Fernández, Á. G., Mata-Torres, C. and Escobar, R. A., “Materials corrosion for thermal energy storage systems in concentrated solar power plants,” Renew. Sustain. Energy Rev. **86**(March 2017), 22–44 (2018).

[14] Barlev, D., Vidu, R. and Stroeve, P., “Innovation in concentrated solar power,” Sol. Energy Mater. Sol. Cells **95**(10), 2703–2725 (2011).

[15] Murdock, H. E., [Renewables 2019 Global Status Report Collaborative] (2019).

[16] Solargis., “GLOBAL SOLAR ATLAS,” World Bank Gr., 2019, <https://worldbank-atlas.com>.

[17] NREL., “NREL: Concentrating Solar Power Projects - Concentrating Solar Power Projects with Operational Plants,” 2019, <https://solarpaces.nrel.gov/by-technology/power-tower> (15 November 2019).

[18] U.S. Department of Energy., “2014: The Year of Concentrating Solar Power” (2014).

[19] Abengoa., “Abengoa Solar” (2008).

[20] E. ZARZA MOYA., “Concentrating Solar Power Technology, Principles, Developments and Applications,7 Parabolic-trough concentrating solar

power (CSP) systems," 197–239 (2012).

[21] Kelly, B. and Kearney, D., "Thermal storage commercial plant design study for a 2-tank indirect molten salt system" (2006).

[22] Yang, H. J., Lim, S. Y. and Yoo, S. H., "The environmental costs of photovoltaic power plants in South Korea: A choice experiment study," Sustain. **9**(10), 1–13 (2017).

[23] Fthenakis, V. M., "Overview of potential hazards," 6–8 (2003).

[24] Lamnatou, C. and Chemisana, D., "Photovoltaic/thermal (PVT) systems: A review with emphasis on environmental issues," Renew. Energy **105**, 270–287 (2017).

[25] Sims, D., "Rare earths and other chemicals damaging the environmental value of renewables," 2019, <https://new.engineering.com/story/rare-earths-and-other-chemicals-damaging-the-environmental-value-of-renewables> (6 May 2020).

[26] -Galvan, R., F., Barranco, V., Galvan, J. C., Batlle, Sebastian FeliuFajardo, S. and García., "We are IntechOpen , the world ' s leading publisher of Open Access books Built by scientists , for scientists TOP 1 %," Intech **i**(tourism), 13 (2016).

[27] NUNEZ, C., "How Green Are Those Solar Panels, Really," Natl. Geogr. Mag., 2014, <https://www.nationalgeographic.com/news/energy/2014/11/141111-solar-panel-manufacturing-sustainability-ranking/> (6 May 2020).

[28] Andreani, L. C., Bozzola, A., Kowalczewski, P., Liscidini, M. and Redorici, L., "Silicon solar cells: Toward the efficiency limits," Adv. Phys. X **4**(1) (2019).

[29] Mustafa, R. J., Gomaa, M. R., Al-Dhaifallah, M. and Rezk, H., "Environmental impacts on the performance of solar photovoltaic systems," Sustain. **12**(2), 1–17 (2020).

[30] Ahmed, H., McCormack, S. J. and Doran, J., “External Quantum Efficiency Improvement with Luminescent Downshifting Layers: Experimental and Modelling,” Int. J. Spectrosc. **2016**, 1–7 (2016).

[31] Xie, J. bo, Fu, J. xun, Liu, S. yu and Hwang, W. sing., “Assessments of carbon footprint and energy analysis of three wind farms,” J. Clean. Prod. **254** (2020).

[32] Nazir, M. S., Ali, N., Bilal, M. and Iqbal, H. M. N., “Potential environmental impacts of wind energy development: A global perspective,” Curr. Opin. Environ. Sci. Heal. **13**, 85–90 (2020).

[33] Erickson, W. P., Wolfe, M. M., Bay, K. J., Johnson, D. H. and Gehring, J. L., “A comprehensive analysis of small-passerine fatalities from collision with turbines at wind energy facilities,” PLoS One **9**(9) (2014).

[34] Pezy, J. P., Raoux, A. and Dauvin, J. C., “The environmental impact from an offshore windfarm: Challenge and evaluation methodology based on an ecosystem approach,” Ecol. Indic. **114**(November 2019), 106302 (2020).

[35] Leung, D. Y. C. and Yang, Y., “Wind energy development and its environmental impact: A review,” Renew. Sustain. Energy Rev. **16**(1), 1031–1039 (2012).

[36] Arnett, E. B., Inkley, D. B., Johnson, D. H., Larkin, R. P., Manes, S., Manville, A. M., Mason, J. R., Morrison, M. L., Strickland, M. D. and Thresher, R., “Impacts of Wind Energy Facilities on Wildlife and Wildlife Habitat,” Wildl. Soc. Tech. Rev. 07-2(September), 1–51 (2007).

[37] Lintott, P. R., Richardson, S. M., Hosken, D. J., Fensome, S. A. and Mathews, F., “Ecological impact assessments fail to reduce risk of bat casualties at wind farms,” Curr. Biol. **26**(21), R1135–R1136 (2016).

[38] Saidur, R., Rahim, N. A., Islam, M. R. and Solangi, K. H., “Environmental impact of wind energy,” Renew. Sustain. Energy Rev. **15**(5), 2423–2430 (2011).

[39] Hao, S., Kuah, A. T. H., Rudd, C. D., Wong, K. H., Lai, N. Y. G., Mao, J. and Liu, X., “A circular economy approach to green energy: Wind turbine, waste, and material recovery,” Sci. Total Environ. **702**, 135054 (2020).

[40] Bošnjaković, M. and Tadijanović, V., “Environment impact of a concentrated solar power plant,” Teh. Glas. **13**(1), 68–74 (2019).

[41] Brand, B., Boudghene Stambouli, A. and Zejli, D., “The value of dispatchability of CSP plants in the electricity systems of Morocco and Algeria,” Energy Policy **47**, 321–331 (2012).

[42] Price, H., Kearney, D., Redell, F., Charles, R. and Morse, F., “Dispatchable solar power plant,” AIP Conf. Proc. **2033** (2018).

[43] Yasin, A. M., “The Impact of Dispatchability of Parabolic Trough CSP Plants over PV Power Plants in Palestinian Territories,” Int. J. Photoenergy **2019** (2019).

[44] Li, R., Zhang, H., Wang, H., Tu, Q. and Wang, X., “Integrated hybrid life cycle assessment and contribution analysis for CO2 emission and energy consumption of a concentrated solar power plant in China,” Energy **174**, 310–322 (2019).

[45] Achkari, O. and El Fadar, A., “Latest developments on TES and CSP technologies – Energy and environmental issues, applications and research trends,” Appl. Therm. Eng. **167**(August 2019), 114806 (2020).

[46] Nieto-Maestre, J., Muñoz-Sánchez, B., Fernández, A. G., Faik, A., Grosu, Y. and García-Romero, A., “Compatibility of container materials for Concentrated Solar Power with a solar salt and alumina based nanofluid: A study under dynamic conditions,” Renew. Energy **146**, 384–396 (2020).

[47] California ISO., “Energy and environmental goals drive change” (2016).

[48] Denholm, P., O’Connell, M., Brinkman, G. and Jorgenson, J., “Overgeneration from Solar Energy in California: A Field Guide to the Duck Chart (NREL/TP-6A20-65023),” Tech. Rep.(November), 46 (2015).

[49] Gasia, J., Miró, L. and Cabeza, L. F., “Review on system and materials requirements for high temperature thermal energy storage. Part 1: General requirements,” Renew. Sustain. Energy Rev. **75**(December 2016), 1320–1338 (2017).

[50] Bonk, A., Sau, S., Uranga, N., Hernaiz, M. and Bauer, T., “Advanced heat transfer fluids for direct molten salt line-focusing CSP plants,” Prog. Energy Combust. Sci. **67**, 69–87 (2018).

[51] Lovegrove, K. and Pye, J., “Fundamental principles of concentrating solar power (CSP) systems,” Conc. Sol. Power Technol. Princ. Dev. Appl., 16–67 (2012).

[52] Fernández, a. G., Lasanta, M. I. and Pérez, F. J., “Molten salt corrosion of stainless steels and low-Cr steel in CSP plants,” Oxid. Met. **78**, 329–348 (2012).

[53] Lovegrove, K. and Csiro, W. S., “Introduction to concentrating solar power (CSP) technology,” Conc. Sol. Power Technol. Princ. Dev. Appl., 3–15 (2012).

[54] Casati, E., Casella, F. and Colonna, P., “Design of CSP plants with optimally operated thermal storage,” 371–387 (2015).

[55] Dehghani-Sanij, A. R., Tharumalingam, E., Dusseault, M. B. and Fraser, R., “Study of energy storage systems and environmental challenges of batteries,” Renew. Sustain. Energy Rev. **104**(November 2018), 192–208 (2019).

[56] Gallegos, M. V., Falco, L. R., Peluso, M. A., Sambeth, J. E. and Thomas, H. J., “Recovery of manganese oxides from spent alkaline and zinc-carbon batteries. An application as catalysts for VOCs elimination,” Waste Manag. **33**(6), 1483–1490 (2013).

[57] Godt, J., Scheidig, F., Grosse-Siestrup, C., Esche, V., Brandenburg, P., Reich, A. and Groneberg, D. A., “The toxicity of cadmium and resulting hazards for human health,” J. Occup. Med. Toxicol. **1**(1), 1–6 (2006).

[58] Mousavi, S. R., Balali-Mood, M., Riahi-Zanjani, B., Yousefzadeh, H. and Sadeghi, M., “Concentrations of mercury, lead, chromium, cadmium, arsenic and aluminum in irrigation water wells and wastewaters used for agriculture in mashhad, northeastern Iran,” Int. J. Occup. Environ. Med. **4**(2), 80–86 (2013).

[59] Mezei, F., [Basics Concepts] (2011).

[60] Tarragó, O., “Lead Toxicity Case Studies in Environmental Medicine,” Lead Toxic. Case Stud. Environ. Med. (2015).

[61] Bernard, A., “Cadmium & its adverse effects on human health,” Indian J. Med. Res. **128**(4), 557–564 (2008).

[62] European Commission., “Report on Raw Materials for Battery Applications - COMMISSION STAFF WORKING DOCUMENT,” Comm. Staff Work. Doc., 1–48 (2018).

[63] Sarbu, I. and Sebarchievici, C., “A comprehensive review of thermal energy storage,” Sustain. **10**(1) (2018).

[64] IEA., “Technology Roadmap,” 2010, <https://www.iea.org/roadmaps/>.

[65] Pérez, F. J., Encinas-Sánchez, V., García-Martín, G., Lasanta, M. I. and De Miguel, M. T., “Dynamic pilot plant facility for applications in CSP: Evaluation of corrosion resistance of A516 in a nitrate molten salt mixture,” AIP Conf. Proc. **1850**(December 2016), 226–231 (2017).

[66] Kuravi, S., Goswami, Y., Stefanakos, E. K., Ram, M., Jotshi, C., Pendyala, S., Trahan, J., Sridharan, P., Rahman, M. and Krakow, B., “Thermal Energy Storage technologies and systems for Concentrating Solar Power Plants,” Technol. Innov. **14**(2), 81–91 (2013).

[67] Tian, Y. and Zhao, C.-Y., “A review of solar collectors and thermal energy storage in solar thermal applications,” 538–553 (2013).

[68] Kuravi, S., Goswami, D. Y., Stefanakos, E. K., Ram, M., Jotshi, C., Trahan, J., Sridharan, P., Rahman, M. and Krakow, B., “Thermal energy storage for

concentrating solar power plants," Clean energy Res. center, Univ. South Florida.

[69] Kenisarin, M. M., "High-temperature phase change materials for thermal energy storage," Renew. Sustain. Energy Rev. **14**(3), 955–970 (2010).

[70] Diaz, P. ., "Analysis and Comparison of different types of Thermal Energy Storage Systems: A Review," J. Adv. Mech. Eng. Sci. **2**(1), 33–46 (2016).

[71] Pfleger, N., Bauer, T., Martin, C., Eck, M. and Wörner, A., "Thermal energy storage - overview and specific insight into nitrate salts for sensible and latent heat storage," Beilstein J. Nanotechnol. **6**(1), 1487–1497 (2015).

[72] Kuravi, S., Goswami, D. Y., Stefanakos, E. K., Ram, M., Jotshi, C., Trahan, J., Sridharan, P., Rahman, M. and Krakow, B., "THERMAL ENERGY STORAGE FOR CONCENTRATING SOLAR POWER PLANTS Sarada Kuravi, D. Yogi Goswami, Elias K. Stefanakos, Manoj Ram, Chand Jotshi, Swetha Pendyala, Jamie Trahan, Prashanth Sridharan, Muhammad Rahman and Burton Krakow Clean Energy Research Center, U," Technol. Innov. **14**(Feburary), 81–91 (2012).

[73] Rutberg, M., Hastbacka, M., Cooperman, A. and Bouza, A., "Thermal energy storage," ASHRAE J. **55**(6), 62–66 (2013).

[74] Breidenbach, N., Martin, C., Jockenhöfer, H. and Bauer, T., "Thermal Energy Storage in Molten Salts: Overview of Novel Concepts and the DLR Test Facility TESIS," Energy Procedia **99**(March), 120–129 (2016).

[75] Tian, Y. and Zhao, C.-Y., "A review of solar collectors and thermal energy storage in solar thermal applications," Appl. Energy **104**, 538–553 (2013).

[76] Gill, D. D., Bradshaw, R. W. and Siegel, N. P., "Compatibility Testing in Nitrate Salts At Temperatures Up To 700 ° C," 1–6 (2011).

[77] Nissen, D. A. and Meeker, D. E., "Nitrate/Nitrite Chemistry in NaN03-KN03 Melts," Inorg. Chem. **22**(5), 716–721 (1983).

[78] Novello, F., Dedry, O. and V, D. N., "High Temperature Corrosion

Resistance of Metallic Materials in Harsh Conditions."

[79] Silverman, M. D. and Engel, J. R., "Survey of Technology for Storage of Thermal Energy in Heat Transfer Salt," 32 (1977).

[80] Vignarooban, K., Xu, X., Arvay, A., Hsu, K. and Kannan, A. M., "Heat transfer fluids for concentrating solar power systems - A review," Appl. Energy **146**, 383–396 (2015).

[81] Raade, J. W. and Padowitz, D., "Development of Molten Salt Heat Transfer Fluid With Low Melting Point and High Thermal Stability," J. Sol. Energy Eng. **133**(3), 031013 (2011).

[82] Peng, Q., Yang, X., Ding, J., Wei, X. and Yang, J., "Design of new molten salt thermal energy storage material for solar thermal power plant," Appl. Energy **112**, 682–689 (2013).

[83] Delise, T., Tizzoni, A. C., Votyakov, E. V., Turchetti, L., Corsaro, N., Sau, S. and Licoccia, S., "Modeling the Total Ternary Phase Diagram of NaNO3–KNO3–NaNO2 Using the Binary Subsystems Data," Int. J. Thermophys. **41**(1) (2020).

[84] Steinmann, W. D., "Thermal energy storage systems for concentrating solar power (CSP) plants," Conc. Sol. Power Technol. Princ. Dev. Appl., 362–394 (2012).

[85] Cleantech, A., "Azocleantech."

[86] Olivares, R. I., Chen, C. and Wright, S., "The Thermal Stability of Molten Lithium–Sodium–Potassium Carbonate and the Influence of Additives on the Melting Point," J. Sol. Energy Eng. **134**(4), 041002 (2012).

[87] Zhang, H. L., "Concentrated solar power plants: Review and design methodology," Renew. Sustain. Energy Rev. **22**, 466–481 (2013).

[88] Dunn, R. I., Hearps, P. J. and Wright, M. N., "Molten-salt power towers: Newly commercial concentrating solar storage," Proc. IEEE **100**(2), 504–515 (2012).

[89] Agüero, A., Audigié, P., Rodríguez, S., Encinas-Sánchez, V., De Miguel, M. T. and Pérez, F. J., “Protective coatings for high temperature molten salt heat storage systems in solar concentration power plants,” AIP Conf. Proc. **2033**(November), 1–9 (2018).

[90] Khorsand, S., Sheikhi, A., Raeissi, K. and Golozar, M. A., “Hot Corrosion Behavior of Inconel 625 Superalloy in Eutectic Molten Nitrate Salts,” Oxid. Met., 1–18 (2018).

[91] Benages-Vilau, R., Calvet, T., Cuevas-Diarte, M. A. and Oonk, H. A. J., “The NaNO3-KNO3 phase diagram,” Phase Transitions **89**(1), 1–20 (2016).

[92] Kramer, C. M. and Wilson, C. J., “The phase diagram of NaNO3-KNO3,” Thermochim. Acta **42**(3), 253–264 (1980).

[93] Merzlyakov, K. S. and Uglev, N. P., “Phase Diagram of the NaNO2 - KNO3 System in the 0 to 1 Molar Fraction Range of Concentrations of KNO3,” Russ. J. Phys. Chem. A **90**(4), 882–883 (2016).

[94] Mohammad, M. Bin, Cadusch, P., Brooks, G. A. and Rhamdhani, M. A., “The Binary Alkali Nitrate and Chloride Phase Diagrams: NaNO3-KNO3, LiNO3-NaNO3, LiNO3-KNO3, and NaCl-KCl,” Metall. Mater. Trans. B Process Metall. Mater. Process. Sci. **49**(6), 3580–3593 (2018).

[95] Tizzoni, A. C., Sau, S., Corsaro, N., Giaconia, A., D’Ottavi, C. and Licoccia, S., “Thermal fluids for CSP systems: Alkaline nitrates/nitrites thermodynamics modelling method,” AIP Conf. Proc. **1734**(May) (2016).

[96] Zhang, X., Tian, J., Xu, K. and Gao, Y., “Thermodynamic Evaluation of Phase Equilibria in NaNo3-KNO 3 System,” J. Phase Equilibria **24**(5), 441–446 (2003).

[97] Bauer, T., Laing, D. and Tamme, R., “Overview of PCMs for Concentrated Solar Power in the Temperature Range 200 to 350°C,” Adv. Sci. Technol. **74**, 272–277 (2010).

[98] Bene, O., Konings, R. J. M., Wurzer, S., Sierig, M. and Dockendorf, A., “A DSC study of the NaNO3-KNO3 system using an innovative encapsulation technique,” Thermochim. Acta **509**(1–2), 62–66 (2010).

[99] Delise, T., Tizzoni, A. C., Ferrara, M., Corsaro, N., D’Ottavi, C., Giaconia, A., Turchetti, L., Annesini, M. C., Telling, M., Sau, S. and Licoccia, S., “New solid phase of KNO3 - NaNO3 salt mixtures studied by neutron scattering and differential scanning calorimetry analysis,” AIP Conf. Proc. **2033**(November 2018) (2018).

[100] Bradshaw, R. W. and Goods, S. H., “Corrosion Resistance of Stainless Steels During Thermal Cycling in Alkali Nitrate,” Sandia Rep. **SAND2001-8**(September), 1–39 (2001).

[101] Tortorelli, P. F., Bishop, P. S. and DiStefano, J. R., “Selection of Corrosion-Resistant Materials for Use in Molten Nitrate Salts,” Oak Ridge Natl. Lab., 62 (1989).

[102] Soleimani Dorcheh, A. and Galetz, M. C., “Slurry aluminizing: A solution for molten nitrate salt corrosion in concentrated solar power plants,” Sol. Energy Mater. Sol. Cells **146**, 8–15 (2016).

[103] Slusser, J. W., Titcomb, J. B., Heffelfinger, M. T. and Dunbobbin, B. R., “Corrosion in Molten Nitrate-Nitrite Salts,” J. Met. **37**(7), 24–27 (1985).

[104] Goods, S. H. and Bradshaw, R. W., “Corrosion of Stainless Steels and Carbon Steel by Molten Mixtures of Commercial Nitrate Salts,” J. Mater. Eng. Perform. **13**(1), 78–87 (2004).

[105] Fernández, A. G., Lasanta, M. I. and Pérez, F. J., “Molten salt corrosion of stainless steels and low-Cr steel in CSP plants,” Oxid. Met. **78**(5–6), 329–348 (2012).

[106] Kruizenga, A. M., Gill, D. D., Laford, M. and Mcconohy, G., “Corrosion of High Temperature Alloys in Solar Salt at 400 , 500 , and 680 ° C,” Sandia Rep. **SAND 2013**-(September), 1–45 (2013).

[107] Bose, S., [High temperature coatings], Butterworth-Heinemann (2007).

[108] Tortorelli, P. F., Bishop, P. S. and DiStefano, J. R., [Selection of Corrosion-Resistant Materials for Use in Molten Nitrate Salts], Oak Ridge National Laboratory, Tennessee (1989).

[109] “NREL: Concentrating Solar Power Projects - Atacama-1.”, 2015.

[110] Pacio, J. and Wetzel, T., “Assessment of liquid metal technology status and research paths for their use as efficient heat transfer fluids in solar central receiver systems,” Sol. Energy **93**, 11–22 (2013).

[111] Avila-Marin and L., A., “Volumetric receivers in Solar Thermal Power Plants with Central Receiver System technology: A review,” Sol. Energy **85**(5), 891–910 (2011).

[112] Boerema, N., Morrison, G., Taylor, R. and Rosengarten, G., “Liquid sodium versus Hitec as a heat transfer fluid in solar thermal central receiver systems,” Sol. Energy **86**(9), 2293–2305 (2012).

[113] Pacio, J. and Wetzel, T., “Assessment of liquid metal technology status and research paths for their use as efficient heat transfer fluids in solar central receiver systems,” Sol. Energy **93**, 11–22 (2013).

[114] Cabeza, L. F., [Advances in thermal energy storage systems], Elsevier (2015).

[115] Flora, G., Gupta, D. and Tiwari, A., “Toxicity of lead: A review with recent updates,” Interdiscip. Toxicol. **5**(2), 47–58 (2012).

[116] Gurr, M., Bau, S., Burmeister, F., Wirth, M., Piedra-Gonzalez, E., Krebser, K., Preußner, J. and Pfeiffer, W., “Investigation of the corrosion behavior of NiVAl multilayer coatings in hot salt melts,” Surf. Coatings Technol. **279**, 101–111 (2015).

[117] Kearney, D., Kelly, B., Herrmann, U., Cable, R., Pacheco, J., Mahoney, R., Price, H., Blake, D., Nava, P. and Potrovitza, N., “Engineering aspects of a molten salt heat transfer fluid in a trough solar field,” Energy **29**(5–6), 861–

870 (2004).

[118] Moore, R., Vernon, M., Ho, C. K., Siegel, N. P., Kolb, G. J., Laboratories, S. N. and Albuquerque, P. O. B., “Design considerations for concentrating solar power tower systems employing molten salt,” Sandia Natl. Lab. **SAND 2010**-(September) (2010).

[119] Spiegel, M. and Mentz, J., “High temperature corrosion beneath nitrate melts,” Mater. Corros. **65**(3), 276–281 (2014).

[120] Audigié, P., Encinas-Sánchez, V., Juez-Lorenzo, M., Rodríguez, S., Gutiérrez, M., Pérez, F. J. and Agüero, A., “High temperature molten salt corrosion behavior of aluminide and nickel-aluminide coatings for heat storage in concentrated solar power plants,” Surf. Coatings Technol. **349**(May), 1148–1157 (2018).

[121] Singh, H., Sidhu, B. S., Puri, D. and Prakash, S., “Use of plasma spray technology for deposition of high temperature oxidation/corrosion resistant coatings - A review,” Mater. Corros. **58**(2), 92–102 (2007).

[122] Singh, H., Sidhu, B. S., Puri, D. and Prakash, S., “Use of plasma spray technology for deposition of high temperature oxidation/corrosion resistant coatings - A review,” Mater. Corros. **58**(2), 92–102 (2007).

[123] Cinca, N. and Guilemany, J. M., “Thermal spraying of transition metal aluminides: An overview,” Intermetallics **24**, 60–72 (2012).

[124] Singh, H., Puri, D. and Prakash, S., “Some studies on hot corrosion performance of plasma sprayed coatings on a Fe-based superalloy,” Surf. Coatings Technol. **192**(1), 27–38 (2005).

[125] Board, N. materials advisory., [Coatings for High-Temperature Structural Materials: Trends and Opportunities], National academy press, Washington D. C. (1996).

[126] Glatzmaier, G. C. and Gomez, J. C., “Determining the Cost Benefit of High-Temperature Coatings for Concentrating Solar Power Thermal Storage

Using Probabilistic Cost Analysis," J. Sol. Energy Eng. **137**(4), 041006 (2015).

[127] Gomez, J., "Degradation mechanisms and deveopment of protective coatings for TES and HTF containment materials," NREL Rep.(October 2012) (2013).

[128] Sunshot., "Molten Salt - Concept Definition & Capital Cost Estimate, B&V PROJECT NO. 042839," US Dep. energy(042839) (2016).

[129] Kelly, B. and Kearney, D., "Thermal Storage Commercial Plant Design Study for a 2-Tank Indirect Molten Salt System: Final Report; May 13, 2002 - December 31, 2004" (2002).

[130] Podchernyaeva, I. a, Panasyuk, a D., Teplenko, M. a and Podol, V. I., "Protective Coatings on Heat-Resistant Nickel Alloys (Review)," Powder Metall. Met. Ceram. **39**(9–10), 434–444 (2000).

[131] Starosta, R., "Properties of Thermal Spraying Ni-Al Alloy Coatings," Adv. Mater. Sci. **9**(1) (2009).

[132] Sidhu, B. S. and Prakash, S., "Degradation Behavior of Ni₃Al Plasma-Sprayed Boiler Tube Steels in an Energy Generation System," J. Mater. Eng. Perform. **14**(3), 356–362 (2005).

[133] Sidhu, B. S. and Prakash, S., "Evaluation of the corrosion behaviour of plasma-sprayed Ni3Al coatings on steel in oxidation and molten salt environments at 900 oC," Surf. Coatings Technol. **166**, 89–100 (2003).

[134] Mishra, S. B., Chandra, K., Prakash, S. and Venkataraman, B., "Characterisation and erosion behaviour of a plasma sprayed Ni3Al coating on a Fe-based superalloy," Mater. Lett. **59**(28), 3694–3698 (2005).

[135] Singh, H., Prakash, S. and Puri, D., "Some observations on the high temperature oxidation behaviour of plasma sprayed Ni3Al coatings," Mater. Sci. Eng. A **444**(1–2), 242–250 (2007).

[136] Mishra, S. C., Satapathy, a., Chaithanya, M., Ananthapadmanabhan, P. V.

and Sreekumar, K. P., “Wear Characteristics of Plasma Sprayed Nickel--Aluminum Composite Coatings,” J. Reinf. Plast. Compos. **28**(23), 2931–2940 (2009).

[137] Sampath, S., Jiang, X. ., Matejicek, J., Prchlik, L., Kulkarni, a and Vaidya, a., “Role of thermal spray processing method on the microstructure, residual stress and properties of coatings: an integrated study for Ni–5 wt.%Al bond coats,” Mater. Sci. Eng. A **364**(1–2), 216–231 (2004).

[138] Deshpande, S., Sampath, S. and Zhang, H., “Mechanisms of oxidation and its role in microstructural evolution of metallic thermal spray coatings—Case study for Ni–Al,” Surf. Coatings Technol. **200**(18–19), 5395–5406 (2006).

[139] Kumar, S., Selvarajan, V., Padmanabhan, P. V. a and Sreekumar, K. P., “Characterization and comparison between ball milled and plasma processed iron-aluminium thermal spray coatings,” Mater. Sci. Eng. A **486**, 287–294 (2008).

[140] Montero, C., Navío, R., Llorente, P., Romero, M. C. and Martínez, J., “CRS sales: Abengoa’s molten salt pilot power tower plant celebrates one year of uninterrupted operation,” Energy Procedia **49**(April 1996), 488–497 (2014).

[141] Bielecki, A., Ernst, S., Skrodzka, W. and Wojnicki, I., “Concentrated Solar Power Plants with Molten Salt Storage: Economic Aspects and Perspectives in the European Union,” Int. J. Photoenergy **2019**, 1–10 (2019).

[142] Abengoa., “Abengoa Solar,” 2011.

[143] Kruizenga, A. M., Gill, D. D. and Laford, M., “Materials Corrosion of High Temperature Alloys Immersed in 600 ° C Binary Nitrate Salt,” Sandia Rep. **SAND 2013**-(March), 1–57 (2013).

[144] Nishikawa, S., Horii, Y. and Ikeuchi, K., “Effect of phosphorus content on stress corrosion cracking susceptibility of shielded metal arc weld metals

for 600 type alloy in high temperature pressurised pure water," Weld. Int. **27**(10), 747–757 (2013).

[145] Bradshaw, A., Simms, N. J. and Nicholls, J. R., "Development of hot corrosion resistant coatings for gas turbines burning biomass and waste derived fuel gases," Surf. Coatings Technol. **216**, 8–22 (2013).

[146] Susan, D. F., Misiolek, W. Z. and Marder, A. R., "Reaction Synthesis of Ni-Al – Based Particle Composite Coatings," Metall. Mater. Trans. a **32**(February) (2001).

[147] Nicholls, J. R., "Designing Oxidation-Resistant Coatings," Jom **52**(1), 28–35 (2000).

[148] Goward, G. W., "Progress in coatings for gas turbine airfoils," Surf. Coatings Technol. **108**–**109**(1–3), 73–79 (1998).

[149] Loghman-Estarki, M., Nejati, M., Shoja-Razavi, R., Jamali, H. and Pakseresht, A., "Evaluation of hot corrosion behavior of plasma sprayed ceria and yttria stabilized zirconia thermal barrier coatings in the presence of Na2SO4+V2O5 molten salt," Ceram. Int. **35**, 693–702 (2015).

[150] Saricimen, H., Quddus, a. and Ul-Hamid, a., "Hot corrosion behavior of plasma and HVOF sprayed Co- and Ni-based coatings at 900°C," Prot. Met. Phys. Chem. Surfaces **50**(3), 391–399 (2014).

[151] Zhou, Y., Peng, X. and Wang, F., "Oxidation of a novel electrodeposited Ni-Al nanocomposite film at 1050 °C," Scr. Mater. **50**(12), 1429–1433 (2004).

[152] Cinca, N. and Guilemany, J. M., "Thermal spraying of transition metal aluminides: An overview," Intermetallics **24**, 60–72 (2012).

[153] Niu, Y., Zheng, X., Liu, X., Ji, H. and Ding, C., "Influence of powder size on characteristics of air plasma sprayed silicon coatings," Ceram. Int. **38**(7), 5897–5905 (2012).

[154] Tsai, P. C., Lee, J. H. and Hsu, C. S., "Hot corrosion behavior of laser-

glazed plasma-sprayed yttria-stabilized zirconia thermal barrier coatings in the presence of V 2 O 5," 5143–5147 (2007).

[155] Singh, H., Puri, D. and Prakash, S., "Corrosion Behavior of Plasma-Sprayed Coatings on a Ni-Base Superalloy in Na2SO4 -60Pct V2O5 Environment at 900 ° C," Metall. Mater. Trans. A **36**(April), 1007–1015 (2005).

[156] Keyvani, A., "Microstructural stability oxidation and hot corrosion resistance of nanostructured Al 2 O 3 / YSZ composite compared to conventional YSZ TBC coatings," J. Alloys Compd. **623**, 229–237 (2015).

[157] Somasundaram, B., Kadoli, R. and Ramesh, M. R., "Evaluation of Cyclic Oxidation and Hot Corrosion Behavior of HVOF-Sprayed WC-Co/NiCrAlY Coating," J. Therm. Spray Technol. **23**(6), 1000–1008 (2014).

[158] Sidhu, T. S., Prakash, S. and Agrawal, R. D., "Hot Corrosion Resistance of High-Velocity Oxyfuel Sprayed Coatings on a Nickel-Base Superalloy in Molten Salt Environment," J. Therm. Spray Technol. **15**(3), 387–399 (2006).

[159] Prasad, K., Mukherjee, S., Antony, K., Manikandan, M., Arivarasu, M., K, D. R. and Arivazhagan, N., "Investigation on Hot Corrosion Behavior of Plasma Spray Coated Nickel Based Superalloy in Aggressive Environments at 900 ° C," Int. J. chemtech Res. **6**(1), 416–431 (2014).

[160] Saladi, S., Menghani, J. V and Prakash, S., "Characterization and Evaluation of Cyclic Hot Corrosion Resistance of Detonation-Gun Sprayed Ni-5Al Coatings on Inconel-718," J. Therm. Spray Technol. **24**(5), 778–788 (2015).

[161] Mahesh, R. a, Jayaganthan, R. and Prakash, S., "Oxidation behavior of HVOF sprayed Ni – 5Al coatings deposited on Ni- and Fe-based superalloys under cyclic condition," Mater. Sci. Eng. A **475**, 327–335 (2008).

[162] Mahesh, R. A., Jayaganthan, R., Prakash, S., Chawla, V. and Chandra, R.,

"High temperature cyclic oxidation behavior of magnetron sputtered Ni-Al thin films on Ni- and Fe-based superalloys," Mater. Chem. Phys. **114**(2–3), 629–635 (2009).

[163] Mahesh, R. A., Jayaganthan, R. and Prakash, S., "A study on hot corrosion behaviour of Ni-5Al coatings on Ni- and Fe-based superalloys in an aggressive environment at 900ºC," J. Alloys Compd. **460**(1–2), 220–231 (2008).

[164] Trent, M. C., Goods, S. H. and Bradshaw, R. W., "Comparison of corrosion performance of grade 316 and grade 347H stainless steels in molten nitrate salt," AIP Conf. Proc. **1734** (2016).

[165] Kruizenga, A. and Gill, D., "Corrosion of iron stainless steels in molten nitrate salt," Energy Procedia **49**, 878–887 (2013).

[166] Bradshaw, R. W. and Goods, S. H., "Corrosion of Alloys and Metals by Molten Nitrates," Sandia Rep. **SAND 2000**-(August), 1–34 (2001).

[167] Kumar, S., Selvarajan, V., Padmanabhan, P. V. a. and Sreekumar, K. P., "Characterization and comparison between APS coatings prepared from ball milled and plasma processed nickel–aluminium powders," Mater. Sci. Eng. A **486**(1–2), 287–294 (2008).

[168] Goods, S. H. and Bradshaw, R. W., "Corrosion of Stainless Steels and Carbon Steel by Molten Mixtures of Commercial Nitrate Salts," J. Mater. Eng. Perform. **13**(1), 78–87 (2004).

[169] Fernández, A. G., Galleguillos, H., Fuentealba, E. and Pérez, F. J., "Corrosion of stainless steels and low-Cr steel in molten Ca(NO3)2-NaNO3-KNO3 eutectic salt for direct energy storage in CSP plants," Sol. Energy Mater. Sol. Cells **141**, 7–13 (2015).

[170] Soleimani Dorcheh, A., Durham, R. N. and Galetz, M. C., "Corrosion behavior of stainless and low-chromium steels and IN625 in molten nitrate salts at 600oC," Sol. Energy Mater. Sol. Cells **144**(3), 109–116 (2016).

[171] Fernández, A., G., ., Rey, A., Lasanta, I., Mato, S., Brady, M. P. and Pérez, F. J., “Corrosion of alumina-forming austenitic steel in molten nitrate salts by gravimetric analysis and impedance spectroscopy,” Mater. Corros. **65**(3), 267–275 (2014).

[172] Kruizenga, A. and Gill, D., “Corrosion of iron stainless steels in molten nitrate salt,” Energy Procedia **49**, 878–887 (2013).

[173] Jia, Q., Li, D., Li, S., Zhang, Z. and Zhang, N., “High-temperature oxidation resistance of NiAl intermetallic formed in Situ by thermal spraying,” Coatings **8**(8) (2018).

[174] Sidhu, B. S. and Prakash, S., “Degradation Behavior of Ni3Al Plasma-Sprayed Boiler Tube Steels in an Energy Generation System,” J. Mater. Eng. Perform. **14**(3), 356–362 (2005).

[175] Chang, J. T., Davison, a., He, J. L. and Matthews, a., “Deposition of Ni–Al–Y alloy films using a hybrid arc ion plating and magnetron sputtering system,” Surf. Coatings Technol. **200**(20–21), 5877–5883 (2006).

[176] Čelko, L., Klakurková, L. and Švejcar, J., “Diffusion in Al-Ni and Al-NiCr interfaces at moderate temperatures,” Defect Diffus. Forum **297**–**301**(April), 771–777 (2010).

[177] Audigié, P., Encinas-Sánchez, V., Juez-Lorenzo, M., Rodríguez, S., Gutiérrez, M., Pérez, F. J. and Agüero, A., “High temperature molten salt corrosion behavior of aluminide and nickel-aluminide coatings for heat storage in concentrated solar power plants,” Surf. Coatings Technol. **349**(June), 1148–1157 (2018).

[178] Gonzalez-Rodriguez, J. G., Cuellar-Hernández, M., Gonzalez-Castañeda, M., Salinas-Bravo, V. M., Porcayo-Calderon, J. and Rosas, G., “Effect of heat treatment and chemical composition on the corrosion behavior of FeAl intermetallics in molten (Li + K)carbonate,” J. Power Sources **172**(2), 799–804 (2007).

[179] Tortorelli, P. F. Bishop, P. ., “Influence of Compositional Modifications on

the Corrosion of Iron Aluminides by Molten Nitrate Salts” (1991).

[180] Sidhu, B. S. and Prakash, S., “Evaluation of the corrosion behaviour of plasma-sprayed Ni 3 Al coatings on steel in oxidation and molten salt environments at 900 8C,” Surf. Coatings Technol. **166**, 89–100 (2003).

[181] Mishra, S. B., Chandra, K. and Prakash, S., “Studies on erosion-corrosion behaviour of plasma sprayed Ni3Al coating in a coal-fired thermal power plant environment at 540°C,” Anti-Corrosion Methods Mater. **64**(5), 540–549 (2017).

[182] Fotovvati, B., Namdari, N. and Dehghanghadikolaei, A., “On coating techniques for surface protection: A review,” J. Manuf. Mater. Process. **3**(1) (2019).

[183] Jilani, A., Abdel-wahab, M. S. and Hammad, A. H., “Advance Deposition Techniques for Thin Film and Advance Deposition Techniques for Thin Film and Coating Coating,” Mod. Technol. Creat. Thin-film Syst. Coatings **i**, 13 (2016).

[184] Baptista, A., Silva, F., Porteiro, J., Míguez, J. and Pinto, G., “Sputtering physical vapour deposition (PVD) coatings: A critical review on process improvement andmarket trend demands,” Coatings **8**(11) (2018).

[185] Fayomi, O. S. I., Akande, I. G., Abioye, O. P. and Fakehinde, O. B., “New trend in thin film composite coating deposition: A mini review,” Procedia Manuf. **35**, 1007–1012 (2019).

[186] Mbam, S. O., Nwonu, S. E., Orelaja, O. A., Nwigwe, U. S. and Gou, X. F., “Thin-film coating; Historical evolution, conventional deposition technologies, stress-state micro/nano-level measurement/models and prospects projection: A critical review,” Mater. Res. Express **6**(12) (2019).

[187] Waser, R., Schneller, T., Hoffmann-eifert, S. and Ehrhart, P., “Advanced chemical deposition techniques - from research to production,” Integr. Ferroelectr. **36**(1–4), 3–20 (2001).

[188] Tejero-Martin, D., Rezvani Rad, M., McDonald, A. and Hussain, T., [Beyond Traditional Coatings: A Review on Thermal-Sprayed Functional and Smart Coatings], Springer US (2019).

[189] Liu, M. J., Zhang, G., Lu, Y. H., Han, J. Q., Li, G. R., Li, C. X., Li, C. J. and Yang, G. J., “Plasma spray–physical vapor deposition toward advanced thermal barrier coatings: a review,” Rare Met. (2020).

[190] Moore, B., Asadi, E. and Lewis, G., “Deposition methods for Microstructured and Nanostructured coatings on metallic bone implants: A review,” Adv. Mater. Sci. Eng. **2017** (2017).

[191] Mouadji, Y., Bradai, M. A. and Younes, R., “In fl uence of heat treatment on microstructure and tribological properties of flame spraying Fe – Ni – Al alloy coating,” 0–1 (2018).

[192] Jain, A., Ong, S. P., Hautier, G., Chen, W., Richards, W. D., Dacek, S., Cholia, S., Gunter, D., Skinner, D., Ceder, G. and Persson, K. A., “Commentary: The materials project: A materials genome approach to accelerating materials innovation,” APL Mater. **1**(1) (2013).

[193] Speakman, S. a and Ph, D., “Introduction to X-Ray Powder Diffraction Data Analysis An X-ray diffraction pattern is a plot of the intensity of X-rays scattered at different angles by a sample,” Mater. Sci.

[194] ICDD., “Powder Diffraction File -2,” Int. Cent. Diffr. Data database.

[195] Zhao, J., Deng, Y., Wei, H., Zheng, X., Yu, Z., Shao, Y., Shield, J. E. and Huang, J., “Strained hybrid perovskite thin films and their impact on the intrinsic stability of perovskite solar cells,” Sci. Adv. **3**(11) (2017).

[196] Bindu, P. and Thomas, S., “Estimation of lattice strain in ZnO nanoparticles: X-ray peak profile analysis,” J. Theor. Appl. Phys. **8**(4), 123–134 (2014).

[197] Fewster, P. F. and Andrew, N. L., “Strain analysis by X-ray diffraction,” Thin Solid Films **319**(1–2), 1–8 (1998).

[198] Girgsdies, F. and Group, E. M., “Peak Profile Analysis in X-ray Powder

Diffraction Peak Profile Analysis in X-ray Powder Diffraction Peak Profile Analysis in X-ray Powder Diffraction" (1200).

[199] Goossens, S., De Pauw, B., Geernaert, T., Salmanpour, M. S., Sharif Khodaei, Z., Karachalios, E., Saenz-Castillo, D., Thienpont, H. and Berghmans, F., "Aerospace-grade surface mounted optical fibre strain sensor for structural health monitoring on composite structures evaluated against in-flight conditions," Smart Mater. Struct. **28**(6) (2019).

[200] Nasiri-Tabrizi, B., "Thermal treatment effect on structural features of mechano-synthesized fluorapatite-titania nanocomposite: A comparative study," J. Adv. Ceram. **3**(1), 31–42 (2014).

[201] Konieczny, M., "Mechanical properties and deformation behavior of laminated Ni-(Ni2Al3+NiAl3) and Ni-(Ni3Al+NiAl) composites," Mater. Sci. Eng. A **586**, 11–18 (2013).

[202] Cho, G. S., Lee, K. R., Choe, K. H., Lee, K. W. and Ikenaga, A., "Fabrication of Ni-Al intermetallic compounds on the Al casting alloy by SHS process," Inst. Cast Met. Eng. - 67th World Foundry Congr. wfc06 Cast. Futur. **1**, 361–370 (2006).

[203] Cao, J., Song, X. G., Wu, L. Z., Qi, J. L. and Feng, J. C., "Characterization of Al/Ni multilayers and their application in diffusion bonding of TiAl to TiC cermet," Thin Solid Films **520**(9), 3528–3531 (2012).

[204] ASTM International., "Standard Practice for Preparing , Cleaning , and Evaluating Corrosion Test," Significance **90**(Reapproved 2011), 1–9 (1999).

[205] Sequeira, C., [High Temperature Corrosion in Molten Salts], Trans Tech Publications (2003).

[206] Fernández, Á. G. and Cabeza, L. F., "Molten salt corrosion mechanisms of nitrate based thermal energy storage materials for concentrated solar power plants: A review," Sol. Energy Mater. Sol. Cells **194**(October 2018), 160–165 (2019).

[207] Bradshaw, R. W. and Goods, S. H., “Corrosion of Alloys and Metals by Molten Nitrates” (2001).

[208] Kramer, C. M. and Munir, Z. A., “ Thermal Decomposition of NaNO 3 and KNO 3 ,” ECS Proc. Vol. **1981**–**9**, 494–505 (1981).

[209] Spiegel, M. and Mentz, J., “High temperature corrosion beneath nitrate melts,” Mater. Corros. **65**(3), 276–281 (2014).

[210] Qiu, S., Solomon, L. and Fang, M., “Study of material compatibility for a thermal energy storage system with phase change material,” Energies **11**(3), 4–6 (2018).

[211] Trent, M. C., Goods, S. H. and Bradshaw, R. W., “Comparison of corrosion performance of grade 316 and grade 347H stainless steels in molten nitrate salt,” AIP Conf. Proc. **1734**(2016) (2016).

[212] Gurr, M., Bau, S., Burmeister, F., Wirth, M., Piedra-Gonzalez, E., Krebser, K., Preußner, J. and Pfeiffer, W., “Investigation of the corrosion behavior of NiVAl multilayer coatings in hot salt melts,” Surf. Coatings Technol. **279**, 101–111 (2015).

[213] Kumar, M., Singh, H. and Singh, N., “Study of Ni-20Cr coatings for high temperature applications - A review,” Arch. Metall. Mater. **58**(2), 523–528 (2013).

[214] Trent, M. C., Goods, S. H. and Bradshaw, R. W., “Comparison of corrosion performance of grade 316 and grade 347H stainless steels in molten nitrate salt,” AIP Conf. Proc. **1734** (2016).

[215] Soleimani Dorcheh, A., Durham, R. N. and Galetz, M. C., “Corrosion behavior of stainless and low-chromium steels and IN625 in molten nitrate salts at 600 °c,” Sol. Energy Mater. Sol. Cells **144**(3), 109–116 (2016).

[216] Kumar, D. and Pandey, K., “Optimization of the process parameters in generic thermal barrier coatings using the Taguchi method and grey relational analysis,” Proc. Inst. Mech. Eng. Part L J. Mater. Des. Appl.

231(7), 600–610 (2017).

[217] Kumar, S., Selvarajan, V., Padmanabhan, P. V. a and Sreekumar, K. P., “Characterization and comparison between ball milled and plasma processed nickel-aluminium powders,” Surf. Coatings Technol. **486**(3–4), 287–294 (2008).

[218] Goods, S. H. and Bradshaw, R. W., “Corrosion of Stainless Steels and Carbon Steel by Molten Mixtures of Commercial Nitrate Salts,” J. Mater. Eng. Perform. **13**(1), 78–87 (2004).

[219] Loghman-Estarki, M. R., Shoja Razavi, R., Edris, H., Bakhshi, S. R., Nejati, M. and Jamali, H., “Comparison of hot corrosion behavior of nanostructured ScYSZ and YSZ thermal barrier coatings,” Ceram. Int. **42**(6), 7432–7439 (2016).

[220] Rajendran, R., “Gas turbine coatings – An overview.pdf,” Eng. Fail. Anal. **26**, 355–369 (2012).

[221] Wagner, S. J. and Rubin, E. S., “Economic implications of thermal energy storage for concentrated solar thermal power,” Renew. Energy **61**, 81–95 (2014).

[222] Zhang, Z., Lim, S. H., Chai, J., Lai, D. M. Y., Cheong, A. K. H., Cheong, K. L., Wang, S. J., Jin, H. and Pan, J. S., “Plasma spray of Ti2AlC MAX phase powders: Effects of process parameters on coatings’ properties,” Surf. Coatings Technol. **325**, 429–436 (2017).

[223] Liu, M., Steven Tay, N. H., Bell, S., Belusko, M., Jacob, R., Will, G., Saman, W. and Bruno, F., “Review on concentrating solar power plants and new developments in high temperature thermal energy storage technologies,” Renew. Sustain. Energy Rev. **53**, 1411–1432 (2016).